STRUCTURE AND STABILITY OF BUOYANT DIFFUSION FLAMES

Thesis by

Graham Christopher Fleming

In Partial Fulfillment of the Requirements

for the degree of

Doctor of Philosophy

California Institute of Technology

Pasadena, California

1982

(Submitted March 17, 1982)

ACKNOWLEDGEMENTS

I wish to express my appreciation to my advisor, Professor F. E. Marble, who inspired this work. His guidance throughout the course of my graduate studies was invaluable.

Sincere thanks also to Professor T. Kubota for many helpful discussions and to Professor E. E. Zukoski and Mr. B. Cetegen for their helpful comments and suggestions.

Many people contributed to making my stay at the California Institute of Technology enjoyable. Ms. D. Eckerman's understanding and encouragement were much appreciated as was the friendship of my roommates, especially Dr. G. Yates, with whom I also had valuable discussions on my research. The support and encouragement of my parents has also greatly helped to sustain me.

I was fortunate to receive an Earle C. Anthony fellowship and a Fulbright Travel Grant as well as support from the California Institute of Technology, which made my graduate study possible.

This work was also supported in part by NASA Grant NAG 3-70, Department of Energy Contract EX-76-G-03-1305 and National Bureau of Standards Grant G 8 9014.

ABSTRACT

The structure and stability of the convecting fluid flow generated by a diffusion flame in gaseous reactants has been investigated. The flame extends vertically upwards from a solid horizontal boundary, and separates the fuel from the oxidizer which can be of a different density. Real fuels are modelled by choosing appropriate values for the density difference and stoichiometric ratio of the reaction.

A self-similar solution for the steady flow is obtained incorporating the Howarth transformation, which allows the large density variations inherent in the combustion of gases to be accommodated. The stoichiometric ratio and fuel/oxidizer density ratio are varied to examine their effects on the structure and flow properties of the flame.

An Orr-Sommerfeld equation governing the stability of buoyant flows is developed, incorporating all the variable density terms. Two different steady flows are studied, the symmetric flame (unit stoichiometry), and a flame with the stoichiometric ratio corresponding to methane burning in air. It was found that using the Boussinesq approximation which neglects density variations except for a buoyancy term is not applicable for the flame, and also introduced inaccuracy in the stability diagram for the buoyant plume. Although the flame bears a superficial similarity to the buoyant plume, the several differences cause a large difference in their stability. Empirically interpreting the stability diagrams to obtain an expected transition point gives $Re_T \approx 250$ for the flame compared to the less stable buoyant plume with $Re_T \approx 140$. A new unstable region consisting of waves with negative phase velocity but positive group velocity was found for both the buoyant flame and the buoyant plume.

The local analysis is inappropriate for disturbances with wavelengths long compared to the flame thickness, therefore an analysis treating the flame and associated plume as negligibly thin was undertaken. This showed that the

primary cause of instability was centrifugal forces generated by the momentum flux following a curved path. Reasonably good agreement was obtained with the local analysis.

TABLE OF CONTENTS

Chapter	Title	Page
	Acknowledgements	ii
	Abstract	iii
	Table of Contents	v
	List of Illustrations	vii
	List of Tables	xi
	List of Symbols	xii
1	Introduction	1
	References	6
2	The Structure of Buoyant Diffusion Flames	8
	2.1 The Governing Equations	9
	2.2 Numerical Solution	20
	2.3 Results	21
	References	26
3	Formulation of the Local Stability Problem	47
	3.1 Governing Equations	48
	3.2 Boundary and Matching Conditions	57
	3.2.1 Matching Conditions at the Flame	57
	3.2.2 Replacement of the Boundary Conditions at Infinity	63
	3.3 Numerical Solution	66
	3.4 Inviscid Stability Equation	72
	References	74
4	The Instability of Buoyant Diffusion Flames	76
	References	89

TABLE OF CONTENTS (Cont'd)

Chapter	Title	Page
5	The Stability of Buoyant Diffusion Plumes	110
	5.1 Steady Solution	111
	5.2 Linear Stability Analysis	114
	References	118
6	Stability of a Buoyant Flame Sheet to Long Wavelength Disturbances	128
	6.1 Formulation	128
	6.2 Asymptotic Solution	136
	References	145
7	Concluding Remarks	149

LIST OF ILLUSTRATIONS

Figure Number	Caption	Page
2.1	Geometry for Buoyant Diffusion Flame	28
2.2	Velocity, Temperature and Concentration Profiles for Symmetric Flame	29
2.3	Velocity, Temperature and Concentration Profiles for Flame with $\tilde{\varphi} = 0.232$	30
2.4	Velocity, Temperature and Concentration Profiles for Flame with $\tilde{\varphi} = 0.058$	31
2.5	Velocity, Temperature and Concentration Profiles for Flame with $\tilde{\varphi} = 0.058$ after inverting Howarth Transformation	32
2.6	Velocity, Temperature and Concentration Profiles for Flame with $\tilde{\varphi} = 0.029$	33
2.7	Variation of maximum vertical velocity, U_{max}, entrainment of oxidiser, $\dot{m}e$, and mass flux through the flame, $\dot{m}_f$ with stoichiometry.	34
2.8	Variation of fuel consumption, $\dot{m}_F$, buoyancy, β, and enthalpy thickness on each side of flame, $\delta_{H\pm}$ with stoichiometry	35
2.9	Velocity, Temperature and Concentration Profiles for Symmetric Flame	36
2.10	Velocity, Temperature and Concentration Profiles for Flame with $\tilde{\varphi} = 1, \frac{\rho^*_{F\infty}}{\rho^*_{O\infty}} = 0.25, \frac{T^*_f}{T^*_{O\infty}} = 7$	37
2.11	Velocity, Temperature and Concentration Profiles for Flame with $\tilde{\varphi} = 1, \frac{\rho^*_{F\infty}}{\rho^*_{O\infty}} = 0.125, \frac{T^*_f}{T^*_{O\infty}} = 7$	38
2.12	Variation of maximum vertical velocity, U_{max}, entrainment of oxidiser, $\dot{m}e$, and mass flux through the flame, $\dot{m}_f$ with density ratio at infinity.	39
2.13	Variation of fuel consumption, $\dot{m}_F$, buoyancy, β, and enthalpy thickness on each side of flame, $\delta_{H\pm}$ with density ratio at infinity.	40
2.14	Velocity, Temperature and Concentration Profiles for Methane/Air Flame ($\tilde{\varphi} = 0.058, \frac{\rho^*_{F\infty}}{\rho^*_{O\infty}} = 0.552, \frac{T^*_f}{T^*_{O\infty}} = 7.58$)	41

LIST OF ILLUSTRATIONS (Cont'd)

Figure Number	Caption	Page
2.15	Velocity, Temperature and Concentration Profiles for Methane/Air Flame ($\tilde{\varphi} = 0.029, \frac{\rho^*_{F\infty}}{\rho^*_{O\infty}} = 0.069, \frac{T^*_f}{T^*_{O\infty}} = 7.83$)	42
4.1	Neutral stability and amplification contours for symmetric buoyant diffusion flame using Boussinesq approximation. Frequency-Reynolds number diagram with local non-dimensionalisation.	91
4.2	Neutral stability and amplification contours for symmetric buoyant diffusion flame using Boussinesq approximation. Wave number-Reynolds number diagram with local non-dimensionalisation.	92
4.3	Stability of symmetric buoyant diffusion flame using Boussinesq approximation. Variation of wave-number and amplification rates with frequency at Re = 10.	93
4.4	Variation of the exponent in the asymptotic expression for the disturbance quantities with frequency.	94
4.5	Inviscid asymptote for the stability of symmetric buoyant diffusion flame using Boussinesq approximation. Variation of wave-number and amplification rates with frequency.	95
4.6	Neutral stability and amplification contours for symmetric buoyant diffusion flame using Boussinesq approximation. Frequency-Reynolds number diagram with global non-dimensionalisation.	96
4.7	Neutral stability and amplification contours for symmetric buoyant diffusion flame using Boussinesq approximation. Wave number-Reynolds number diagram with global non-dimensionalisation.	97
4.8	Neutral stability and amplification contours for asymmetric buoyant diffusion flame ($\tilde{\varphi} = 0.058$) using Boussinesq approximation. Frequency-Reynolds number diagram with local non-dimensionalisation.	98
4.9	Neutral stability and amplification contours for asymmetric buoyant diffusion flame ($\tilde{\varphi} = 0.058$) using Boussinesq approximation. Wave-number-Reynolds number diagram with local non-dimensionalisation.	99

LIST OF ILLUSTRATIONS (Cont'd)

Figure Number	Caption	Page
4.10	Neutral stability and amplification contours for symmetric buoyant diffusion flame with $\left(\frac{T_f}{T_\infty}-1\right)=6$. Frequency-Reynolds number diagram with local non-dimensionalisation.	100
4.11	Neutral stability and amplification contours for symmetric buoyant diffusion flame with $\left(\frac{T_f}{T_\infty}-1\right)=6$. Wave-number-Reynolds number diagram with local non-dimensionalisation.	101
4.12	Stability of symmetric buoyant diffusion flame with $\left(\frac{T_f}{T_\infty}-1\right)=6$. Variation of wave-number and amplification rates with frequency at Re = 10.	102
4.13	Inviscid asymptote for the stability of symmetric buoyant diffusion flame with $\left(\frac{T_f}{T_\infty}-1\right)=6$. Variation of wave-number and amplification rates with frequency.	103
4.14	Neutral stability and amplification contours for symmetric buoyant diffusion flame with $\left(\frac{T_f}{T_\infty}-1\right)=6$. Frequency-Reynolds number diagram with global non-dimensionalisation.	104
4.15	Neutral stability and amplification contours for symmetric buoyant diffusion flame with $\left(\frac{T_f}{T_\infty}-1\right)=6$. Wave-number-Reynolds number diagram with global non-dimensionalisation.	105
4.16	Neutral stability and amplification contours for asymmetric buoyant diffusion flame ($\tilde{\varphi}=0.058$) with $\left(\frac{T_f}{T_\infty}-1\right)=6$. Frequency-Reynolds number diagram with global non-dimensionalisation.	106
4.17	Neutral stability and amplification contours for asymmetric buoyant diffusion flame ($\tilde{\varphi}=0.058$)with $\left(\frac{T_f}{T_\infty}-1\right)=6$. Wave-number-Reynolds number diagram with global non-dimensionalisation.	107

LIST OF ILLUSTRATIONS (Cont'd)

Figure Number	Caption	Page
4.18	Variation of inviscid asymptotes with temperature.	108
4.19	Variation of inviscid asymptotes with flame temperature with the non-dimensionalisation independent of temperature.	109
5.1	Neutral stability and amplification contours for a plane buoyant plume using Boussinesq approximation. Frequency-Reynolds number diagram with local non-dimensionalisation.	120
5.2	Neutral stability and amplification contours for a plane buoyant plume using Boussinesq approximation. Wave-number-Reynolds number diagram with local non-dimensionalisation.	121
5.3	Inviscid asymptote for the stability of a plane buoyant plume using Boussinesq approximation. Variation of wave-number and amplification rates with frequency.	122
5.4	Stability of a plane buoyant plume using Boussinesq approximation. Variation of wave-number and amplification rates with frequency at Re = 10.	123
5.5	Neutral stability and amplification contours for a plane buoyant plume with $Q_p = 58.6 Btu/htft$. Frequency-Reynolds number diagram with local non-dimensionalisation.	124
5.6	Neutral stability and amplification contours for a plane buoyant plume with $Q_p = 58.6 Btu/hrft$. Wave-number-Reynolds number diagram with local non-dimensionalisation.	125
5.7	Neutral stability and amplification contours for a plane buoyant plume. Frequency-Reynolds number diagram with global non-dimensionalisation.	126
5.8	Neutral stability and amplification contours for a plane buoyant plume. Wave-number-Reynolds number diagram with global non-dimensionalisation.	127
6.1	Geometry for perturbed flame	146
6.2	Control volume for momentum balance across flame	147
6.3	Integration contour in $\mathcal{Z} = \xi + i\chi$ plane	148

LIST OF TABLES

Table Number	Title	Page
2.1	Streamfunction ξ and Temperature ϑ for a symmetric flame	43
2.2	Streamfunction ξ and Temperature ϑ for a flame with $\tilde{\varphi} = 0.058$, $\tilde{M} = \tilde{T}_\infty = 0$, $Pr = 0.72$. (η_E is the similarity variable after inverting the Howarth Transformation for $\tilde{T}_f = 6$)	44
2.3	Streamfunction ξ and Temperature ϑ for a flame with $\tilde{\varphi} = 0.058$, $\tilde{M} = 0.81$, $\tilde{T}_\infty = 0$, $\tilde{T}_f = 6.58$, $Pr = 0.72$.	45
2.4	Flow parameters for the flames shown in figures (2.2)-(2.6), figures (2.9)-(2.11) and figures (2.14)-(2.15)	46

LIST OF SYMBOLS

a_i	Constants in asymptotic form of ξ and ϑ
A	Constant for entrainment velocity for chapter six
A_i, B_i	Amplitude of dimensionless horizontal velocity and temperature disturbances relative to vertical velocity disturbance
b_i	Deviation from boundary condition
c	Phase velocity of disturbance $= \frac{\beta}{\alpha}$
c_G	Group velocity
c_p	Specific heat at constant pressure
c^r	Ratio of disturbance phase velocity to maximum steady velocity
C, C_1	Constants of integration
C_i	Constants for integrated flow properties of flame in chapter six
D	Binary diffusion coefficient
f	Vertical velocity disturbance
$\mathbf{f}_i$	Real or imaginary part of a disturbance quantity (Page 68)
F	Fuel
Fr	Froude number $= \frac{u_0^{*2}}{g^* x^*}$
g	Gravitational acceleration
h	Enthalpy
I	$\int_{-\infty}^{\infty} \xi' \vartheta d\eta$
I	Integral from chapter six
j	jth mesh point
J	Number of mesh points
J^*	Integrated momentum flux in the flame
k	Thermal conductivity
$k_0, k_1, \ldots$	Coefficients in wavenumber expansion
$k(x)$	Wavenumber in chapter six
l	Length scale

L	Length of flame in transverse direction
Le	Lewis number $= \frac{Pr}{Sc} = \frac{\rho c_p D}{\lambda}$
m, m_2	Disturbance quantities for coefficients of viscosity
$\dot{m}_i$	Volumetric mass producton rate of species i
$\dot{m}_o$	Dimensionless oxidizer entrainment rate
$\dot{m}_f$	Dimensionless mass flux through the flame
$\dot{m}_F$	Dimensionless fuel consumption rate
m^*	Integrated flame density
M	Mach number
M_i	Molecular weight of species i
$\tilde{M}$	Molecular weight ratio parameter. Equation (2.35)
M^*	Integrated mass flux in flame
O	Oxidizer
p	Pressure
P	Product
Pr	Prandtl number $= \frac{\rho c_p \nu}{\lambda}$
$\dot{q}$	Volumetric heat release rate
q_c	Heat produced per mole of fuel
Q_p^*	Heat generated per unit length of line source
$\bar{Q}$	Dimensionless heating parameter. Equation (5.6)
Q	Heat released by one mole of fuel
$\tilde{Q}$	Effective heating value of fuel. Equation (2.34)
r	Density disturbance
R_O	Universal gas constant
R	In chapter six, $\sqrt{x^2 + y^2}$
R_k	Right-hand side of disturbance equation
R_i	Gas constant for species i

Re — Reynolds number $= \dfrac{u_0^* \delta^*}{\nu_\infty^*}$

$$= 2\sqrt{2}\left[\frac{\left(\frac{T_f}{T_\infty} - 1\right) g^* x^{*3}}{\nu_\infty^{*2}}\right]^{\frac{1}{4}}$$

R_{kl} — Coefficient matrix for disturbance equation

s, $\tilde{s}$ — Temperature disturbance

S — Exponent in x dependence of long wavelength instability

Sc — Schmidt number $= \dfrac{\nu}{D}$

t — Time

T — Temperature

$\tilde{T}_\infty$ — Parameter involving fuel to oxidizer ratio. Equation (2.36)

$\tilde{T}_f$ — Parameter involving flame to oxidizer temperature ratio. Equation (2.32)

u — Vertical velocity

u_o — Velocity scale

$$= 2\left[\left(\frac{T_f}{T_\infty} - 1\right) g^* x^*\right]^{\frac{1}{2}}$$

U_{max} — Dimensionless maximum vertical velocity

v — Horizontal velocity

V — Flow quantity

w^* — Average vertical velocity in the flame plume

W — Complex velocity potential

x, y — Dimensionless vertical and horizontal coordinates

Y_i — Mass fraction of species i

z — Boundary condition variable

z — Complex variable in chapter six

$\tilde{z}$ — Complex variable in chapter six

Z — Schvab-Zeldovich variable

Greek

α Disturbance wave number

β Disturbance frequency

$\tilde{\beta}$ Buoyancy

γ Ratio of specific heats

δ Boundary layer thickness

$$= \left[\frac{4\nu_\infty^{*2} x^*}{\left(\frac{T_f}{T_\infty} - 1 \right) g^*} \right]^{\frac{1}{4}}$$

δ_H Dimensionless enthalpy thickness. Equation (2.51)

Δ Real or imaginary part of a disturbance quantity

ε Strain rate tensor

η Similarity variable

ϑ Non-dimensional steady temperature

κ Normalised mass fraction

λ Thermal conductivity

λ Exponent for time dependence of $\tilde{\zeta}$ in chapter six

λ Exponent in asymptotic behaviour of disturbances

$\lambda_{i\pm}$ Exponent in asymptotic behaviour of disturbances

μ Dynamic viscosity

μ_1, μ_2 Coefficients of viscosity

ν Kinematic viscosity

π Pressure disturbance

ρ Density

τ Stress tensor

τ Time scale in chapter six

φ Horizontal velocity disturbance

φ In chapter six, velocity potential for flow outside flame and its plume

φ_i Moles of species i consumed or produced by reaction of one mole of fuel

$\tilde{\varphi}$ Effective stoichiometric ratio. Equation (2.33)

ξ Dimensionless steady velocity streamfunction

ψ Velocity streamfunction

ζ Flame position

ζ Position of flame and thin plume with time dependence removed in chapter six

$\tilde{\zeta}$ Position of flame and thin plume in chapter six

Subscripts

e Edge of boundary layer

f At the flame

F In the fuel

i Species i

i, j, k, l Indices

I Imaginary part

J At the last mesh point

O In the oxidizer

P In the product

R Real part

x, y Spatial coordinates

∞ At infinity

$+ -$ In the fuel or oxidizer respectively

Superscripts

J Last mesh point

L Evaluated at the limiting stability curve $\alpha_R = 0$

N Evaluated at the neutral curve $\alpha_I = 0$

0 Mesh point at $Y = 0$

ν Iterate

$*$ Dimensional quantity

$+$ Non-dimensionalised with Reynolds number independent physical scales

$-$ Non-dimensionalised with temperature independent physical scales

$'$ Differentiation with respect to temperature and y or η respectively

Chapter 1.

INTRODUCTION

The stability of a two-dimensional laminar jet is one of the classic examples of hydrodynamic stability theory. The problem has been studied analytically by Pai, reference (1.1), 1951, for large Reynolds numbers, and by Curle, reference (1.2), 1956, and Tatsumi and Kakutani, reference (1.3), 1958, who established the position of the neutral stability curve and the existence of a critical Reynolds number below which the flow was stable. Kaplan, reference (1.4), 1964, improved the accuracy of the solution numerically and added several temporal amplification rate curves. More recently, the spatial stability of laminar jets has been studied, including the effects of removing the parallel flow assumption, by Haaland, reference (1.5), 1972, Bajaj and Garg, reference (1.6), 1977, and Garg, reference (1.7), 1981. They found that removing the parallel flow assumption resulted in improved agreement between the experimentally determined and the calculated critical Reynolds numbers.

Another problem, closely related but differing in some essential aspects, is the two-dimensional buoyant plume generated by a line heat source. Unlike the laminar jet, the buoyant plume does not conserve momentum, since buoyancy is accelerating the flow. The velocity at the centerline of the plume is therefore increasing with height, while the temperature decreases due to entrainment of the external fluid. A self-similar description of the flow has been developed by Fujii, reference (1.8), 1963, Gebhart, Pera and Schorr, reference (1.9), 1970, and Fujii, Morioka and Uehara, reference (1.10), 1973.

Because this flow has something of the character of an accelerated layer or jet, one intuitively expects the solution to be in some sense more stable. The stability was first studied by Pera and Gebhart, reference (1.11), 1971, who obtained the neutral stability curve and demonstrated the importance of

including the buoyancy term in the Orr-Sommerfeld equation. While their results showed the buoyant plume to first become unstable at lower Reynolds numbers than the jet, the results of Haaland and Sparrow, reference (1.12), 1973, and Hieber and Nash, reference (1.13), 1975, who included non-parallel effects as well as calculating several constant amplification rate curves, show that the expected Reynolds number for transition to turbulence is larger in the case of the plume, since the amplification rates are somewhat lower than for the jet.

The physical situation of interest in the following work is the buoyant or naturally convecting laminar diffusion flame. The fuel and oxidizer are separated by a thin reaction zone which is idealised as a vertical flame sheet extending upwards from a solid horizontal boundary. Real fuels are modelled by allowing the stoichiometric ratio of the reaction to vary and the fuel and oxidizer density to differ. Because the flame position is taken as fixed, a density difference between fuel and oxidizer results in a buoyancy driven flow upwards and towards the flame in the lighter fluid. This problem has practical significance for diffusion flames where buoyancy is important, such as candle flames, bunsen burners and natural fires.

A self-similar solution is developed in Chapter 2, which is similar to the buoyant plume in some respects, but differs from it in several important areas. The presence of a reaction causes both a discontinuity in the temperature gradient and a constant temperature to occur at the flame. The buoyant diffusion flame is thus essentially different to the buoyant plume in that, because of the sensible heat released along the length of the flame, the "buoyancy" is not conserved but increases with distance along the flow direction. Furthermore, the buoyant flame can be very asymmetric due to both the unequal consumption of fuel and oxidizer by the reaction and the external velocity caused by the density difference between fuel and oxidizer. The stoichiometric ratio and the density ratio of fuel to oxidizer are varied to examine their effects on both the structure

of the flame, and the properties of the flame such as buoyancy, oxidizer entrainment and fuel consumption.

There is some evidence that laminar shear zones which support combustion processes are more stable than corresponding isothermal regions, for example the stabilising effect of combustion on the wake behind cylindrical flame holders observed by Zukoski and Marble, reference (1.14), 1955. Certainly if the shear layer is in a favorable pressure gradient, the acceleration resulting from the gradient is enhanced by the reduced density of the combustion products. Further, the increased temperature results in a higher viscosity and locally lower values of the Reynolds number. This may well be reflected in an increase of the critical Reynolds number based upon external (cold) gas conditions. An examination of the combustion layer in the absence of pressure gradient, however, failed to show an increased stability, Blackshear, reference (1.15),1956.

In Chapters 3 and 4, the Tollmien-Schlichting theory of small disturbances is used to formulate the stability problem for the buoyant diffusion flame. It is assumed that at sufficiently large heights above the start of the flame, the flow can be approxmated locally by a parallel flow, which is then perturbed by small sinusoidal disturbances. The effect of buoyancy causes a coupling between the equations of momentum and energy increasing the order of the disturbance equations from fourth order, in the case of the laminar jet, to sixth order, in the case of the buoyant flows. Pera and Gebhart, reference (1.11), 1971, found that this coupling could not be neglected for the buoyant plume, since it destabilised the flow considerably at low Reynolds numbers.

The present analysis differs from that of the buoyant plume in three respects. Firstly the steady flow differs considerably from that of the buoyant plume as previously discussed. Secondly, the presence of the flame alters the matching conditions to be applied within the flow and thirdly, the very large effect of density variation must be accounted for. Chapter 3 is therefore devoted to

obtaining the pertinent governing equations starting from the disturbance equations for compressible fluid flow derived by Lees and Lin, reference (1.16), 1946, and to developing the appropriate boundary and matching conditions and presenting the numerical methods to be employed. As a check on the results, two different numerical algorithms are used, these being a shooting method developed by Hieber and Gebhart, reference (1.17), 1971, and a difference method due to Keller and Cebeci, given in Cebeci and Bradshaw, reference (1.18), 1977.

In Chapter 4, the results from the stability analysis are presented for several of the steady solutions obtained in Chapter 2. Unlike the buoyant plume, the flame eventually becomes unstable to disturbances of all frequencies as the Reynolds number, or height above the start of the flame, is increased, however the most amplified frequencies are around 5-10 Hz. The necessity of considering large density variations in the case of the flame, is exhibited by the large increase in stability of the flow as the flame temperature is increased. The most notable feature of the stability diagrams, however, is the existence of an instability for waves with negative phase velocity, wave crests moving downwards, but with positive group velocity. Although in the parallel flow analysis, these disturbances seem to be very important in the stability of flames, they have very long wavelengths, so an analysis including non-parallel effects might considerably change this region of the stability diagram.

As a check on the numerical algorithms, and to determine whether this negative phase velocity region exists for the buoyant plume, this flow is subjected to a parallel-flow stability analysis in Chapter 5. Comparison with the results of Gebhart and Pera, reference (1.11), 1971, gives good agreement for the neutral stability curve over the range of Reynolds numbers they considered. Extending their calculations to include several constant amplification rate curves and lower Reynolds numbers showed that a negative phase velocity region, positive group velocity region also exists for the buoyant plume. It should be noted that

non-parallel effects included in the analysis of Haaland and Sparrow, reference (1.12), 1973, and Hieber and Nash, reference (1.13), 1975, alter the stability diagram considerably at low Reynolds number. They did not consider negative phase velocity waves however, so it is not known how this region will be affected, except that an even greater change is expected since the parallel-flow assumption is very poor for these long wavelength disturbances. Removal of the Boussinesq approximation led to considerably improved agreement with experimental results obtained by Pera and Gebhart, reference (1.11), 1971, but did not have as dramatic effect as it did for the flame.

Finally in Chapter 6, the effect of the flow properties changing with Reynolds number is examined by assuming disturbances of wavelength long compared to the thickness of the flame and associated convecting fluid. It is found that the instability arises primarily due to centrifugal forces generated by the momentum flux in the flame flowing along a curved path, balanced by the force necessary to overcome the inertia of the surrounding fluid. Limited comparison with the results of Chapter 4 gave good agreement for disturbance amplification rates.

References.

(1.1) S. I PAI, On the Stability of Two-Dimensional Laminar Jet Flow of Gas, *J. Aero. Sci.* **18**, 731, (1951)

(1.2) N. CURLE, On Hydrodynamic Stability in Unlimited Fields of Viscous Flow, *Proc. Roy. Soc. Series A* **238** 489, (1956)

(1.3) T. TATSUMI and T. KAKUTANI, The Stability of a Two-Dimensional Laminar Jet, *JFM* **4** 261, (1958)

(1.4) R. E. KAPLAN, The Stability of Laminar Incompressible Boundary Layers in the Presense of Compliant Boundaries, *MIT Report ASRL TR116-1* Chapter 8, (1964)

(1.5) S. E. HAALAND, Contributions to Linear Stability Theory of Nearly Parallel Flows, *PhD thesis, Fluid Mechanics Program, University of Minnesota, Minneapolis, Minn.*, (1972)

(1.6) A. K. BAJAJ and V. K. GARG, Linear Stability of Jet Flows, *J. App. Mech.* **44** 378, (1977)

(1.7) V. K. GARG, Spatial Stability of the Non-Parallel Bickley Jet, *JFM* **102** 127, (1981)

(1.8) T. FUJII, Theory of Steady Laminar Natural Convection above a Horizontal Line Heat Source and a Point Heat Source, *Int. J. Heat Mass Trans.* **6**, 597, (1963)

(1.9) B. GEBHART, L. PERA and A. W. SCHORR, Steady Laminar Natural Convection Plumes above a Horizontal Line Heat Source, *Int. J. Heat Mass Trans.* **13**, 161, (1970)

(1.10) T. FUJII, I. MORIOKA and H. UEHARA, Buoyant Plume above a Horizontal Line Heat Source, *Int. J. Heat Mass Trans.* **16**, 755, (1973)

(1.11) L. PERA and B. GEBHART, On the Stability of Laminar Plumes: Some Numerical Solutions and Experiments, *Int. J. Heat Mass Trans.* **14**, 975, (1971)

(1.12) S. E. HAALAND and E. M. SPARROW, Stability of Buoyant Boundary Layers and Plumes, Taking Account of Nonparallelism of the Basic Flows, *J. Heat Trans.* **95c** 295, (1973)

(1.13) C. A. HIEBER and E. J. NASH, Natural Convection above a Line Heat Source: Higher-Order Effects and Stability, *Int. J. Heat Mass Trans.* **18** 1473, (1975)

(1.14) E. E. ZUKOSKI and F. E. MARBLE, The Role of Wake Transition in the Process of Flame Stabilization on Bluff Bodies, *Combustion Researches and Reviews 1955*, AGARD, Butterworths Scientific Publications, London, p. 167, (1955)

(1.15) P. L. BLACKSHEAR, Growth of Disturbances in a Flame -Generated Shear Region, *NACA TN 3830*, (1956)

(1.16) L. LEES and C. C. LIN, Investigation of the Stability of the Laminar Boundary Layer in a Compressible Fluid, *NACA TN 1115*, (1946)

(1.17) C. A. HIEBER and B. GEBHART, Stability of Vertical Natural Convection Boundary Layers: Some Numerical Solutions, *JFM* **48**, 625, (1971)

(1.18) T. CEBECI and P. BRADSHAW, Momentum Transfer in Boundary Layers, *McGraw-Hill* , Chapter 9, (1977)

Chapter 2.

THE STRUCTURE OF BUOYANT DIFFUSION FLAMES

In this chapter it is shown that a self-similar solution may be obtained for the free convective plume generated by a vertical diffusion flame. The Boussinesq approximation, which was used by Pohlhausen, reference (2.1), 1930, for the free convection boundary layer on a vertical hot plate, is too restrictive when considering the large temperature differences associated with combustion processes and has been replaced by the Howarth Transformation for variable density flows, reference (2.2), 1948. This transformation was also employed by Kosdon, Williams and Buman, reference (2.3), 1969, and later by Kim, De Ris and Kroesser, reference (2.4), 1971, in their investigations of the laminar free convective burning of fuel surfaces and gave good agreement with experimental measurements of burning-rates for several fuels.

This work was extended to include the overfire region by Pagni and Shih, reference (2.5), 1977, using an integral technique, and by Ahmad and Faeth, reference (2.6), 1978, and Groff and Faeth, reference (2.7), 1978, using a numerical procedure. Shih and Pagni, reference (2.8), 1978, and Kinoshita and Shih, reference (2.9), 1980, examined forced, free and mixed-mode diffusion flames adjacent to vertical fuel surfaces and above free standing fuel slabs, and found that the limit of free convective burning gave a good description of the flow if the Froude number was less than one. The self-similar solution of Kosdon, Williams and Buman was also incorporated by Fernández-Pello and Williams, reference (2.10), 1977, and Fernández-Pello, reference (2.11), 1978, in their treatments of flame spread over vertical and inclined fuel surfaces.

Consider the buoyant diffusion flame, shown in figure (2.1), for which no motion of either reactant is present upstream of the point at which the flame originates. The fuel at $y^* = \infty$ may have a different density from that of the

oxidizer at $y^* = -\infty$, thus only one of the reactants need be quiescent at large $|y|$, while the other may rise due to the effects of buoyancy. Although the work covered here is restricted by the assumption of unit Lewis number, wide ranges in the stoichiometry of the chemical reaction and in the density ratio of the fuel to oxidizer at infinity have been considered.

2.1. The Governing Equations

The governing boundary layer equations for a steady laminar diffusion flame are reference (2.12), 1965.

Continuity:

$$\frac{\partial(\rho^* u^*)}{\partial x^*} + \frac{\partial(\rho^* v^*)}{\partial y^*} = 0 \tag{2.1}$$

where the superscript * denotes a dimensional variable.

Vertical Momentum:

$$\rho^* u^* \left[\frac{\partial u^*}{\partial x^*}\right] + \rho^* v^* \left[\frac{\partial u^*}{\partial y^*}\right] = \frac{\partial}{\partial y^*}\left[\mu^* \frac{\partial u^*}{\partial y^*}\right] + g^*(\rho_\infty^* - \rho^*) \tag{2.2}$$

Here the pressure gradient is fixed by the external hydrostatic pressure gradient, $-\frac{\partial p^*}{\partial x^*} = \rho_\infty^* g^*$, since $p^* = p^*(x^*)$ under the boundary layer assumption.

Energy:

$$\rho^* u^* \left[\frac{\partial h^*}{\partial x^*}\right] + \rho^* v^* \left[\frac{\partial h^*}{\partial y^*}\right] = \frac{\partial}{\partial y^*}\left[\left[\frac{\lambda^*}{c_p^*}\right]\frac{\partial h^*}{\partial y^*}\right] + \dot{q}^* \tag{2.3}$$

where the specific enthalpy

$$h^* = \int_{T_\infty^*}^{T^*} c_p^* dT^* \tag{2.4}$$

and the volumetric heat release rate is $\dot{q}^*$.

Species:

$$\rho^* u^* \left[\frac{\partial Y_i}{\partial x^*}\right] + \rho^* v^* \left[\frac{\partial Y_i}{\partial y^*}\right] = \frac{\partial}{\partial y^*}\left[\rho^* D_i^* \frac{\partial Y_i}{\partial y^*}\right] + \dot{m}_i^* \tag{2.5}$$

where the mass fraction, diffusivity and volumetric mass-production of species i are respectively Y_i, D_i^* and m_i^*.

State:

$$\rho^* T^* \left[\sum_i Y_i R_i^*\right] = \rho_\infty^* R_\infty^* T_\infty^* \tag{2.6}$$

where the gas constant for species i is given by

$$R_i^* = \frac{R_0^*}{M_i^*} \tag{2.7}$$

R_0^* is the universal gas constant and M_i^* the molecular weight of species i, and the subscript ∞ refers to the ambient conditions at $y^* = -\infty$ (i.e. in the oxidizer).

Chemistry:

$$F + \varphi_o O \rightarrow \varphi_p P + Q^* \tag{2.8}$$

where F, O, and P are one mole of Fuel, Oxidizer and Product, Q^* is the heat produced by one mole of fuel and φ_o and φ_p are the amounts of oxidizer consumed and product generated by the reaction of one mole of fuel.

These equations have incorporated the following physical approximations; the gases are all ideal, velocities are much less than the speed of sound, $x^* << \frac{R^* T_\infty^*}{g^*}$ so that the variation in ρ_∞^* implied by hydrostatic equilibrium can be neglected leaving ρ_∞^* independent of position, no species diffusion driven by pressure and temperature gradients, constant specific heat, no radiation and a single global chemical reaction.

This last assumption is valid for reactions with fast chemical kinetics in which case the reaction takes place inside a sheet much thinner than the boundary layer thickness. This flame sheet will be taken to have negligible thickness, both oxidizer and reactant being totally consumed on the plane at $y^* = 0$. Applying this approximation along with the Howarth Transformation

$$\left.\begin{aligned} \tilde{x}^* &= x^* \\ \tilde{y}^* &= \int_0^{y^*} \left[\frac{\rho^*}{\rho_\infty^*}\right] dy^* \end{aligned}\right\} \tag{2.9}$$

and defining

$$\left.\begin{aligned} \tilde{u}^* &= u^* \\ \tilde{v}^* &= \left[\frac{\rho^*}{\rho_\infty^*}\right] v^* + u^* \int_0^{y^*} \frac{\partial}{\partial x^*}\left[\frac{\rho^*}{\rho_\infty^*}\right] dy^* \end{aligned}\right\} \tag{2.10}$$

with the additional assumptions that $\rho^* \lambda^* = \rho_\infty^* \lambda_\infty^*$, $\rho^* \mu^* = \rho_\infty^* \mu_\infty^*$, $\rho^{*2} D_i^* = \rho_\infty^{*2} D_{i\infty}^*$ and that c_p^* is constant, (2.1) and (2.2) reduce to

$$\frac{\partial \tilde{u}^*}{\partial \tilde{x}^*} + \frac{\partial \tilde{v}^*}{\partial \tilde{y}^*} \tag{2.11}$$

$$\tilde{u}^* \frac{\partial \tilde{u}^*}{\partial \tilde{x}^*} + \tilde{v}^* \frac{\partial \tilde{u}^*}{\partial \tilde{y}^*} = \left(\frac{\rho_\infty^*}{\rho^*} - 1 \right) g^* + \nu_\infty^* \frac{\partial^2 \tilde{u}^*}{\partial \tilde{y}^{*2}} \tag{2.12}$$

$$\tilde{u}^* \frac{\partial T^*}{\partial \tilde{x}^*} + \tilde{v}^* \frac{\partial T^*}{\partial \tilde{y}^*} = \frac{\lambda_\infty^*}{\rho_\infty^* c_p^*} \frac{\partial^2 T^*}{\partial \tilde{y}^{*2}} \qquad \tilde{y}^* \neq 0 \tag{2.13}$$

$$\tilde{u}^* \frac{\partial Y_F}{\partial \tilde{x}^*} + \tilde{v}^* \frac{\partial Y_F}{\partial \tilde{y}^*} = D_{F\infty}^* \frac{\partial^2 Y_F}{\partial \tilde{y}^{*2}} \qquad \tilde{y}^* > 0 \tag{2.14}$$

$$\tilde{u}^* \frac{\partial Y_O}{\partial \tilde{x}^*} + \tilde{v}^* \frac{\partial Y_O}{\partial \tilde{y}^*} = D_{O\infty}^* \frac{\partial^2 Y_O}{\partial \tilde{y}^{*2}} \qquad \tilde{y}^* < 0 \tag{2.15}$$

The assumption that the molecular weights of oxidizer and products are the same combined with the equation of state (2.6) reduces the buoyancy term in equation (2.12) to

$$\left.\begin{aligned} \left(\frac{\rho_\infty^*}{\rho^*} - 1 \right) g^* &= \left(\frac{T^*}{T_\infty^*} - 1 \right) g^* \left[\left(\frac{M_O^*}{M_F^*} - 1 \right) Y_F + 1 \right] + g^* \left(\frac{M_O^*}{M_F^*} - 1 \right) Y_F \qquad \tilde{y}^* \geq 0 \\ \left(\frac{\rho_\infty^*}{\rho^*} - 1 \right) g^* &= \left(\frac{T^*}{T_\infty^*} - 1 \right) g^* \qquad \tilde{y}^* \leq 0 \end{aligned}\right\} \tag{2.16}$$

To obtain the boundary and matching conditions at $\tilde{y}^* = 0$, equations (2.3) and (2.5) must be examined. The flame sheet approximation is equivalent to assuming that the mass and heat production terms in these equations are delta

functions situated at $\tilde{y}^* = 0$. If the mass consumption of fuel is given by $\dot{m}_F^* = -\dot{m}^*(x^*)\,\delta(y^*)$, then equation (2.8) gives

$$\left.\begin{aligned} \dot{m}_O^* &= -\varphi_O \dot{m}^*(x^*)\,\delta(y^*) \\ \dot{q}^* &= Q^*\,\dot{m}^*(x^*)\,\delta(y^*) \end{aligned}\right\} \qquad (2.17)$$

Integrating equations (2.3) and (2.5) then gives

$$\varphi_O \rho^* D_F^* \left[\frac{\partial Y_F}{\partial y^*}\right] = -\rho^* D_O^* \left[\frac{\partial Y_O}{\partial y^*}\right] \qquad (2.18)$$

and assuming c_p^* is const

$$\lambda^* \left[\frac{\partial T^*}{\partial y^*}\right] = -Q^* \rho^* D_F^* \left[\frac{\partial Y_F}{\partial y^*}\right] \qquad (2.19)$$

where the square brackets indicate jumps in the quantities inside from $y^* = 0^+$ to $y^* = 0^-$. Using $Y_F = 0$ for $y^* < 0$ and $Y_O = 0$ for $y^* > 0$ and the conditions for application of the Howarth Transformation, these equations reduce to

$$\varphi_O D_{F\infty}^* \frac{\partial Y_F}{\partial \tilde{y}^*} = -D_{O\infty}^* \frac{\partial Y_O}{\partial \tilde{y}^*} \qquad \tilde{y}^* = 0 \qquad (2.20)$$

and

$$\frac{\partial T^*}{\partial \tilde{y}^*}(\tilde{x}^*,0^+) - \frac{\partial T^*}{\partial \tilde{y}^*}(\tilde{x}^*,0^-) = -\frac{Q^*}{c_p^*}\left[\frac{\rho^* c_p^* D_{F\infty}^*}{\lambda_\infty^*}\right]\frac{\partial Y_F}{\partial \tilde{y}^*}(\tilde{x}^*,0) \qquad (2.21)$$

These two conditions along with continuity of T^*, u^*, v^* and $\mu^* \dfrac{\partial u^*}{\partial y^*}$ make up the

matching conditions at $\tilde{y}^* = 0$.

The governing equations (2.11) - (2.15), with the addition of (2.16), the matching conditions at $\tilde{y}^* = 0$ and boundary conditions at infinity, can now be solved by a similarity transformation. Introducing the streamfuction ψ^* such that

$$\tilde{u}^* = \frac{\partial \psi^*}{\partial \tilde{y}^*}, \quad \tilde{v}^* = -\frac{\partial \psi^*}{\partial \tilde{x}^*} \tag{2.22}$$

where

$$\left.\begin{aligned} \psi^* &= 4\nu_\infty^* \left[\frac{\left[\left(\frac{T_f^*}{T_{O\infty}^*} - 1 \right) g^* \tilde{x}^{*3} \right]^{\frac{1}{4}}}{4\nu_\infty^{*2}} \right] \xi(\eta) \\ \eta &= \left[\frac{\left[\left(\frac{T_f^*}{T_{O\infty}^*} - 1 \right) g^* \right]^{\frac{1}{4}}}{4\nu_\infty^{*2} \tilde{x}^*} \right] \tilde{y}^* \end{aligned}\right\} \tag{2.23}$$

where T_f^* is the constant temperature at the flame. The dimensionless temperature and normalised mass fractions are

$$\left.\begin{aligned} \vartheta &= \frac{T^* - T_{O\infty}^*}{T_f^* - T_{O\infty}^*} \\ \kappa_F &= \frac{Y_F}{Y_{F_\infty}} \\ \kappa_O &= \frac{Y_O}{Y_{O_\infty}} \end{aligned}\right\} \tag{2.24}$$

By substituting for T^*, Y_F and y^* in equation (2.19), $\left[\frac{T_f^*}{T_{O\infty}^*} - 1\right]$ is found to be constant. The governing equations now become

$$\left.\begin{aligned} &\xi''' + 3\xi\xi'' - 2(\xi')^2 + \vartheta = 0 \qquad \eta < 0 \\ &\xi''' + 3\xi\xi'' - 2(\xi')^2 + \left[\left[\frac{M_O^*}{M_F^*} - 1\right] Y_{F_\infty} \kappa_F + 1\right] \vartheta \\ &\quad + \frac{\left[\frac{M_O^*}{M_F^*} - 1\right] Y_{F_\infty}}{\left[\frac{T_f^*}{T_{O\infty}^*} - 1\right]} \kappa_F = 0 \qquad \eta > 0 \end{aligned}\right\} \tag{2.25}$$

$$\vartheta'' + 3Pr\,\xi\vartheta' = 0 \qquad \eta \neq 0 \tag{2.26}$$

$$\left.\begin{aligned} &\kappa_F''' + 3Sc_O\xi\kappa_F' = 0 \qquad \eta > 0 \\ &\kappa_O''' + 3Sc_F\xi\kappa_O' = 0 \qquad \eta < 0 \end{aligned}\right\} \tag{2.27}$$

where the prime denotes differentiation by η. From equations (2.22) - (2.23) the transformed velocities are found to be

$$\left.\tilde{u}^* = 4\left[\frac{\left[\frac{T_f^*}{T_{O\infty}^*} - 1\right] g^* \tilde{x}^*}{4}\right]^{\frac{1}{2}} \xi'\right.$$

$$\left.\begin{aligned} \tilde{v}^{*} &= -4\nu_{\infty}^{*}\left[\frac{\left(\frac{T_f^{*}}{T_{O\infty}^{*}}-1\right)g^{*}}{4\nu_{\infty}^{*2}\tilde{x}^{*}}\right]^{\frac{1}{4}}\left(\frac{3}{4}\xi-\frac{1}{4}\eta\,\xi'\right) \\ \vartheta &\to 0 \\ \xi' &\to 0 \\ \kappa_{\vartheta} &\to 1 \end{aligned}\right\} \quad \text{as } \eta \to -\infty \qquad (2.28),\ (2.29)$$

The boundary conditions at infinity are

$$\left.\begin{aligned} \vartheta &\to \vartheta_{F_\infty} = \frac{\left(\frac{T_{F\infty}^{*}}{T_{O\infty}^{*}}-1\right)}{\left(\frac{T_f^{*}}{T_{O\infty}^{*}}-1\right)} \\ \xi' &\to \left\{\frac{\left[\left(\frac{M_O^{*}}{M_F^{*}}-1\right)Y_{F_\infty}+1\right]\left(\frac{T_{F\infty}^{*}}{T_{O\infty}^{*}}-1\right)+\left(\frac{M_O^{*}}{M_F^{*}}-1\right)Y_{F_\infty}}{2\left(\frac{T_f^{*}}{T_{O\infty}^{*}}-1\right)}\right\}^{\frac{1}{2}} \\ &= \left\{\frac{\frac{\rho_{O\infty}^{*}}{\rho_{F\infty}^{*}}-1}{2\left(\frac{T_f^{*}}{T_{O\infty}^{*}}-1\right)}\right\}^{\frac{1}{2}} \end{aligned}\right\} \quad \text{as } \eta \to \infty \qquad (2.30)$$

$$\kappa_F \to 1 \Big]$$

The matching and jump conditions at $\eta = 0$ are

$$\left.\begin{aligned} &\kappa_F = \kappa_O = 0 \\ &\vartheta(0^+) = \vartheta(0^-) = 1 \\ &\xi, \xi', \xi'' \ \textit{continuous} \\ &\kappa_F' = -\frac{D_{O\infty}^* Y_{O_\infty}}{\varphi_O D_{F\infty}^* Y_{F_\infty}} \kappa_O' \end{aligned}\right\} \textit{at } \eta = 0 \qquad (2.31)$$

The remaining matching condition gives $\left[\frac{T_f^*}{T_{O\infty}^*} - 1\right]$ in terms of $\vartheta(0^+)$, $\vartheta(0^-)$, $\kappa_F'(0)$ and the parameter $\frac{Q^* Y_{F_\infty}}{c_p^* T_{O\infty}^*} Le_F$

$$\tilde{T}_f \equiv \left[\frac{T_f^*}{T_{O\infty}^*} - 1\right] = -\frac{Q^* Y_{F_\infty}}{c_p^* T_{O\infty}^*} Le_F \frac{\kappa_F'(0)}{(\vartheta(0^+) - \vartheta(0^-))} \qquad (2.32)$$

where $Le_F = \frac{\rho^* c_p^* D_{F\infty}^*}{\lambda_\infty}$. The solution is dependent on seven parameters. The effective stoichiometric ratio (i.e the effective ratio of fuel/oxidizer consumed at the flame):

$$\tilde{\varphi} \equiv \frac{D_{O\infty}^* Y_{O_\infty}}{\varphi_O D_{F\infty}^* Y_{F_\infty}} \qquad (2.33)$$

The effective heating value of the fuel:

$$\tilde{Q} \equiv \frac{Q^* Y_{F_\infty}}{c_p^* T_{O\infty}^*} Le_F \tag{2.34}$$

The ratio of molecular weights:

$$\tilde{M} \equiv \left[\frac{M_O^*}{M_F^*} - 1\right] Y_{F_\infty} \tag{2.35}$$

The temperature ratio of fuel and oxidizer at infinity:

$$\tilde{T}_\infty \equiv \left[\frac{T_{F\infty}^*}{T_{O\infty}^*} - 1\right] \tag{2.36}$$

as well as the Prandtl number and Schmidt numbers of fuel and oxidizer. The density ratio of fuel to oxidizer at infinity can be expressed in terms of $\tilde{M}$ and $\tilde{T}_\infty$ as

$$\left[\frac{\rho_{O\infty}^*}{\rho_{F\infty}^*} - 1\right] = (\tilde{M}+1)\tilde{T}_\infty + \tilde{M} \tag{2.37}$$

The equations could now be solved for any choice of these seven parameters. The rest of the chapter will deal with the special case when the Lewis number of fuel and oxidizer are unity. This allows the useful simplification

$$\kappa_F = (1-\vartheta)\frac{T_f^* - T_{O\infty}^*}{T_f^* - T_{F\infty}^*} = \frac{(1-\vartheta)\tilde{T}_f}{(\tilde{T}_f - \tilde{T}_\infty)} \qquad \eta < 0$$

$$\left.\begin{aligned} \kappa_O &= (1-\vartheta) \qquad \eta > 0 \end{aligned}\right\} \tag{2.38}$$

then equations (2.31), (2.32), (2.33) and (2.38) give

$$\tilde{T}_f = \left[\frac{T_f^*}{T_{O\infty}^*} - 1\right] = \frac{\tilde{\varphi}\left[\tilde{Q} + \tilde{T}_\infty\right]}{1+\tilde{\varphi}} \tag{2.39}$$

The final form of the governing equations is

$$\left.\begin{aligned} \xi'''+3\xi\xi''-2(\xi')^2 + \vartheta &= 0 \qquad \eta < 0 \\ \xi'''+3\xi\xi''-2(\xi')^2 + (\tilde{M}\kappa_F + 1)\vartheta + \frac{\tilde{M}}{\tilde{T}_f}\kappa_F &= 0 \qquad \eta > 0 \end{aligned}\right\} \tag{2.40}$$

where κ_F is given in terms of ϑ, $\tilde{T}_\infty$, $\tilde{\varphi}$ and $\tilde{Q}$ by equations(2.38) and (2.39).

$$\vartheta' + 3Pr\,\xi\vartheta' = 0 \qquad \eta \neq 0 \tag{2.41}$$

with boundary conditions

$$\xi',\ \vartheta \to 0 \qquad as\ \eta \to -\infty \tag{2.42}$$

$$\left.\begin{aligned} \vartheta &\to \frac{\tilde{T}_\infty}{\tilde{T}_f} \qquad as\ \eta \to \infty \\ \xi' &\to \left[\frac{(\tilde{M}+1)\tilde{T}_\infty + \tilde{M}}{2\tilde{T}_f}\right]^{\frac{1}{2}} \qquad as\ \eta \to \infty \end{aligned}\right\} \tag{2.43}$$

and matching conditions at $\eta = 0$

$$\left.\begin{aligned} \vartheta(0) &= 1 \\ \vartheta(0^+) &= -\vartheta(0^-)\,\frac{\tilde{\varphi}(\tilde{T}_f - \tilde{T}_\infty)}{\tilde{T}_f} \\ \xi,\ \xi',\ \xi'',\ &\textit{continuous} \end{aligned}\right\} \textit{at } \eta = 0 \qquad (2.44)$$

2.2. Numerical Solution

The asymptotic behaviour of ξ and ϑ as $\eta \to -\infty$ is given by

$$\left.\begin{aligned} \xi &\to a_1 + a_2\exp(-3a_1 Pr\,\eta) + a_3\exp(-3a_1\eta) \\ \vartheta &\to -a_2(3a_1 Pr)^3\left[\frac{1}{Pr} - 1\right]\exp(-3a_1 Pr\,\eta) \end{aligned}\right\} \qquad (2.45)$$

where the a_i's are constants to be determined. These expressions are used as the starting point for a shooting method procedure. Values of a_1, a_2 and a_3 are assumed and equations (2.40) and (2.41) integrated from, $\eta = -\eta_e$ to $\eta = \eta_e$where η_e is sufficiently large that equation (2.45) is valid. If the values $b_1 = \vartheta(0)-1$, $b_2 = \xi'(\eta_e)-\xi'(\infty)$ and $b_3 = \vartheta(\eta_e)-\vartheta(\infty)$ are not zero to within a specified tolerance the Jacobian $\frac{\partial b_i}{\partial a_j}$ is approximately determined by taking small deviations about the guessed values of each of the a_i in turn. Newton's method is then used to produce a new guess for the a_i's . This is repeated until the solution converges. Checks are performed to insure the solution is independent of choice of integration end point η_e and mesh size. In general this method required very good guesses for the a_i's, however once one solution has been

found, it is possible to find others by taking small increments in the parameters.

2.3. Results

All the results presented are for $Pr = 0.72$ and $\frac{T^*_{F\infty}}{T^*_{O\infty}} = 1$ (*i.e* $\tilde{T}_\infty = 0$). Figure (2.2) shows the velocity and temperature profiles for a symmetric flame (i.e $\tilde{\varphi} = 1.0$ and $\frac{M^*_O}{M^*_f} = 1.0$). The structure of this problem closely resembles that of free-convection over a vertical heated plate, the latter utilizing the no-slip condition at $y^* = 0$ instead of the zero shear stress condition appropriate to the present problem. A useful check on the numerical computation was obtained by using the no-slip condition and comparing with the results of Ostrach, reference (2.13), 1952, since, although Ostrach used the Boussinesq approximation, the ordinary differential equations obtained in his analysis are identical to the present set of equations except for the lack of a species conservation equation. Removal of the no-slip condition leads to higher peak vertical velocities and higher entrainment velocities. As a consequence, the flame has a somewhat smaller boundary layer thickness than the wall flow, since the increased entrainment aids the flow of reactants to the flame and retards the diffusion of heat away from it.

Three examples of non-unit stoichiometric ratio are shown in figures (2.3) - (2.6). The effective fuel/oxidizer mass consumption ratios are $\tilde{\varphi} = 0.232$, $\tilde{\varphi} = 0.058$ and $\tilde{\varphi} = 0.029$, the last two corresponding to the stoichiometric ratios of methane and hydrogen burning in air. The flames now exhibit a large horizontal flow through the flame in the direction of the fuel. This flow carries hot combustion products to the fuel side of the flame causing the maximum vertical velocity to be displaced into the fuel. It also dilutes the fuel near the flame, decreasing the concentration gradients and thus decreasing the diffusion velocity of the fuel while doing the reverse in the oxidizer. Fuel and oxidizer are thereby supplied to the flame in the stoichiometric ratio. As a consequence, the

thermal and species boundary layers are considerably increased in the fuel and decreased in the oxidizer. In figure (2.5), the Howarth Transformation has been inverted for the case of $\tilde{\varphi} = 0.058$ with $\left(\frac{T_f^*}{T_{O\infty}^*} - 1\right) = 6$. Note the large horizontal velocity through the flame and the increased asymmetry of the flame.

In figures (2.7) and (2.8), some parameters of interest have been plotted against $\tilde{\varphi}$. These parameters are:

The maximum vertical velocity

$$U_{\max} \equiv \frac{u_{\max}^*}{4}\left(\frac{\tilde{Q}\, g^* x^*}{4}\right)^{\frac{-1}{2}} \tag{2.46}$$

Note that the velocity has been normalised using $\tilde{Q}$, the effective heating value of the fuel, rather than $\left(\frac{T_f^*}{T_{O\infty}^*} - 1\right)$, since $\tilde{Q}$ is more nearly constant for real fuels as the stoichiometric ratio is changed, thus giving a better physical representation of how the peak velocity varies. The relation between $\tilde{Q}$, $\tilde{\varphi}$, and $\left(\frac{T_f^*}{T_{O\infty}^*} - 1\right)$ is given by equation (2.39). $\tilde{Q}$ will also be used in all the following normalisations.

The mass entrainment of oxidizer

$$\dot{m}_e \equiv \frac{v_{O\infty}^*}{4\nu_\infty^*}\left(\frac{\tilde{Q}\, g^*}{4\nu_\infty^{*2} x^*}\right)^{\frac{-1}{4}} \tag{2.47}$$

the mass flux of fluid through the flame

$$\dot{m}_f \equiv \frac{\rho_f^* v_f^*}{4\rho_{O\infty}^* \nu_\infty^*}\left(\frac{\tilde{Q}\, g^*}{4\nu_\infty^{*2} x^*}\right)^{\frac{-1}{4}} \tag{2.48}$$

the fuel consumption rate

$$\dot{m}_F \equiv \frac{\rho_f^* D_F^* \frac{\partial Y_F}{\partial y^*}(x,0)}{\rho_{F_\infty}^* D_{F_\infty}^* \left[\frac{\tilde{Q}\, g^*}{4\nu_\infty^{*2} x^*}\right]^{\frac{1}{4}} Y_{F_-}} \tag{2.49}$$

the buoyancy

$$\beta \equiv \frac{\int_{-\infty}^{0} (\rho_{O_\infty}^* - \rho^*) g^* dy^*}{\rho_{O_\infty}^* g^* \left[\frac{\tilde{Q}^3}{g^*} 4\nu_\infty^{*2} x^*\right]^{\frac{1}{4}}} + \frac{\int_{0}^{\infty} (\rho_{F_\infty}^* - \rho^*) g^* dy^*}{\rho_{O_\infty}^* g^* \left[\frac{\tilde{Q}^3}{g^*} 4\nu_\infty^{*2} x^*\right]^{\frac{1}{4}}} \tag{2.50}$$

and the enthalpy thickness of the boundary layer on each side of the flame

$$\left.\begin{aligned} \delta_{H_+} &\equiv \frac{1}{2}\left[\frac{\tilde{Q}\, g^*}{4\nu_\infty^{*2} x^*}\right]^{\frac{1}{4}} \int_0^\infty \frac{(T^* - T_{O_\infty}^*)}{(T_f^* - T_{O_\infty}^*)} \frac{u^*}{u_{\max}^*} dy^* \\ \delta_{H_-} &\equiv \frac{1}{2}\left[\frac{\tilde{Q}\, g^*}{4\nu_\infty^{*2} x^*}\right]^{\frac{1}{4}} \int_{-\infty}^0 \frac{(T^* - T_{O_\infty}^*)}{(T_f^* - T_{O_\infty}^*)} \frac{u^*}{u_{\max}^*} dy^* \end{aligned}\right\} \tag{2.51}$$

In figure (2.7), $\dot{m}_e$, $U_{\max}$ and $\dot{m}_f$ are plotted against $\tilde{\varphi}$. $U_{\max}$ and $\dot{m}_e$, the oxidizer entrainment, decrease as $\tilde{\varphi} \to 0$ with $\tilde{Q}$ held constant, since the flame temperature is decreasing. On the other hand, the mass flow through the flame, $\dot{m}_f$, increases to a maximum near $\tilde{\varphi} = 0.05$ where it has reached over 60% of the entrained mass. For smaller values of $\tilde{\varphi}$, $\dot{m}_f$ declines since the total mass flux available is decreasing rapidly. This large flow through the flame is again illustrated in figure (2.8) where the ratio of enthalpy thicknesses $\frac{\delta_{H_+}}{\delta_{H_-}}$ has reached

7.63 at $\tilde{\varphi} = 0.058$, showing that most of the hot fluid in the plume is on the fuel side of the flame. Figure (2.8) also shows a decrease in the fuel consumption rate, $\dot{m}_F$, and a decrease in the buoyancy β as $\tilde{\varphi}$ decreases. Although total enthalpy thickness ($\delta_{H_+} + \delta_{H_-}$) has increased, tending to increase the buoyancy due to increased physical size of the plume, the decrease in T_f^* with $\tilde{Q}$ held constant dominates so that the buoyancy decreases. Tables (2.1) and (2.2) give the numerical values of the flow parameters for the cases studied in figures (2.2) and figures (2.4) and (2.5).

Figures (2.9) - (2.13) show the effects of changing the fuel density at infinity for a flame with $\tilde{\varphi} = 1.0$. As the fuel density decreases, it rises in a natural convection flow relative to the oxidizer. This flow has vertical velocities $\sim(height)^{\frac{1}{2}}$ and horizontal velocities $\sim(height)^{\frac{-1}{4}}$ towards the flame. The non-zero vertical velocity, which becomes a boundary condition on the boundary layer flow at $y^* = \infty$, imposes a shear on the basic flow. The maximum vertical velocity, shown in figure (2.12), is thus displaced towards the fuel and increases as $\frac{\rho^*_{F\infty}}{\rho^*_{O\infty}}$ is decreased. The horizontal flow, which would be present even in the absence of a reaction, helps to carry fuel to the flame, increasing the concentration and concentration gradient of the fuel near the flame, thus causing a higher fuel consumption rate, and decreasing the enthalpy thicknesses, shown in figure (2.13). The buoyancy added to the flow by the combustion process decreases as $\frac{\rho^*_{F\infty}}{\rho^*_{O\infty}}$ decreases, since the total thickness of the boundary layer has decreased. Figure (2.12) also shows a small mass flux through the flame and an increase in the mass of oxidizer entrained.

In figures (2.14) and (2.15), the two special cases of methane and hydrogen burning in air are presented. These exhibit the combined effects of non-unit stoichiometric ratio and a fuel - oxidizer density difference at infinity. The

hydrogen/air flame has the most severe asymmetries of any practical combustion reaction. The numerical values for the methane/air flame are given in table (2.3). In table (2.4), numerical values for $\xi(0)$, $\xi'(0)$, $\xi''(0)$ and $\vartheta^{+}(0)$ are presented for all the cases studied.

These solutions are valid in the absence of any mean translational velocity ahead of the point at which the flame is initiated. The importance of an external uniform flow, is measured by the Froude number

$$Fr = \frac{U_{\infty}^{*2}}{g^{*}x^{*}}$$

which is a measure of the relative importance of the buoyant velocity (proportional to $\left[\left(\frac{T_f^{*}}{T_{O_{\infty}}^{*}}-1\right)g^{*}x^{*}\right]^{\frac{1}{2}}$) and external velocity U_{∞}^{*}. If the Froude number is much smaller than one, the present solutions constitute a close approximation; if it is much greater than one, the flow will be described to first order by a shear flow in the absence of gravity.

References.

(2.1) E. POHLHAUSEN, In E. Schmidt and W. Beckmann, Das Temperatur- und Geschwindigkeitsfeld vor einer Wärme abgebenden senkrechter Platte bei natürlicher Konvektion. *Tech. Mech. Thermodyn.* 1,1 (1930)

(2.2) L. HOWARTH, Concerning the Effect of Compressibility on Laminar Boundary Layers and Their Separation, *Proc. Roy. Soc. Series A* **194**, 16, (1948)

(2.3) F. J. KOSDON, F. A. WILLIAMS and C. BUMAN, Combustion of Vertical Cellulosic Cylinders in Air, *Twelth Symposium (International) on Combustion*, p 253, The Combustion Institute (1969)

(2.4) J. S. KIM, J. DE RIS and F. WILLIAM KROESSER, Laminar Free-Convective Burning of Fuel Surfaces, *Thirteenth Symposium (International) on Combustion* , p 949, The Combustion Institute (1971)

(2.5) P. J. PAGNI and T. M SHIH, Excess Pyrolyzate, *Sixteenth Symposium (International) on Combustion* , p. 1329, The Combustion Institute (1977)

(2.6) T. AMHAD and G. M. FAETH, An Investigation of the Laminar Overfire Region Along Upright Surfaces, *J. of Heat Trans.*, **100**, 112, (1978)

(2.7) E. G. GROFF and G. M. FAETH, Laminar Combustion of Vertical Free-Standing Fuel Surfaces, *Comb. and Flame*, **32**, 139, (1978)

(2.8) T. M. SHIH and P. J. PAGNI, Laminar Mixed-Mode, Forced and Free, Diffusion Flames, *J. Heat Trans.*, **100**, 253, (1978)

(2.9) C. M. KINOSHITA and P. J. PAGNI, Laminar Wake Flame Heights, *J. Heat Trans.*, **102**, 104, (1980)

(2.10) A. FERNÁNDEZ-PELLO and F. A. WILLIAMS, A Theory of Laminar Flame Spread Over Flat Surfaces of Solid Combustibles, *Comb. and Flame*, **28**, 251, (1977)

(2.11) A. C. FERNÁNDEZ-PELLO, A Theoretical Model for the Upward Laminar Spread of Flames Over Vertical Fuel Surfaces, *Comb. and Flame*, **31**, 135, (1978)

(2.12) F. A. WILLIAMS, *Combustion Theory*, Addison-Wesley, Chapter 1, (1965)

(2.13) S. OSTRACH, An Analysis of Laminar Free-Convection Flow and Heat Transfer about a Flat Plate Parallel to the Direction of the Generating Body Force, *NACA TN 2635*, (1952)

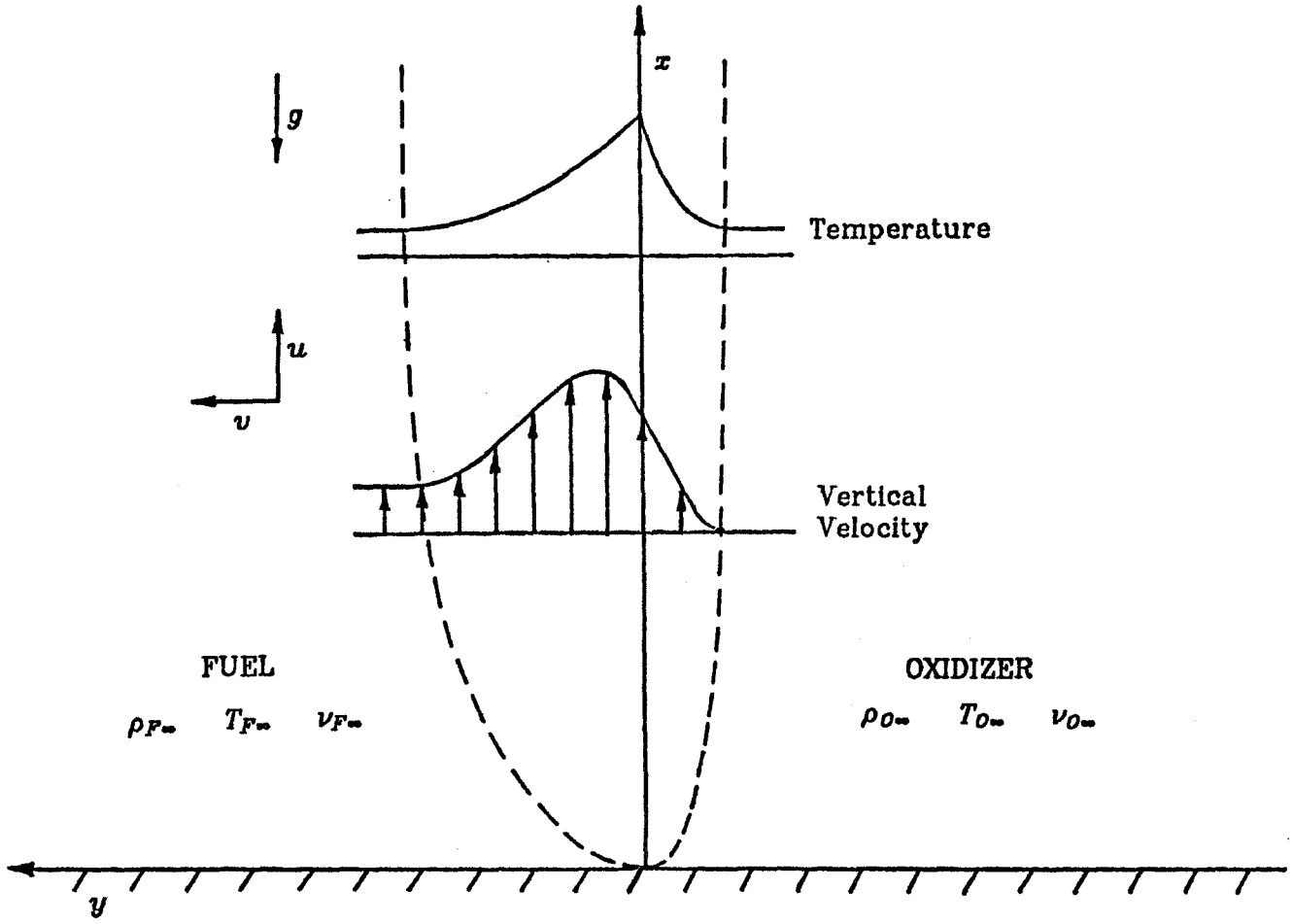

Figure (2.1) Geometry for Buoyant Diffusion Flame

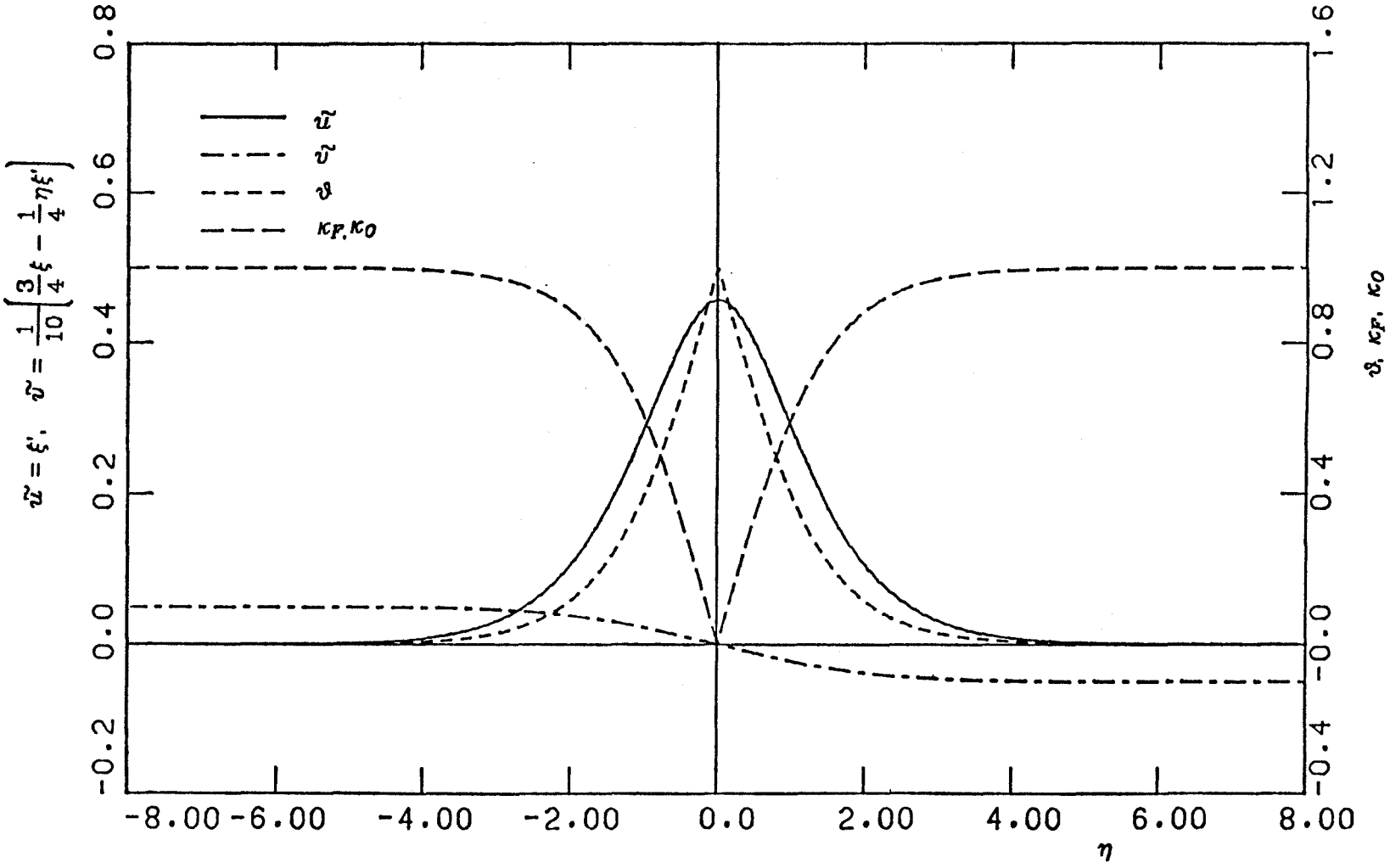

Figure (2.2) Velocity, Temperature and Concentration Profiles for Symmetric Flame

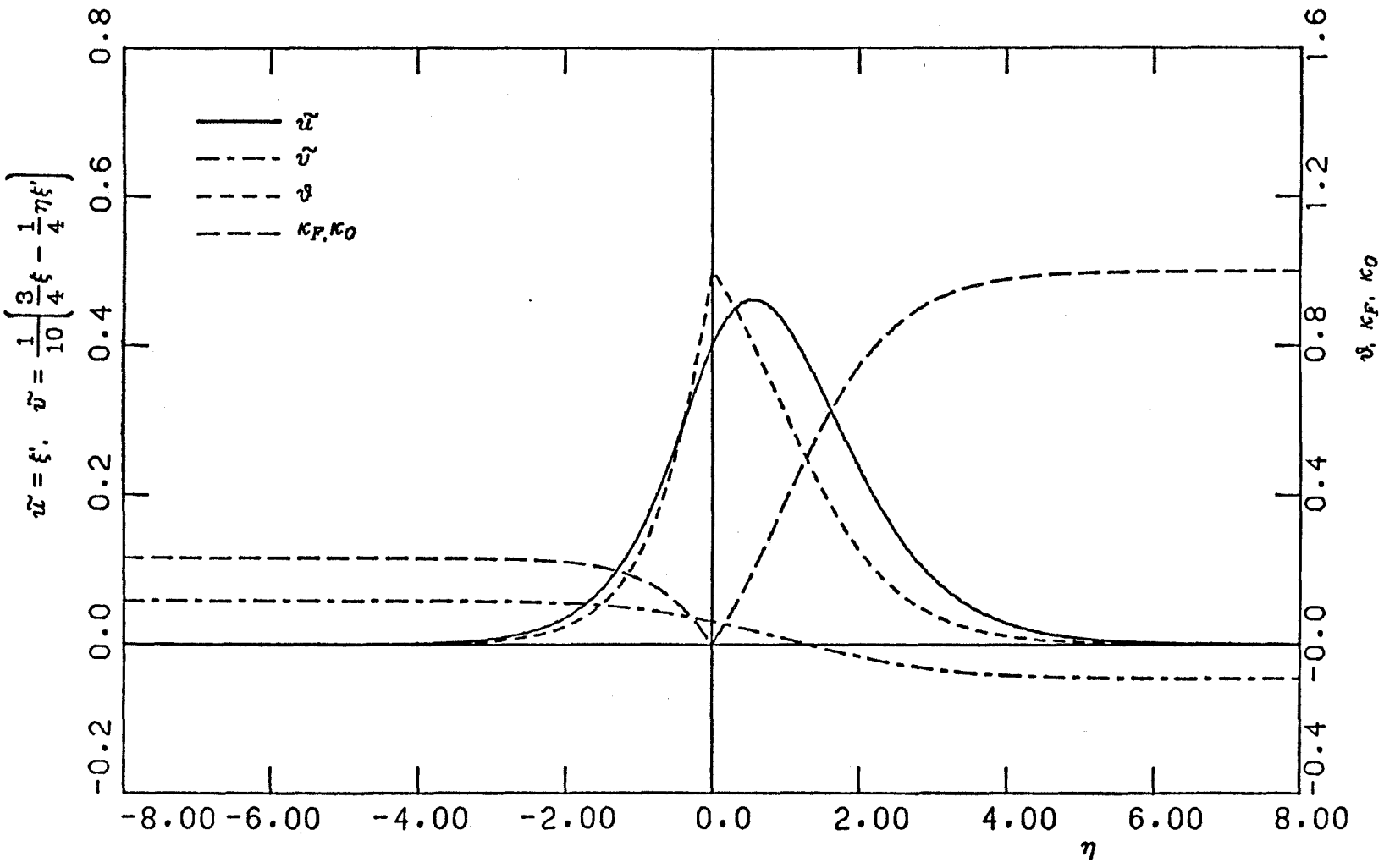

Figure (2.3) Velocity, Temperature and Concentration Profiles for Flame with $\tilde{\varphi} = 0.232$

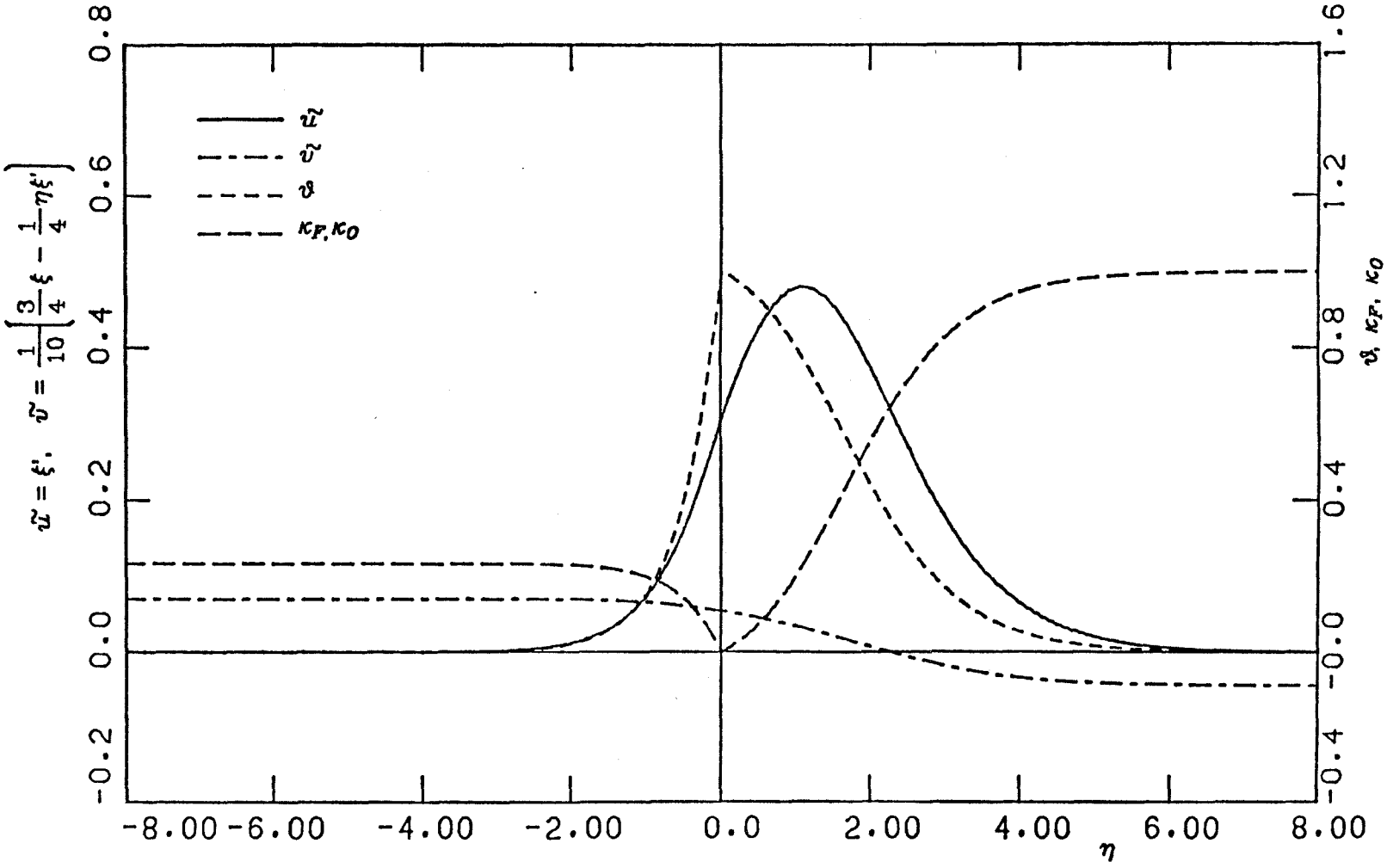

Figure (2.4) Velocity, Temperature and Concentration Profiles for Flame with $\tilde{\varphi} = 0.058$

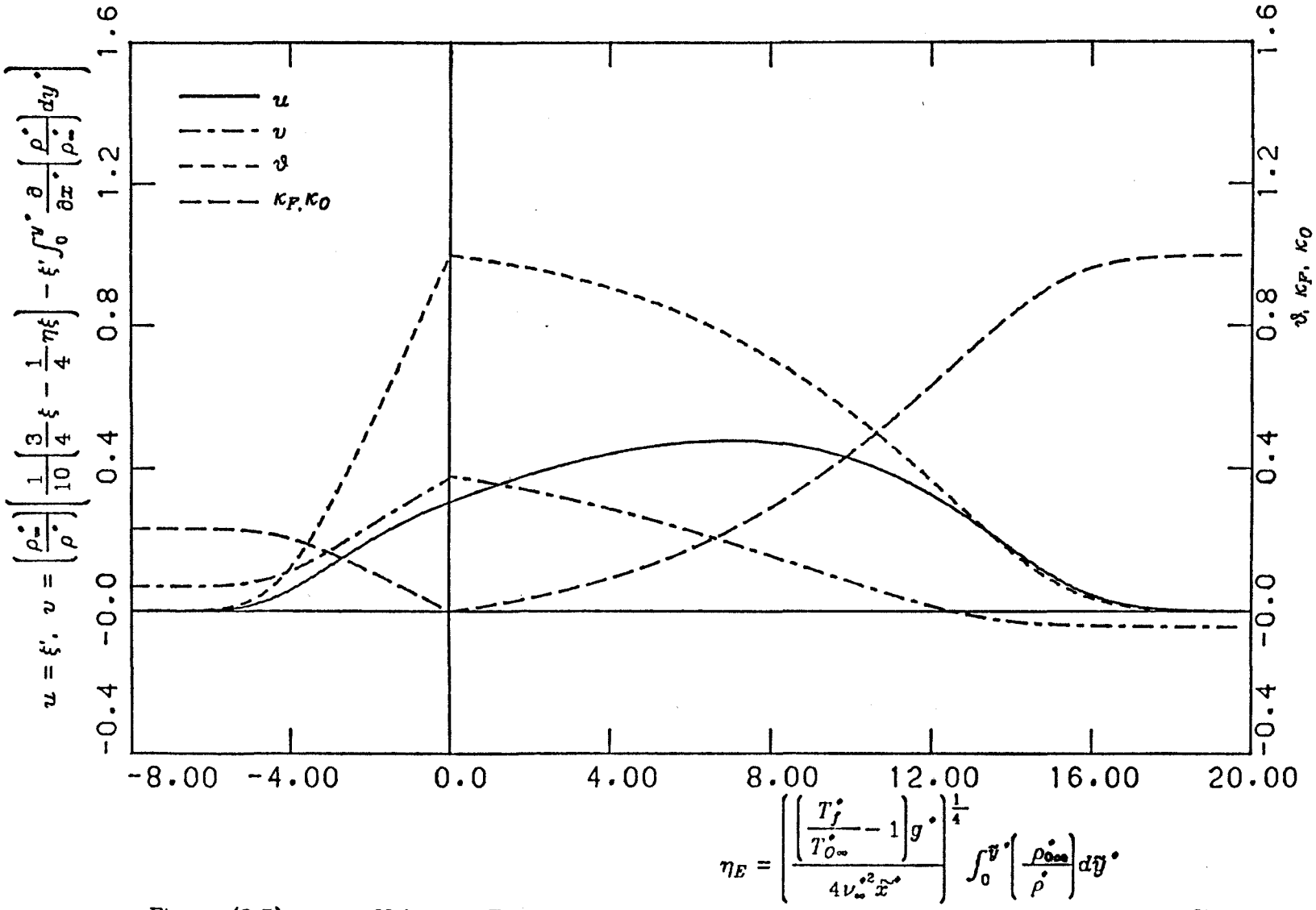

Figure (2.5) Velocity, Temperature and Concentration Profiles for Flame with $\tilde{\varphi} = 0.058$ after Inverting Howarth Transformation

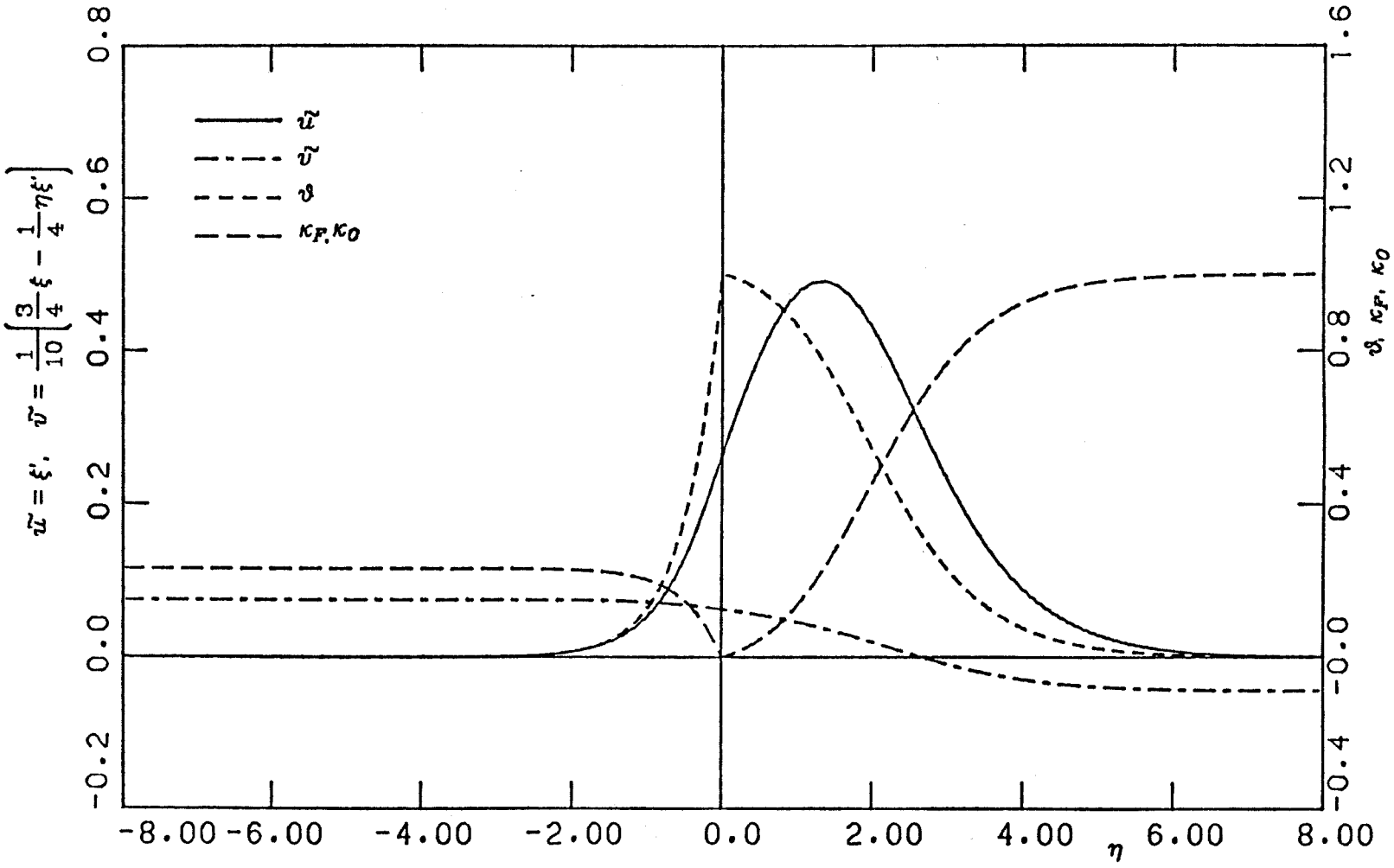

Figure (2.6) Velocity, Temperature and Concentration Profiles for Flame with $\tilde{\varphi} = 0.029$

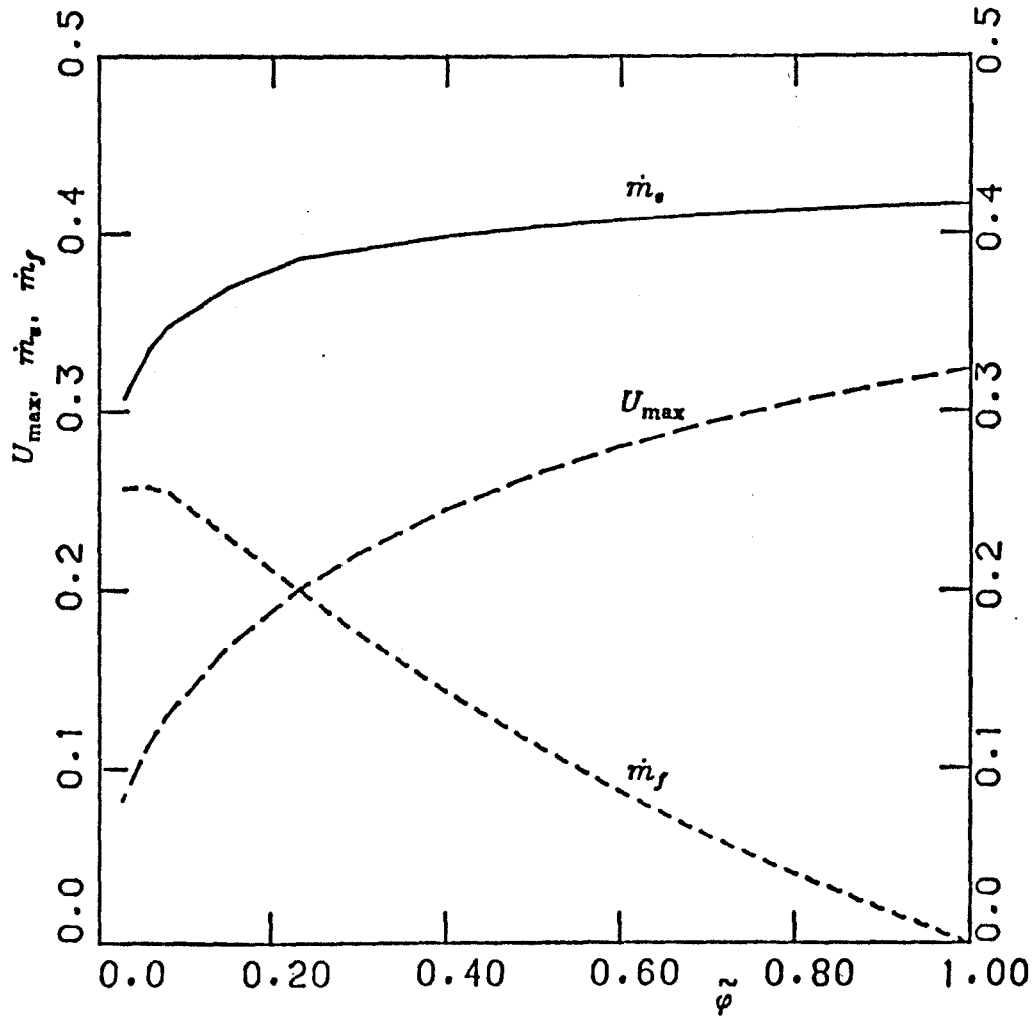

Figure (2.7) Variation of maximum vertical velocity, U_{max}, entrainment of oxidiser, $\dot{m}e$, and mass flux through the flame, $\dot{m}_f$ with stoichiometry.

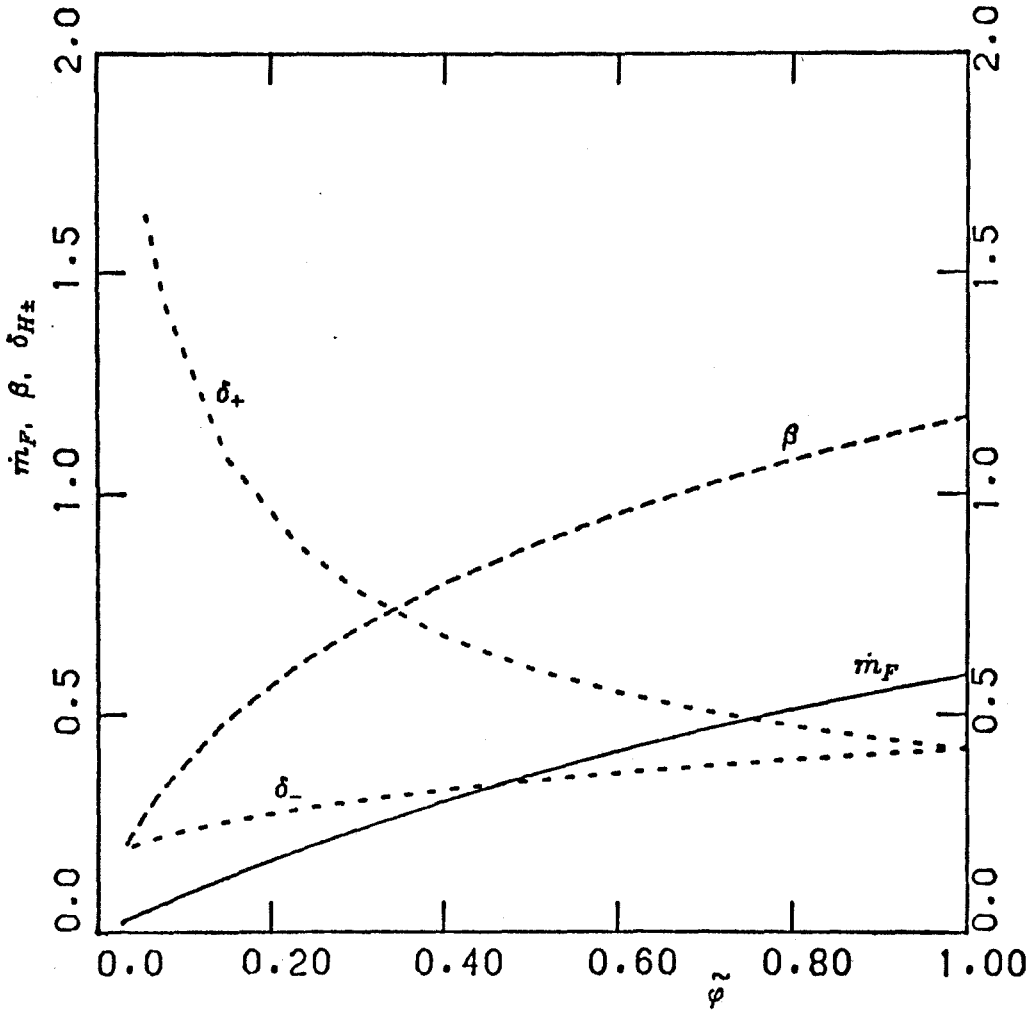

Figure (2.8) Variation of fuel consumption, $\dot{m}_F$, buoyancy, β, and enthalpy thickness on each side of flame, $\delta_{H\pm}$ with stoichiometry

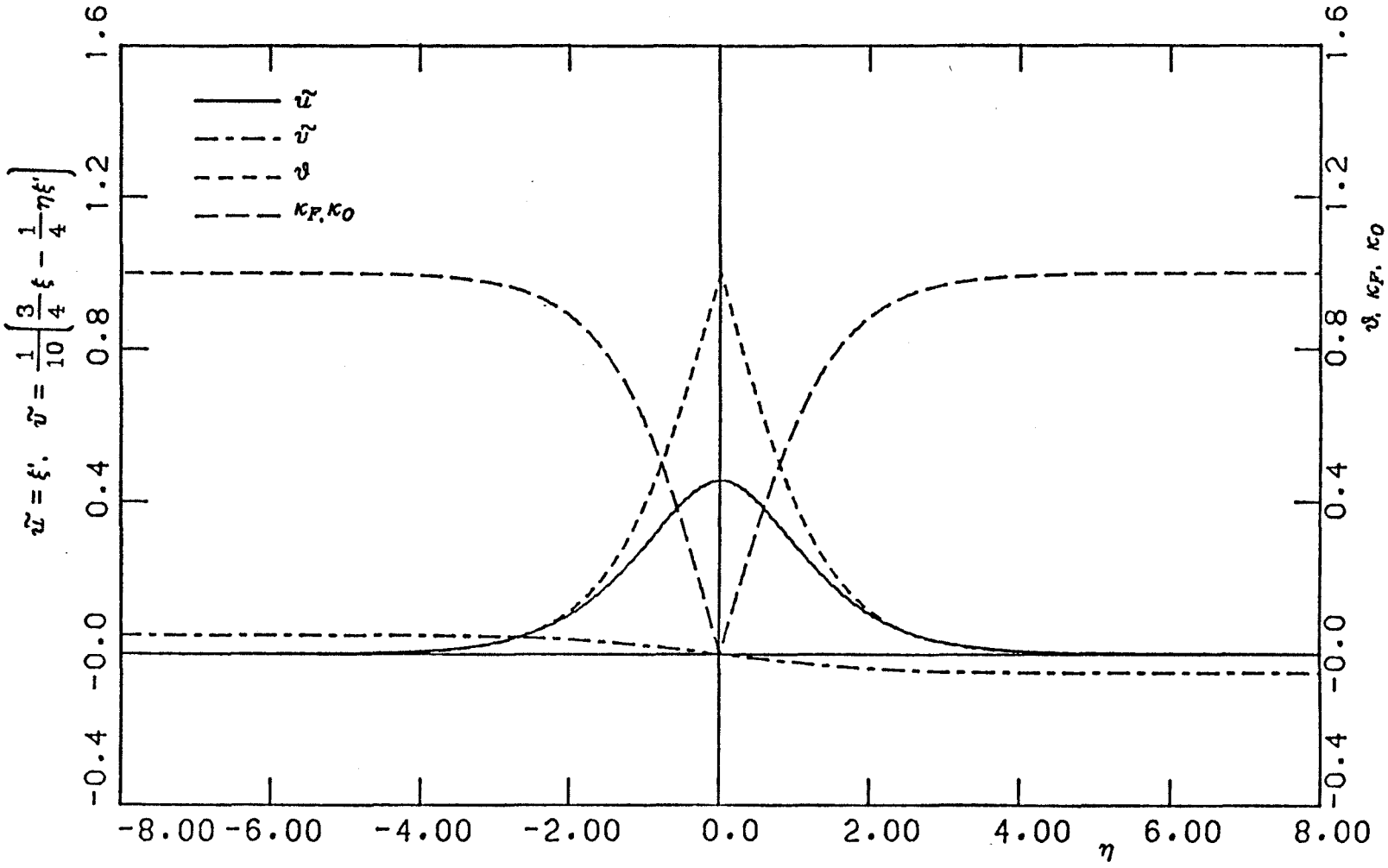

Figure (2.9) **Velocity, Temperature and Concentration Profiles for Symmetric Flame.**

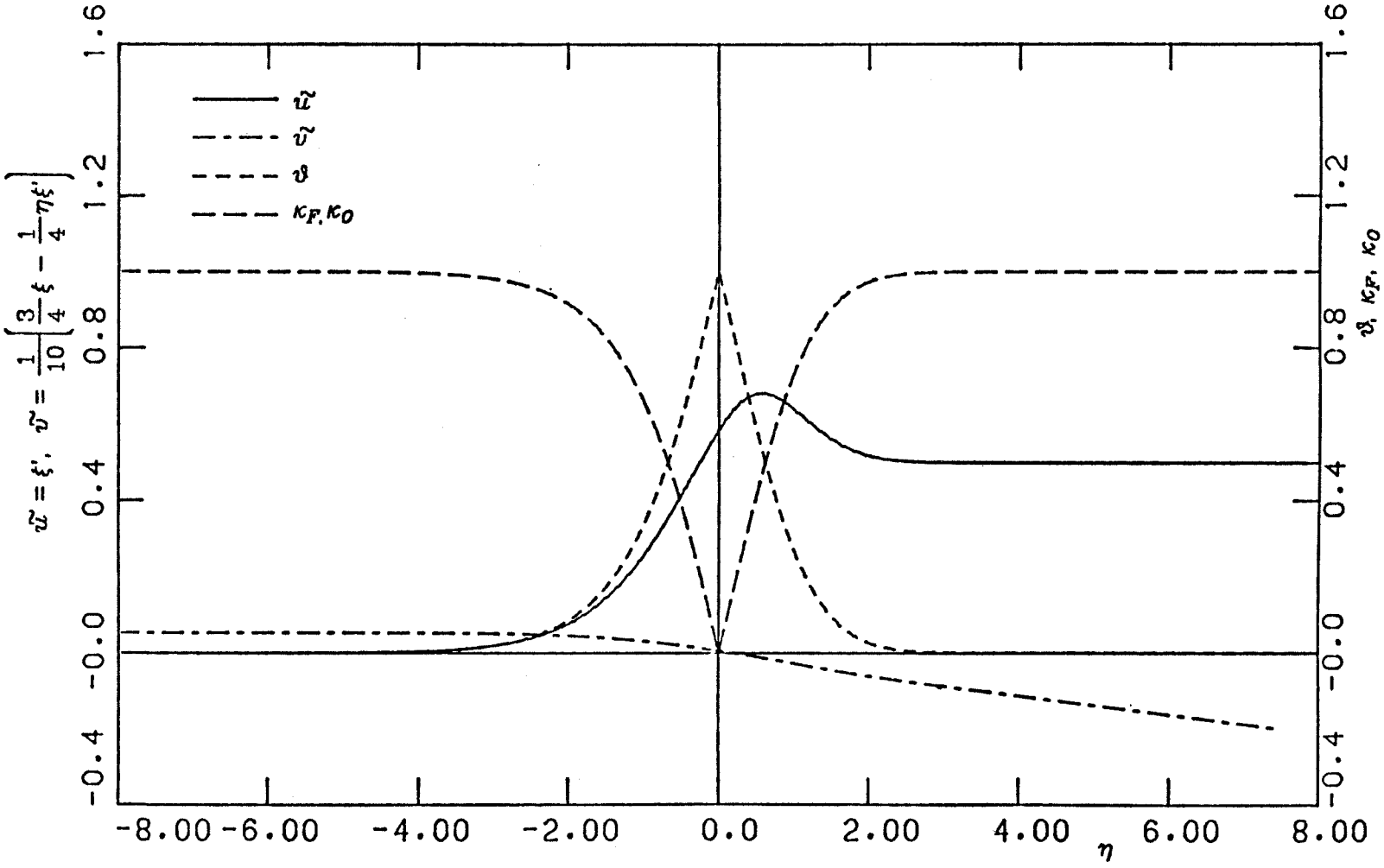

Figure (2.10) Velocity, Temperature and Concentration Profiles for Flame with $\tilde{\varphi} = 1$, $\frac{\dot{\rho}_{F_\infty}}{\dot{\rho}_{O_\infty}} = 0.25$, $\frac{T_f^*}{T_{O_\infty}^*} = 7$

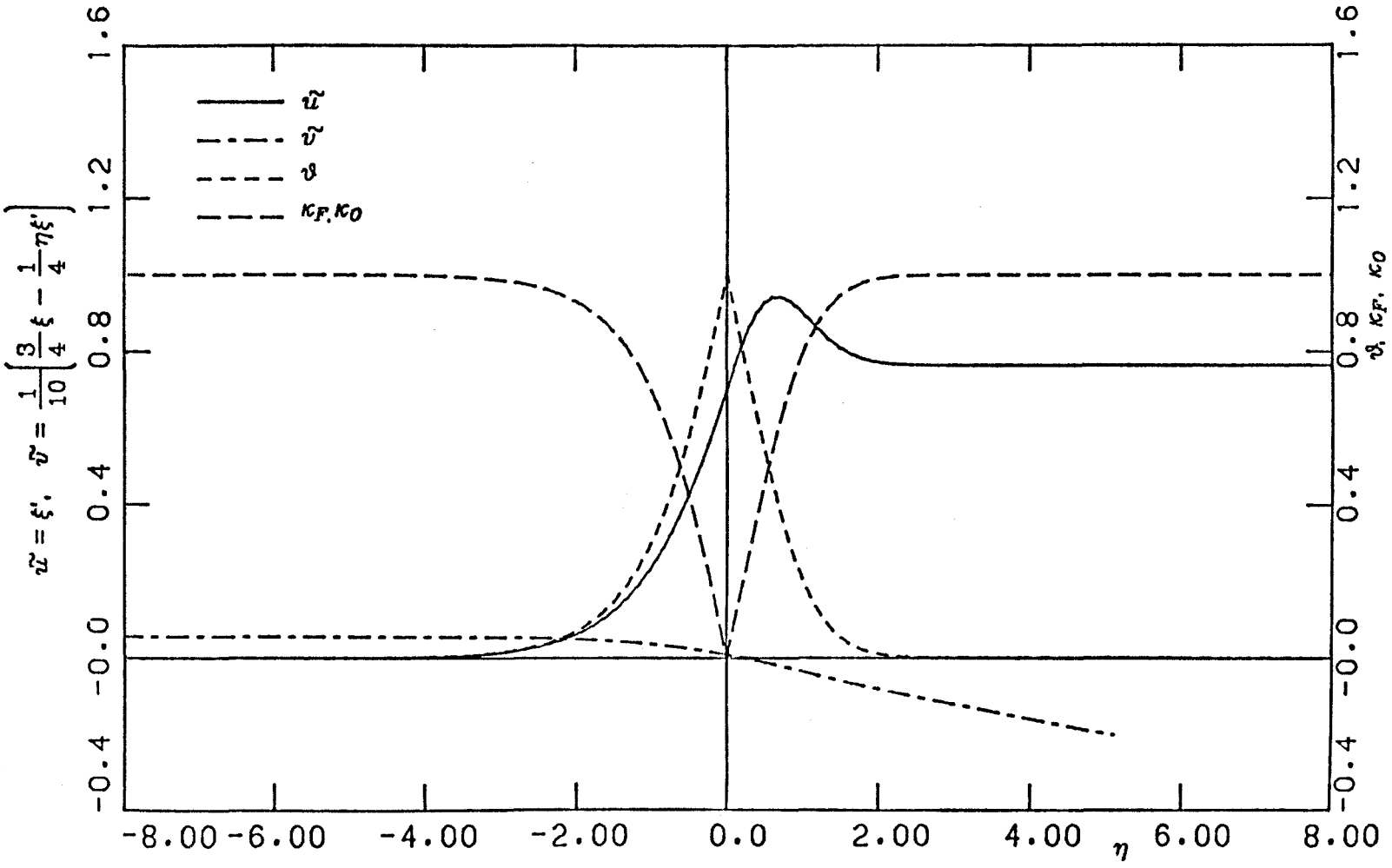

Figure (2.11) Velocity, Temperature and Concentration Profiles for Flame with $\tilde{\varphi} = 1$, $\frac{\dot{\rho}_{F_\infty}}{\dot{\rho}_{O_\infty}} = 0.125$, $\frac{T_f^*}{T_{O_\infty}^*} = 7$

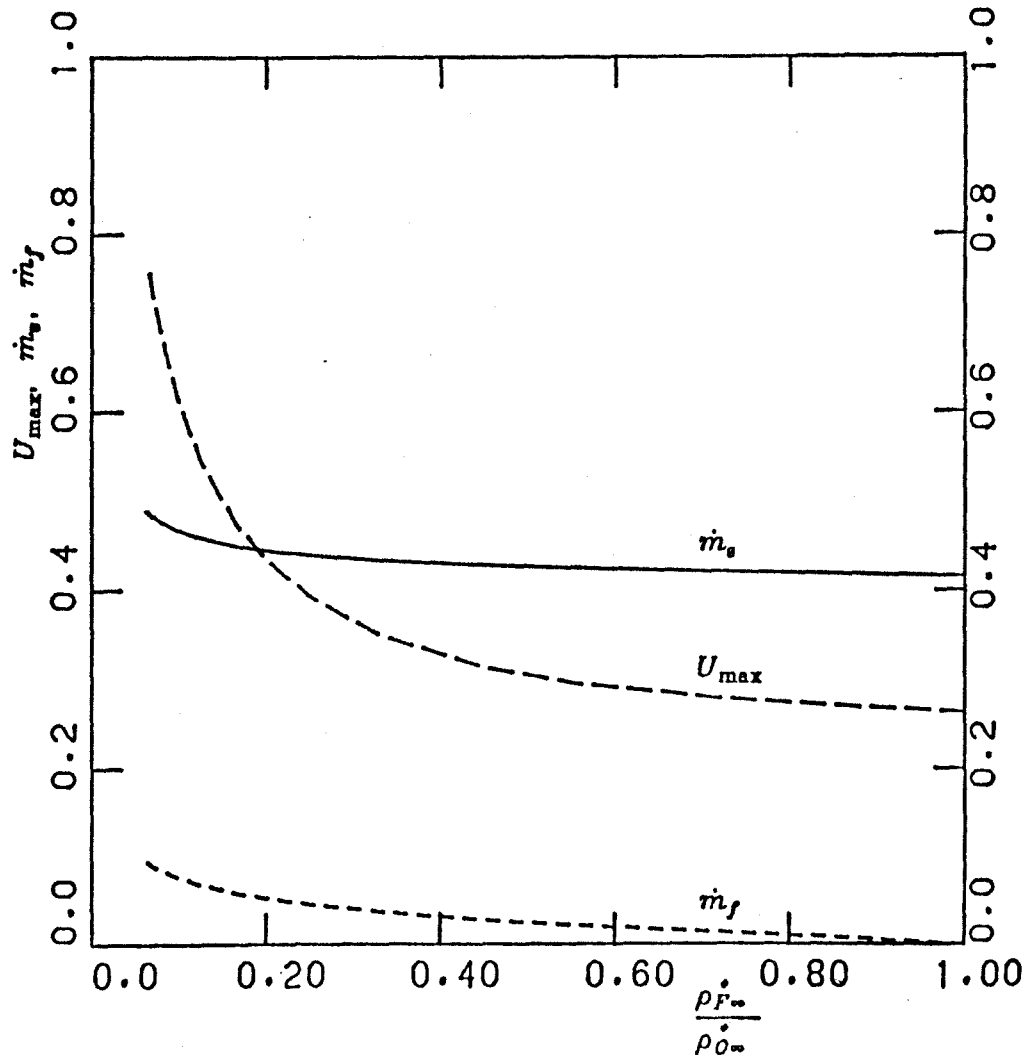

Figure (2.12) Variation of maximum vertical velocity, U_{max}, entrainment of oxidiser, $\dot{m}e$, and mass flux through the flame, $\dot{m}_f$ with density ratio at infinity.

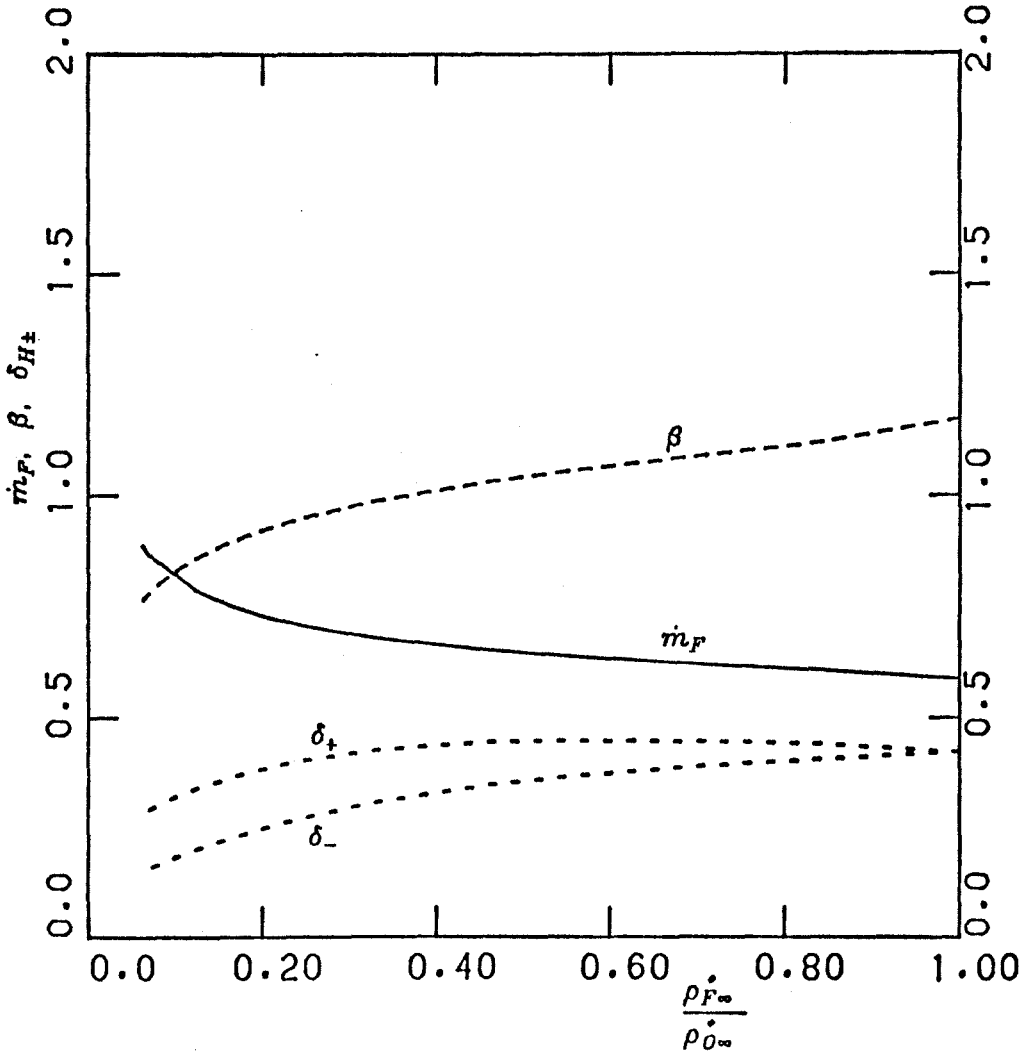

Figure (2.13) Variation of fuel consumption, $\dot{m}_F$, buoyancy, β, and enthalpy thickness on each side of flame, $\delta_{H\pm}$ with density ratio at infinity.

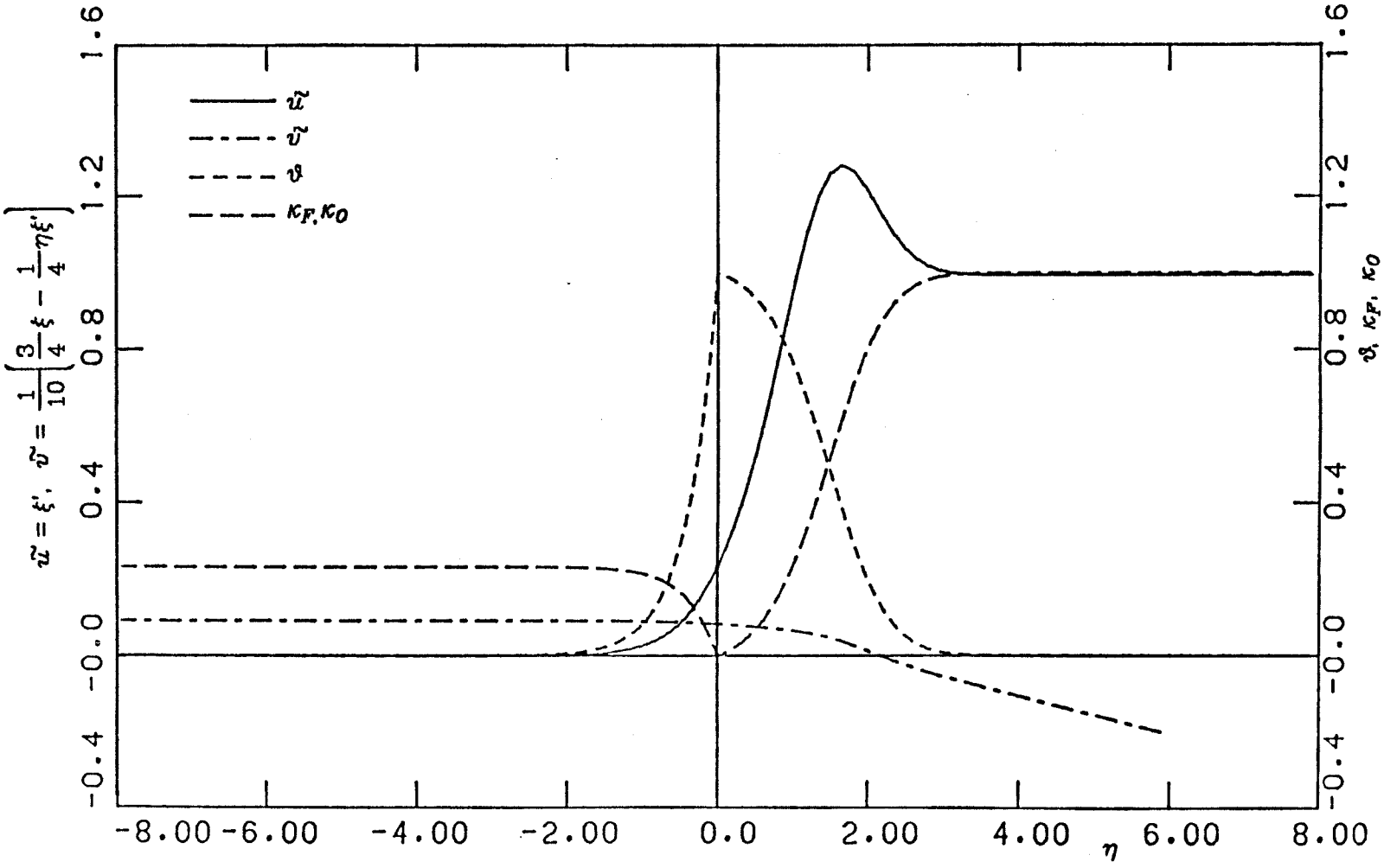

Figure (2.14) Velocity, Temperature and Concentration Profiles for Methane/Air Flame ($\tilde{\varphi} = 0.058$, $\frac{\dot{\rho}_{F\infty}}{\dot{\rho}_{O\infty}} = 0.552$, $\frac{\dot{T}_f}{\dot{T}_{O\infty}} = 7.58$)

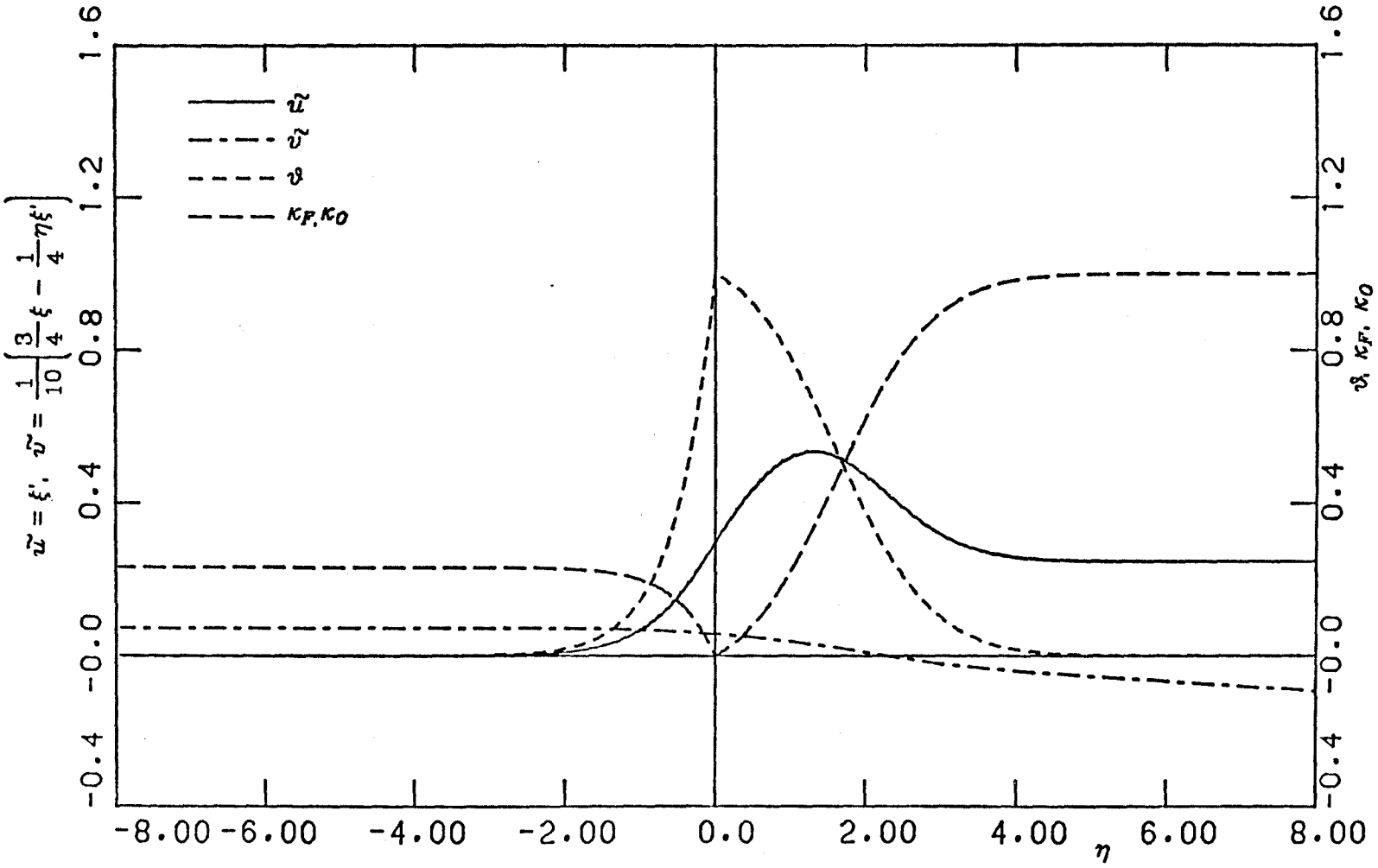

Figure (2.15) Velocity, Temperature and Concentration Profiles for Hydrogen/Air Flame ($\tilde{\varphi} = 0.029$, $\frac{\rho^*_{F\infty}}{\rho^*_{O\infty}} = 0.069$, $\frac{T^*_f}{T^*_{O\infty}} = 7.83$)

Table (2.1). Streamfunction ξ and Temperature ϑ for a Symmetric Flame.

($\tilde{\varphi} = 1$, $\tilde{M} = \tilde{T}_\infty = 0$, $Pr = 0.72$)

η	ξ	ξ'	ξ''	ξ'''	ϑ	ϑ'	ϑ''
0.0	0.0000	0.4573	0.0000	-0.5817	1.0000	-0.7010	0.0000
0.2	0.0907	0.4467	-0.1018	-0.4340	0.8607	-0.6874	0.1347
0.4	0.1775	0.4187	-0.1734	-0.2838	0.7267	-0.6485	0.2487
0.6	0.2574	0.3792	-0.2163	-0.1479	0.6026	-0.5902	0.3282
0.8	0.3288	0.3338	-0.2343	-0.0375	0.4915	-0.5198	0.3692
1.0	0.3909	0.2868	-0.2333	0.0430	0.3950	-0.4448	0.3756
1.2	0.4436	0.2414	-0.2190	0.0946	0.3134	-0.3713	0.3558
1.4	0.4877	0.1997	-0.1970	0.1219	0.2461	-0.3036	0.3198
1.6	0.5238	0.1628	-0.1715	0.1310	0.1915	-0.2439	0.2760
1.8	0.5531	0.1311	-0.1454	0.1278	0.1479	-0.1933	0.2309
2.0	0.5766	0.1045	-0.1208	0.1173	0.1136	-0.1514	0.1886
2.2	0.5953	0.0826	-0.0987	0.1032	0.0868	-0.1175	0.1511
2.4	0.6100	0.0648	-0.0796	0.0880	0.0661	-0.0906	0.1193
2.6	0.6214	0.0506	-0.0635	0.0733	0.0502	-0.0694	0.0932
2.8	0.6304	0.0393	-0.0502	0.0600	0.0380	-0.0530	0.0721
3.0	0.6373	0.0303	-0.0394	0.0484	0.0287	-0.0403	0.0554
3.2	0.6427	0.0234	-0.0307	0.0386	0.0217	-0.0305	0.0424
3.4	0.6468	0.0179	-0.0238	0.0305	0.0164	-0.0231	0.0323
3.6	0.6499	0.0137	-0.0184	0.0239	0.0123	-0.0175	0.0245
3.8	0.6523	0.0105	-0.0142	0.0187	0.0093	-0.0132	0.0186
4.0	0.6542	0.0080	-0.0109	0.0145	0.0070	-0.0099	0.0141
4.2	0.6556	0.0061	-0.0083	0.0112	0.0053	-0.0075	0.0106
4.4	0.6566	0.0046	-0.0064	0.0086	0.0040	-0.0056	0.0080
4.6	0.6574	0.0035	-0.0048	0.0066	0.0030	-0.0042	0.0060
4.8	0.6580	0.0027	-0.0037	0.0051	0.0022	-0.0032	0.0045
5.0	0.6585	0.0020	-0.0028	0.0039	0.0017	-0.0024	0.0034
5.4	0.6591	0.0012	-0.0016	0.0022	0.0009	-0.0014	0.0019
5.8	0.6595	0.0007	-0.0009	0.0013	0.0005	-0.0008	0.0011
6.2	0.6597	0.0004	-0.0005	0.0007	0.0003	-0.0004	0.0006
6.6	0.6598	0.0002	-0.0003	0.0004	0.0002	-0.0002	0.0004
7.0	0.6599	0.0001	-0.0002	0.0002	0.0002	-0.0001	0.0002
7.4	0.6599	0.0001	-0.0001	0.0001	0.0000	-0.0001	0.0001

Table (2.2). Streamfunction ξ and Temperature ϑ for a Flame with $\tilde{\varphi} = 0.058$, $\tilde{M} = \tilde{T}_- = 0$, $Pr = 0.72$ (η_E is the similarity variable after inverting the Howarth transformation for $\tilde{T}_f = 6$.)

η	η_E	ξ	ξ'	ξ''	ξ'''	ϑ	ϑ'	ϑ''
0.0	0.0000	-0.7092	0.3064	0.2956	-0.1833	1.0000	1.7458	2.6743
-0.2	-1.2113	-0.7644	0.2459	0.2996	0.1075	0.7004	1.2693	2.0958
-0.4	-2.1157	-0.8078	0.1891	0.2640	0.2265	0.4849	0.9034	1.5764
-0.6	-2.8011	-0.8407	0.1411	0.2153	0.2500	0.3327	0.6326	1.1487
-0.8	-3.3320	-0.8649	0.1030	0.1670	0.2278	0.2268	0.4375	0.8174
-1.0	-3.7590	-0.8825	0.0739	0.1253	0.1886	0.1539	0.2999	0.5717
-1.2	-4.1120	-0.8950	0.0523	0.0917	0.1476	0.1041	0.2043	0.3949
-1.4	-4.4153	-0.9038	0.0367	0.0659	0.1112	0.0702	0.1385	0.2703
-1.6	-4.6849	-0.9099	0.0255	0.0467	0.0816	0.0473	0.0936	0.1839
-1.8	-4.9318	-0.9142	0.0176	0.0328	0.0588	0.0318	0.0631	0.1246
-2.0	-5.1633	-0.9172	0.0121	0.0228	0.0418	0.0214	0.0425	0.0842
-2.4	-5.5987	-0.9206	0.0057	0.0109	0.0204	0.0096	0.0192	0.0382
-2.8	-6.0147	-0.9221	0.0026	0.0051	0.0097	0.0043	0.0087	0.0173
-3.2	-6.4219	-0.9229	0.0012	0.0024	0.0046	0.0020	0.0039	0.0078
-3.6	-6.8251	-0.9232	0.0005	0.0011	0.0021	0.0009	0.0018	0.0035
-4.0	-7.2266	-0.9234	0.0002	0.0005	0.0010	0.0004	0.0008	0.0016
-4.4	-7.6273	-0.9234	0.0001	0.0002	0.0004	0.0002	0.0004	0.0007
-4.8	-8.0275	-0.9235	0.0001	0.0001	0.0002	0.0001	0.0002	0.0003
0.0	0.0000	-0.7092	0.3064	0.2956	-0.1833	1.0000	-0.1013	-0.1551
0.2	1.3865	-0.6423	0.3616	0.2550	-0.2237	0.9764	-0.1356	-0.1882
0.4	2.7403	-0.5652	0.4078	0.2062	-0.2630	0.9453	-0.1761	-0.2150
0.6	4.0518	-0.4798	0.4436	0.1502	-0.2960	0.9057	-0.2208	-0.2288
0.8	5.3102	-0.3885	0.4675	0.0887	-0.3165	0.8570	-0.2663	-0.2235
1.0	6.5048	-0.2937	0.4789	0.0248	-0.3189	0.7994	-0.3087	-0.1958
1.1	7.0750	-0.2457	0.4798	-0.0068	-0.3123	0.7676	-0.3272	-0.1736
1.2	7.6255	-0.1978	0.4775	-0.0375	-0.3002	0.7340	-0.3432	-0.1467
1.4	8.6641	-0.1035	0.4643	-0.0939	-0.2609	0.6629	-0.3663	-0.0818
1.6	9.6150	-0.0128	0.4406	-0.1408	-0.2056	0.5884	-0.3755	-0.0104
1.8	10.4762	0.0722	0.4088	-0.1756	-0.1414	0.5136	-0.3706	0.0578
2.0	11.2486	0.1503	0.3713	-0.1973	-0.0764	0.4410	-0.3532	0.1147
2.2	11.9365	0.2205	0.3307	-0.2065	-0.0176	0.3730	-0.3259	0.1552
2.4	12.5463	0.2825	0.2894	-0.2051	0.0302	0.3111	-0.2922	0.1783
2.6	13.0860	0.3364	0.2492	-0.1953	0.0650	0.2563	-0.2556	0.1857
2.8	13.5645	0.3824	0.2116	-0.1799	0.0871	0.2089	-0.2183	0.1807
3.0	13.9903	0.4212	0.1775	-0.1612	0.0981	0.1687	-0.1839	0.1673
3.4	14.7170	0.4804	0.1209	-0.1215	0.0968	0.1075	-0.1243	0.1290
3.8	15.3231	0.5200	0.0797	-0.0859	0.0797	0.0670	-0.0806	0.0906
4.2	15.8506	0.5459	0.0512	-0.0581	0.0593	0.0412	-0.0508	0.0599
4.6	16.3285	0.5623	0.0322	-0.0381	0.0414	0.0250	-0.0315	0.0382
5.0	16.7755	0.5725	0.0198	-0.0244	0.0277	0.0150	-0.0193	0.0238
5.4	17.2037	0.5787	0.0120	-0.0154	0.0181	0.0090	-0.0117	0.0146
5.8	17.6205	0.5824	0.0071	-0.0096	0.0115	0.0053	-0.0071	0.0089
6.2	18.0302	0.5846	0.0040	-0.0059	0.0073	0.0030	-0.0043	0.0054
6.6	18.4358	0.5858	0.0022	-0.0035	0.0045	0.0017	-0.0026	0.0033
7.0	18.8388	0.5865	0.0011	-0.0021	0.0028	0.0009	-0.0016	0.0020
7.4	19.2403	0.5868	0.0004	-0.0012	0.0017	0.0004	-0.0009	0.0012
7.8	19.6409	0.5869	0.0001	-0.0007	0.0011	0.0001	-0.0006	0.0007

Table (2.3). Streamfunction ξ and Temperature ϑ for a Flame with $\tilde{\varphi} = 0.058$, $\tilde{M} = 0.81$, $\tilde{T}_\infty = 0$, $\tilde{T}_f = 6.58$ and $Pr = 0.72$

η	ξ	ξ'	ξ''	ξ'''	ϑ	ϑ'	ϑ''
0.0	-0.7469	0.2991	0.3138	-0.1179	1.0000	1.8136	2.9259
-0.2	-0.8004	0.2362	0.3063	0.1558	0.6911	1.2978	2.2436
-0.4	-0.8418	0.1789	0.2630	0.2558	0.4723	0.9098	1.6543
-0.6	-0.8726	0.1316	0.2100	0.2642	0.3201	0.6281	1.1838
-0.8	-0.8951	0.0947	0.1600	0.2319	0.2156	0.4286	0.8287
-1.0	-0.9111	0.0671	0.1180	0.1870	0.1446	0.2901	0.5709
-1.2	-0.9224	0.0469	0.0851	0.1432	0.0967	0.1952	0.3889
-1.4	-0.9303	0.0325	0.0603	0.1059	0.0645	0.1308	0.2628
-1.6	-0.9357	0.0223	0.0422	0.0765	0.0430	0.0874	0.1767
-1.8	-0.9394	0.0152	0.0292	0.0543	0.0286	0.0583	0.1183
-2.0	-0.9419	0.0104	0.0201	0.0380	0.0190	0.0388	0.0790
-2.4	-0.9448	0.0047	0.0093	0.0181	0.0084	0.0172	0.0351
-2.8	-0.9461	0.0021	0.0043	0.0084	0.0037	0.0076	0.0155
-3.2	-0.9467	0.0010	0.0019	0.0039	0.0016	0.0034	0.0069
-3.6	-0.9470	0.0004	0.0009	0.0017	0.0007	0.0015	0.0030
-4.0	-0.9471	0.0002	0.0004	0.0008	0.0003	0.0007	0.0013
-4.4	-0.9471	0.0001	0.0002	0.0003	0.0001	0.0003	0.0006
-4.8	-0.9472	0.0000	0.0001	0.0002	0.0001	0.0001	0.0003
0.0	-0.7469	0.2991	0.3138	-0.1179	1.0000	-0.1052	-0.1697
0.2	-0.6810	0.3593	0.2868	-0.1538	0.9753	-0.1433	-0.2107
0.4	-0.6036	0.4133	0.2519	-0.1956	0.9422	-0.1891	-0.2466
0.6	-0.5162	0.4595	0.2083	-0.2402	0.8992	-0.2410	-0.2687
0.8	-0.4205	0.4960	0.1560	-0.2814	0.8456	-0.2951	-0.2680
1.0	-0.3185	0.5214	0.0966	-0.3107	0.7814	-0.3462	-0.2382
1.2	-0.2127	0.5344	0.0332	-0.3190	0.7078	-0.3883	-0.1784
1.3	-0.1592	0.5361	0.0015	-0.3130	0.6681	-0.4043	-0.1390
1.4	-0.1056	0.5347	-0.0292	-0.2998	0.6270	-0.4160	-0.0949
1.6	0.0004	0.5232	-0.0848	-0.2524	0.5426	-0.4255	0.0003
1.8	0.1030	0.5016	-0.1287	-0.1830	0.4581	-0.4161	0.0926
2.0	0.2005	0.4727	-0.1573	-0.1027	0.3773	-0.3896	0.1687
2.2	0.2918	0.4397	-0.1699	-0.0246	0.3031	-0.3502	0.2207
2.4	0.3763	0.4057	-0.1680	0.0406	0.2377	-0.3031	0.2463
2.6	0.4542	0.3733	-0.1550	0.0864	0.1821	-0.2532	0.2484
2.8	0.5259	0.3442	-0.1348	0.1116	0.1363	-0.2049	0.2327
3.0	0.5922	0.3195	-0.1115	0.1189	0.0999	-0.1609	0.2058
3.4	0.7123	0.2841	-0.0669	0.0987	0.0503	-0.0915	0.1408
3.8	0.8216	0.2642	-0.0346	0.0630	0.0233	-0.0471	0.0836
4.2	0.9251	0.2547	-0.0157	0.0334	0.0100	-0.0222	0.0443
4.6	1.0260	0.2505	-0.0063	0.0152	0.0039	-0.0095	0.0211
5.0	1.1258	0.2489	-0.0023	0.0061	0.0014	-0.0038	0.0092
5.4	1.2252	0.2483	-0.0007	0.0022	0.0005	-0.0014	0.0036
5.8	1.3246	0.2482	-0.0002	0.0007	0.0001	-0.0005	0.0013
6.2	1.4238	0.2481	-0.0001	0.0002	0.0000	-0.0001	0.0004
6.4	1.4734	0.2481	0.0000	0.0001	0.0000	-0.0001	0.0002

Table (2.4). Flow parameters for flames shown in figures (2.2) - (2.6), figures (2.9) - (2.11) and figures (2.14) - (2.15)

φ^*	$\rho_{F\infty}$	$\left(\frac{T_f^*}{T_{O\infty}^*}-1\right)$	$\xi(0)$	$\xi'(0)$	$\xi''(0)$	$\vartheta'_+(0)$
1.0	1.0		0.0	0.4574	0.0	0.7010
0.232	1.0		-0.5078	0.3717	0.2600	0.2902
0.058	1.0		-0.7092	0.3064	0.2956	0.1013
0.029	1.0		-0.8334	0.2651	0.2976	0.05701
1.0	0.25	6.0	-0.0726	0.5858	0.3091	0.8418
1.0	0.125	6.0	-0.1093	0.7020	0.6044	0.9339
0.058	0.5525	6.58	-0.7469	0.2991	0.3138	0.1052
0.029	0.069	6.83	-1.0881	0.2320	0.4266	0.07137

Chapter 3.

FORMULATION OF THE LOCAL STABILITY PROBLEM

In this chapter, the theory for the stability of the buoyant diffusion flame is formulated utilizing the appropriate extension of the Orr-Sommerfeld linearization of the field equations. The steady boundary layer flow, assumed to be essentially parallel over distances comparable to a disturbance wave length, is perturbed by sinusoidal disturbances in the temperature, composition and velocity profiles. The field equations are then linearized by dropping all terms involving the multiplication of disturbance order quantities, resulting in a sixth order system of linear ordinary differential equations. The history and theory of this method is reviewed by Betchov and Criminale, reference (3.1), 1967.

The equations derived in this chapter differ considerably from those used in previous investigations of boundary layer flows. Laminar jet flow, studied analytically by Pai, reference (3.2), 1951, Curle, reference (3.3), 1956, and Tatsumi and Kakutani, reference (3.4), 1958, and numerically by Kaplun, reference (3.5), 1964, is similar to the buoyant flame in that it is a boundary-free flow, however it lacks the coupling of temperature and velocity through the body force term in the equations of motion. Plapp, references (3.6) and (3.7), 1957, obtained the governing disturbance equations for natural convection flows, but neglected variations in density in all but the body force term. These equations were used by Nachtsheim, reference (3.8), 1963, to study the flow over a heated wall and by Pera and Gebhart, reference (3.9), 1971, to study the buoyant plume. Both investigations showed that the coupling due to buoyancy could not be ignored, since it destabilized the flow considerably at low Reynolds numbers.

For the buoyant diffusion flame, it is no longer possible to exclude the effects of density variation in all but the body force term, since these variations can be very large. The equations developed below therefore use the full disturbance

equations for a variable density fluid derived by Lees and Lin, reference (3.10), 1946, and adapt them to the natural convection problem posed by the buoyant flame.

3.1. Governing Equations

The equations describing the non-steady, two dimensional motion of a binary gas mixture, with the x axis vertically upward, are

Continuity:

$$\frac{\partial \rho^*}{\partial t^*} + \frac{\partial}{\partial x^*}\left(\rho^* u^*\right) + \frac{\partial}{\partial y^*}\left(\rho^* v^*\right) = 0 \tag{3.1}$$

Vertical Momentum:

$$\frac{\partial u^*}{\partial t^*} + u^* \frac{\partial u^*}{\partial x^*} + v^* \frac{\partial u^*}{\partial y^*} = \frac{1}{\rho^*}\left(\frac{\partial \tau_{xx}^*}{\partial x^*} + \frac{\partial \tau_{xy}^*}{\partial y^*}\right) - g^* \tag{3.2}$$

Horizontal Momentum:

$$\frac{\partial v^*}{\partial t^*} + u^* \frac{\partial v^*}{\partial x^*} + v^* \frac{\partial v^*}{\partial y^*} = \frac{1}{\rho^*}\left(\frac{\partial \tau_{xy}^*}{\partial x^*} + \frac{\partial \tau_{yy}^*}{\partial y^*}\right) \tag{3.3}$$

Energy:

$$\rho^* \frac{\partial h^*}{\partial t^*} + \rho^* u^* \frac{\partial h^*}{\partial x^*} + \rho^* v^* \frac{\partial h^*}{\partial y^*} = \frac{\partial p^*}{\partial t^*} + u^* \frac{\partial p^*}{\partial x^*} + v^* \frac{\partial p^*}{\partial y^*} + \tag{3.4}$$

$$\left(\tau_{xx}^* \varepsilon_{xx}^* + 2\tau_{xy}^* \varepsilon_{xy}^* + \tau_{yy}^* \varepsilon_{yy}^*\right) + \frac{\partial}{\partial x^*}\left(k^* \frac{\partial T^*}{\partial x^*}\right) + \frac{\partial}{\partial y^*}\left(k^* \frac{\partial T^*}{\partial y^*}\right) + \dot{q}^*$$

Species:

$$\rho^* \frac{\partial Y_i}{\partial t^*} + \rho^* u^* \frac{\partial Y_i}{\partial x^*} + \rho^* v^* \frac{\partial Y_i}{\partial y^*} = \frac{\partial}{\partial x^*}\left[\rho^* D_i^* \frac{\partial Y_i}{\partial x^*}\right] + \frac{\partial}{\partial y^*}\left[\rho^* D_i^* \frac{\partial Y_i}{\partial y^*}\right] + \dot{m}_i^* \quad (3.5)$$

State:

$$p^* = \rho^* R^* T^* \quad (3.6)$$

Here it has been assumed that no species diffusion is driven by pressure or temperature gradients. A superscript * denotes a dimensional quantity, $\varepsilon_{xx}^*, \varepsilon_{xy}^*, \varepsilon_{yy}^*$ are the components of the rate of strain tensor and $\tau_{xx}^*, \tau_{xy}^*, \tau_{yy}^*$ are the components of the stress tensor.

$$\varepsilon_{xx}^* = \frac{\partial u^*}{\partial x^*}, \quad \varepsilon_{xy}^* = \frac{1}{2}\left[\frac{\partial u^*}{\partial y^*} + \frac{\partial v^*}{\partial x^*}\right], \quad \varepsilon_{yy}^* = \frac{\partial v^*}{\partial y^*} \quad (3.7)$$

$$\left.\begin{aligned} \tau_{xx}^* &= -p^* + 2\mu_1^* \frac{\partial u^*}{\partial x^*} + \frac{2}{3}(\mu_2^* - \mu_1^*)\left[\frac{\partial u^*}{\partial x^*} + \frac{\partial v^*}{\partial y^*}\right] \\ \tau_{xy}^* &= \mu_1^*\left[\frac{\partial u^*}{\partial y^*} + \frac{\partial v^*}{\partial x^*}\right] \\ \tau_{yy}^* &= -p^* + 2\mu_1^* \frac{\partial v^*}{\partial y^*} + \frac{2}{3}(\mu_2^* - \mu_1^*)\left[\frac{\partial u^*}{\partial x^*} + \frac{\partial v^*}{\partial y^*}\right] \end{aligned}\right\} \quad (3.8)$$

The coefficients of viscosity μ_1^* and μ_2^* and the coefficients of heat conductivity k^* and diffusion D_i^* are taken to be known functions of temperature.

Consider a motion which is slightly disturbed from a steady state. It is convenient to separate any quantity $V^*(x^*, y^*, t^*)$ describing this motion into a

steady part $\bar{V}^*(x^*,y^*)$ and a small disturbance $\tilde{V}^*(x^*,y^*,t^*)$

$$V^*(x^*,y^*,t^*) = \bar{V}^*(x^*,y^*) + \tilde{V}(x^*,y^*,t^*)$$

By substituting expressions of this type into the governing equations (3.1)-(3.8) and neglecting terms quadratic in the small disturbance, a linear system of disturbance equations is obtained. If the steady flow is parallel or nearly parallel, such as the boundary layer solution developed in chapter 2 for large Reynolds numbers, further simplifications can be made using

$$\bar{v}^* << \bar{u}^*, \quad \frac{\partial \bar{V}^*}{\partial x^*} << \frac{\partial \bar{V}^*}{\partial y^*}$$

The steady flow quantities are therefore taken to be independent of x^*. A sinusoidal form is assumed for the disturbances, and the variables non-dimensionalised as follows

$$\frac{u^*}{u_o^*} = u(y) + f(y)\, e^{i\alpha(x-ct)}$$

$$\frac{v^*}{u_o^*} = \alpha\varphi(y)\, e^{i\alpha(x-ct)}$$

$$\frac{\rho^*}{\rho_\infty^*} = \rho(y) + r(y)\, e^{i\alpha(x-ct)}$$

$$\frac{p^*}{\rho_\infty^* u_o^{*2}} = p(y) + \pi(y)\, e^{i\alpha(x-ct)}$$

$$\left.\begin{aligned}
\frac{T^*}{T_\infty^*} &= T(y) + \tilde{s}\, e^{ia(x-ct)} \\
\frac{\mu_1^*}{\mu_{1\infty}^*} &= \mu(y) + m(y)\, e^{ia(x-ct)} \\
\frac{\mu_2^*}{\mu_{1\infty}^*} &= \mu_2(y) + m_2(y)\, e^{ia(x-ct)} \\
\frac{k^*}{c_{p\infty}^* \mu_{1\infty}^*} &= \frac{1}{Pr}\mu(y) + \frac{1}{Pr} m(y)\, e^{ia(x-ct)} \\
\frac{\rho_\infty^* D_i^*}{\mu_{1\infty}^*} &= \frac{1}{Sc}\mu(y) + \frac{1}{Sc} m(y)\, e^{ia(x-ct)} \\
\alpha^* \delta^* = a, \quad \frac{c^*}{u_o^*} &= c \\
\frac{y^*}{\delta^*} = y, \quad \frac{x^*}{\delta^*} &= x
\end{aligned}\right\} \qquad (3.9)$$

where, for the buoyant diffusion flame,

$$u_o^* = 2\left[\left(\frac{T_f}{T_\infty} - 1\right) g^* x^*\right]^{\frac{1}{2}} \qquad (3.10a)$$

$$\delta^* = \left[\frac{4\nu_\infty^{*2} x^*}{\left(\frac{T_f}{T_\infty} - 1 \right) g^*} \right]^{\frac{1}{4}} \tag{3.10b}$$

Lees and Lin, reference (3.10), 1946, first obtained the disturbance equations for a compressible fluid using the internal energy equation. This was replaced with the enthalpy equation by Lees and Reshotko reference (3.11), 1962. The following equations differ from those of Lees and Reshotko only by the addition of the buoyancy term in the vertical momentum equation and by normalising the pressure by $\rho_\infty^* u_o^{*2}$ rather than p_∞^*.

Continuity:

$$\varphi' = -if + \left[\frac{T'}{T} \right] \varphi + i(u - c) \left[\frac{\tilde{s}}{T} - \gamma M^2 \pi \right] \tag{3.11}$$

Vertical Momentum:

$$\left.\begin{aligned} \alpha\rho\left[i(u-c)f + u'\varphi \right] &= -i\alpha\pi + \frac{\mu}{\mathrm{Re}}\left[f'' + \alpha^2(i\varphi' - 2f) \right] \\ &- \frac{1}{Fr}\left[\gamma M^2 \rho\pi - \frac{\tilde{s}}{T} \right] + \frac{2}{3\mathrm{Re}}(\mu_2 - \mu)\alpha^2(i\varphi' - f) \\ &+ \frac{1}{\mathrm{Re}}\left[mu'' + m'u' + \mu'(f' + i\alpha^2\varphi) \right] \end{aligned}\right\} \tag{3.12}$$

Horizontal Momentum:

$$\alpha^2\rho\left[i(u-c)\varphi\right] = -\pi' + \frac{\mu\alpha}{\mathrm{Re}}\left[2\varphi'' + if' - \alpha^2\varphi\right]$$

$$+ \frac{2\alpha}{3\mathrm{Re}}(\mu_2 - \mu)(\varphi'' + if') + \frac{\alpha}{\mathrm{Re}}\left[imu' + 2\mu'\varphi' + \frac{2}{3}(\mu_2' - \mu')(\varphi' + if)\right] \quad (3.13)$$

Energy:

$$\alpha\rho\left[i(u-c)\tilde{s} + T'\varphi\right] = \frac{1}{Pr\,\mathrm{Re}}\left[\mu(\tilde{s}'' - \alpha^2\tilde{s}) + (mT')' + \mu'\tilde{s}'\right] +$$

$$i\alpha(u-c)\left[1 - \frac{1}{\gamma}\right]\gamma M^2\pi + \left[(\gamma-1)\frac{M^2}{\mathrm{Re}}\right]\left[mu'^2 + 2\mu u'(f' + i\alpha^2\varphi)\right] \quad (3.14)$$

Note that this energy disturbance equation is valid outside the infinitesimal region of the reaction zone.

State:

$$\gamma M^2\pi = \frac{\tau}{\rho} + \frac{\tilde{s}}{T} \quad (3.15)$$

In these equations, a prime denoted differentiation with respect to the non-dimensional variable y. The species disturbance equation has not been given since in the limit of Mach number becoming zero, the energy and species disturbance equations are identical. In the preceding equations, the Reynolds number, Re, Froude number, Fr and Mach number M are

$$\mathrm{Re} = \frac{u_o^*\delta^*}{\nu_\infty^*}, \quad Fr = \frac{u_o^2}{g^*\delta^*}, \quad M = \frac{u_o^*}{(\gamma R^* T_\infty^*)} \quad (3.16)$$

where γ is the ratio of specific heats. Note that in the present case, the

Reynolds and Froude numbers are proportional

$$Fr = \left[\frac{T_f^*}{T_\infty^*} - 1\right]\mathrm{Re}$$

The Mach number is now taken to be zero in equations (3.11)-(3.15). Eliminating the pressure, π , between equations (3.12) and (3.13), substituting for φ' and φ'' from equation (3.11) and for $\rho = T^{-1}$ from the unperturbed equation of state yields

$$\left.\begin{aligned}
&\frac{\alpha}{T}\left[i(u-c)(f' - i\alpha^2\varphi) + iu'(u-c)\frac{\tilde{s}}{T} + u''\varphi\right] - \frac{\alpha T'}{T^2}\left[i(u-c)f\right] = \\
&\frac{\mu}{\mathrm{Re}}\left[f'''' - \alpha^2\left[2f'' + \left[\frac{T'}{T}\right]f' + i\left[\frac{T''}{T}\right]\varphi - (u-c)\frac{\tilde{s}'}{T} - u'\frac{\tilde{s}}{T}\right] + i\alpha^4\varphi\right] + \\
&\frac{2\mu'}{\mathrm{Re}}(f''' - \alpha^2 f') + \frac{1}{\left[\frac{T_f}{T_\infty} - 1\right]\mathrm{Re}}\left[\frac{\tilde{s}'}{T^2} - \frac{2\tilde{s}T'}{T^3}\right] + \\
&\frac{1}{\mathrm{Re}}\left[(mu'')' + (m'u')' + \alpha^2 mu' + \mu''(f' + i\alpha^2\varphi)\right]
\end{aligned}\right\} \quad (3.17)$$

It is now convenient to define the variables s and ϑ by

$$\tilde{s} = \left[\frac{T_f}{T_\infty} - 1\right]s \quad (3.18a)$$

$$T = 1 + \left[\frac{T_f}{T_\infty} - 1\right]\vartheta \tag{3.18b}$$

Since viscosity is a function of temperature

$$\mu' = \frac{\partial \mu}{\partial y} = \frac{\partial \mu}{\partial T}\frac{\partial T}{\partial y} = \left[\frac{T_f}{T_\infty} - 1\right]\dot{\mu}\vartheta' \tag{3.19}$$

where $\dot{\mu} \equiv \frac{\partial \mu}{\partial T}$. Also, the fluctuating viscosity can be related to the temperature fluctuation through

$$m = \tilde{s}\frac{\partial \mu}{\partial T} = \left[\frac{T_f}{T_\infty} - 1\right]s\dot{\mu} \tag{3.20}$$

Substituting for these expressions in equation (3.17) gives

$$\begin{aligned} f''' = {} & \left[\frac{T_f}{T_\infty} - 1\right]\left\{\alpha^2\frac{\vartheta'}{T}\left[1 + 2T\frac{\dot{\mu}}{\mu}\right] - \frac{i\alpha \mathrm{Re}}{\mu T}\frac{\vartheta'}{T}(u - c)\right\} f + \\ & \left\{2\alpha^2 + \frac{i\alpha \mathrm{Re}}{\mu T}(u - c) - \left[\frac{T_f}{T_\infty} - 1\right]\frac{\dot{\mu}}{\mu}\vartheta' - \left[\frac{T_f}{T_\infty} - 1\right]^2\frac{\ddot{\mu}}{\mu}\vartheta'^2\right\} f' - \\ & 2\left[\frac{T_f}{T_\infty} - 1\right]\frac{\dot{\mu}}{\mu}\vartheta' f'' + \\ & \left\{-i\alpha^4 + \frac{\alpha \mathrm{Re}}{\mu T}(u'' + \alpha^2(u - c)) + \left[\frac{T_f}{T_\infty} - 1\right]\left[i\alpha^2\frac{\vartheta'}{T} - i\alpha^2\frac{\dot{\mu}}{\mu}\vartheta' - \right.\right. \end{aligned}$$

$$\left.\frac{\alpha PrRe}{\mu T}\frac{\dot{\mu}}{\mu}u'\vartheta'\right] - \left[\frac{T_f}{T_\infty} - 1\right]^2\left[i\alpha^2\frac{\ddot{\mu}}{\mu}\vartheta'^2\right]\Bigg\}\varphi + \Bigg\}$$

$$\left[\frac{T_f}{T_\infty} - 1\right]\left\{-\alpha^2\frac{u'}{T} + \frac{2\vartheta'}{\mu T^3} + \frac{i\alpha\mathrm{Re}\,(u-c)u'}{\mu T}}{T} - \frac{\dot{\mu}}{\mu}u''' - 2\alpha^2\frac{\dot{\mu}}{\mu}u' + \right.$$

$$\frac{i\alpha Pr\,\mathrm{Re}}{\mu T}\frac{\dot{\mu}}{\mu}(u-c)u' - \left[\frac{T_f}{T_\infty} - 1\right]\left[2\frac{\ddot{\mu}}{\mu}\vartheta'u'' + \frac{\ddot{\mu}}{\mu}u'\vartheta' - (\frac{\dot{\mu}}{\mu})^2u'\vartheta'\right] +$$

$$\left[\frac{T_f}{T_\infty} - 1\right]^2\left[\frac{\dot{\mu}}{\mu}\frac{\ddot{\mu}}{\mu}\vartheta'^2u' - \frac{\dddot{\mu}}{\mu}\vartheta'^2u'\right]\Bigg\}s +$$

$$\left\{\frac{-1}{\mu T^2} - \left[\frac{T_f}{T_\infty} - 1\right]\left[\frac{\alpha^2(u-c)}{T} + 2\frac{\dot{\mu}}{\mu}u''\right] - \left[\frac{T_f}{T_\infty} - 1\right]^2\left[2\frac{\ddot{\mu}}{\mu}u'\vartheta' - 2(\frac{\dot{\mu}}{\mu})^2u'\vartheta'\right]\right\}s' \Bigg\} \quad (3.21)$$

This equation along with continuity

$$\varphi' = -if + \frac{\left[\frac{T_f}{T_\infty} - 1\right]}{T}\left[\vartheta'\varphi + i(u-c)s\right] \quad (3.22)$$

and energy

$$s'' = \frac{\alpha Pr\,\mathrm{Re}}{\mu T}\vartheta'\varphi + \left\{\alpha^2 + \frac{i\alpha Pr\,\mathrm{Re}}{\mu T}(u-c) - \left[\frac{T_f}{T_\infty} - 1\right]\frac{\dot{\mu}}{\mu}\vartheta' - \right\} \quad (3.23)$$

$$\left.\left(\frac{T_f}{T_\infty}-1\right)^2\frac{\ddot{\mu}}{\mu}\vartheta'^2\right\}s-2\left(\frac{T_f}{T_\infty}-1\right)\frac{\dot{\mu}}{\mu}\vartheta's'\Bigg]$$

constitute the governing equations for small sinusoidal disturbances from a parallel steady flow for a variable density fluid. Note taking the limit $\left(\frac{T_f}{T_\infty}-1\right)=0$ in all terms except the Reynolds number results in the same equations as those derived by Plapp, references (3.6), (3.7), 1957, using the Boussinesq approximation, which neglects the effects of density variation in all terms except the body force term in the vertical momentum equation.

3.2. Boundary and Matching Conditions

3.2.1. *Matching Conditions at the Flame.* The presence of a flame sheet within the convecting fluid introduces a set of matching conditions which must be applied there. To obtain the appropriate conditions on the temperature disturbance, s, consider the energy and species conservation equations, (3.4) and (3.5). Neglecting dissipation effects, and with c_p^* constant, these can be written as

$$\rho^* c_p^*\left[\frac{\partial T^*}{\partial t^*}+u^*\frac{\partial T^*}{\partial x^*}+v^*\frac{\partial T^*}{\partial y^*}\right]=\frac{\partial}{\partial x^*}\left[k^*\frac{\partial T^*}{\partial x^*}\right]+\frac{\partial}{\partial y^*}\left[k^*\frac{\partial T^*}{\partial y^*}\right]+\dot{q}^*$$

$$\rho^*\left[\frac{\partial Y_i}{\partial t^*}+u^*\frac{\partial Y_i}{\partial x^*}+v^*\frac{\partial Y_i}{\partial y^*}\right]=\frac{\partial}{\partial x^*}\left[\rho^* D_i^*\frac{\partial Y_i}{\partial x^*}\right]+\frac{\partial}{\partial y^*}\left[\rho^* D_i^*\frac{\partial Y_i}{\partial y^*}\right]+\dot{m}_i^*$$

The difficulty of dealing with the heat and species production terms $\dot{q}^*$ and $\dot{m}_i^*$ can be bypassed by use of the Schvab-Zeldovich variable

$$Z = \frac{c_p^*(T^* - T_\infty^*) + q_c Y_F}{q_c} \tag{3.24a}$$

$$= \frac{f^*}{1+f^*} + \frac{Y_F - f^* Y_O}{1+f^*} \tag{3.24b}$$

where $q_c \equiv \frac{\dot{q}^*}{\dot{m}_F^*}$ and $f^* \equiv \frac{\dot{m}_F^*}{\dot{m}_O^*}$. Assuming unit Lewis number, the governing equation for Z is

$$\rho^* c_p^* \left(\frac{\partial Z}{\partial t^*} + u^* \frac{\partial Z}{\partial x^*} + v^* \frac{\partial Z}{\partial y^*} \right) = \frac{\partial}{\partial x^*} \left(k^* \frac{\partial Z}{\partial x^*} \right) + \frac{\partial}{\partial y^*} \left(k^* \frac{\partial Z}{\partial y^*} \right) \tag{3.25}$$

with boundary conditions

$$Z \to 1 \text{ as } y \to \infty \,, \; Z \to 0 \text{ as } y \to -\infty \tag{3.26}$$

Assume that $Z(x^*, y^*, t^*)$ is known for arbitrary initial conditions. At the flame $Y_F = Y_O = 0$, thus

$$T_f^* - T_\infty^* = \frac{q_c f^*}{c_p^*(1+f^*)} \tag{3.27}$$

The temperature at the flame is therefore always given by the adiabatic flame temperature regardless of the initial conditions, so the disturbance temperature at the flame must vanish. In addition, differentiating equation (3.24b) and evaluating at the flame gives

$$Y_F' + f^* Y_O' = 0 \qquad \textit{at the flame} \tag{3.28}$$

Furthermore, equations (3.24a) and (3.24b) give

$$\frac{T - T_\infty}{T_f - T_\infty} = 1 - Y_F \qquad y > 0$$

$$= 1 - Y_O \qquad y < 0$$

the disturbance mass fractions, $\tilde{Y}_i$, are therefore given by

$$\tilde{Y}_i = -s$$

so equation (3.28) can be used as a condition on the disturbance temperature at the flame. The flame position, no longer constrained to be at $y = 0$, can be taken as

$$y_f = \zeta e^{i\alpha(x - ct)} \tag{3.29}$$

The perturbation in the temperature at the flame now has two components; the temperature disturbance s, and the perturbation imposed on the steady flow by disturbing the flame position away from $y = 0$. This latter component can be evaluated by taking a Taylor series expansion about $y = 0$.

$$T_+^* = T_f^* + \zeta e^{i\alpha(x - ct)}(T_f^* - T_\infty^*)\vartheta_+'(0) + \cdots \qquad at\ y = \zeta e^{i\alpha(x - ct)} \tag{3.30a}$$

$$T_-^* = T_f^* + \zeta e^{i\alpha(x - ct)}(T_f^* - T_\infty^*)\vartheta_-'(0) + \cdots \qquad at\ y = \zeta e^{i\alpha(x - ct)} \tag{3.30b}$$

where the subscripts + and - refer to evaluating the quantity on the fuel and oxidizer side of the flame respectively. Since the temperature at the flame must

remain at the adiabatic flame temperature, the boundary condition on the disturbance temperature is

$$s_+ = -\zeta\,\vartheta_+'(0) \qquad at\ y = \zeta e^{ia(x-ct)} \tag{3.31a}$$

$$s_- = -\zeta\,\vartheta_-'(0) \qquad at\ y = \zeta e^{ia(x-ct)} \tag{3.31b}$$

Expanding the left hand sides in Taylor series about $y = 0$ allows this condition to be applied at $y = 0$. Similarly equation (3.28) gives

$$(s_+' + \zeta\vartheta_+'') + f^*(s_-' + \zeta\vartheta_-'') = 0 \qquad at\ y = 0 \tag{3.32}$$

The matching condition on the velocity distribution must be obtained from the equations of motion (3.2) and (3.3). Density ρ^*, viscosity μ_1^* and velocities u^* and v^* are continuous, therefore integrating equation (3.2) from $y_-^* = \zeta e^{ia(x-ct)} - \varepsilon$ to $y_+^* = \zeta e^{ia(x-ct)} + \varepsilon$ and letting $\varepsilon \to 0$ gives

$$\left[\mu_1^* \frac{\partial u^*}{\partial y^*}\right] = 0$$

where the square brackets denote a jump in the enclosed quantity across the flame. Since μ_1^* is continuous, this becomes

$$\left[f' + \zeta u''\right] = 0 \qquad at\ y = 0 \tag{3.33}$$

Forming the vorticity equation by differentiating equation (3.2) with respect to y^* and equation (3.3) with respect to x^* and integrating from y_-^* to y_+^* gives

$$\left[\frac{\partial}{\partial y^*}\left[\mu_1^*\frac{\partial u^*}{\partial y^*}\right]\right] = -\left[\frac{\partial \mu_1^*}{\partial y^*}\right]\frac{\partial v^*}{\partial x^*} + 2\frac{\partial}{\partial x^*}\left[\mu_1^*\frac{\partial v^*}{\partial y^*}\right] - \mu_1^*\left[\frac{\partial^2 v^*}{\partial x^* \partial y^*}\right] + \left[\frac{\partial}{\partial y^*}(\rho^* u^* v^*)\right]$$

Once again, the disturbance order equation is obtained by expanding the steady solution in Taylor series about $y = 0$ and substituting to get

$$\left[\mu'(f' + \zeta u''(0)) + (m' + \zeta\mu''(0))u'\right] + \left[\mu(f'' + \zeta u'''(0)) + (m + \zeta\mu'(0)u''\right]$$

$$= -\left[\mu'\right] i\alpha^2\varphi + i\mu\alpha^2\left[\varphi'\right]$$

Using the disturbance continuity equation (3.22) to replace φ' and equations (3.19) and (3.20) to replace μ', μ'' and m gives

$$\mu\left[f'' + \zeta u'''(0)\right] = \left(\frac{T_f}{T_\infty} - 1\right)\left[-i\alpha^2\dot{\mu}\varphi\left[\vartheta\right] - (f' + \zeta u''(0))\dot{\mu}\left[\vartheta\right] +\right.$$

$$\left. i\alpha^2\frac{\mu}{T}\left[\varphi\left[\vartheta\right] + i(u - c)\left[s\right]\right] - u'\dot{\mu}\left[s' + \zeta\vartheta'\right]\right] \qquad (3.34)$$

In summary, the matching conditions at $y = 0$ are

$$\left.\begin{array}{l} \varphi\ ,\ f \qquad \textit{continuous} \\ \\ \left[f' + \zeta u''\right] = 0 \\ \\ s_+ = -\zeta\vartheta_+'\ ,\ s_- = -\zeta\vartheta_-' \end{array}\right)$$

$$\left.\begin{aligned} &(s_+' + \zeta\vartheta_+'') + f^*(s_-' + \zeta\vartheta_-'') = 0 \\ &\mu\left[f'' + \zeta u'''\right] = \left(\frac{T_f}{T_\infty} - 1\right)\left[-i\alpha^2\dot{\mu}\varphi\left[\vartheta'\right] - (f' + \zeta u'')\dot{\mu}\left[\vartheta'\right] + \right. \\ &\left. i\alpha^2\frac{\mu}{T}\left[\varphi\left[\vartheta'\right] + i(u-c)\left[s\right]\right] - u'\dot{\mu}\left[s' + \zeta\vartheta'\right]\right] \end{aligned}\right\} \quad (3.35)$$

In the special case of a symmetric undisturbed flow, the disturbance can be expressed as a linear combination of antisymmetric and symmetric disturbances. The matching conditions can then be simplified to give boundary conditions at $y = 0$. For an antisymmetric disturbance

$$\left.\begin{aligned} &f = 0 \\ &f'' = -\zeta u_+''' + \left(\frac{T_f}{T_\infty} - 1\right)\left[\frac{\dot{\mu}}{\mu}(-i\alpha^2\varphi \right. \\ &\left. - (f' + \zeta u'')\vartheta_+') + \frac{i\alpha^2}{T}(\varphi - i\zeta(u-c)\vartheta_+')\right] \\ &s_+ = -\zeta\vartheta_+' \,,\; s_+' = -\zeta\vartheta_+'' \end{aligned}\right\} \quad at\ y = 0 \qquad (3.36)$$

For a symmetric disturbance

$$\varphi = f' = s_+ = \zeta = 0 \qquad at\ y = 0 \qquad (3.37)$$

3.2.2. *Replacement of the boundary conditions at infinity.*

Two different numerical algorithms are used to obtain a solution. These are the shooting method of Hieber and Gebhart, reference (3.12), 1971, and the difference method of Keller and Cebeci described in Cebeci and Bradshaw, reference (3.13), 1977. Both methods require a knowledge of the asymptotic behaviour of the solution as $y \to \infty$. For large y, the governing equations (3.21)-(3.23) reduce to

$$\varphi' = -if - i\left[\frac{T_f}{T_\infty} - 1\right]cs \tag{3.38}$$

$$f''' = (2\alpha^2 - i\beta\mathrm{Re})f' + (-i\alpha^4 - \alpha^2\beta\mathrm{Re})\varphi +$$

$$\left[-1 + \left[\frac{T_f}{T_\infty} - 1\right]\alpha\beta\right]s' \tag{3.39}$$

$$s'' = \alpha^2 s - i\beta PrRe\ s \tag{3.40}$$

Nachtsheim, reference (3.7), 1963, obtained the solution to these equations in the limit $\left[\frac{T_f}{T_\infty} - 1\right] \to 0$. When $\left[\frac{T_f}{T_\infty} - 1\right]$ is non-zero, these solutions are slightly changed and are of the form

$$f \to e^{\lambda x} \tag{3.41a}$$

$$\varphi \to Af\ ,\ s \to Bf \tag{3.41b}$$

where the quantities λ, A and B are given by

$$\lambda_{1\pm} = \pm\alpha\,,\quad A_{1\pm} = \frac{-i}{\lambda_{1\pm}},\quad B_{1\pm} = 0 \tag{3.42a}$$

$$\lambda_{2\pm} = \pm(\alpha^2 - i\beta Re)^{1/2}\,,\quad A_{2\pm} = \frac{-i}{\lambda_{2\pm}},\quad B_{2\pm} = 0 \tag{3.42b}$$

$$\left.\begin{aligned} \lambda_{3\pm} &= \pm(\alpha^2 - i\beta PrRe)^{1/2} \\ A_{3\pm} &= \frac{-i}{\lambda_{3\pm}} + \frac{i\beta^2 \mathrm{Re}^2 Pr(1-Pr)\left(\frac{T_f}{T_\infty} - 1\right)c}{\lambda_{3\pm}\left(\lambda_{3\pm}^2 - i\left(\frac{T_f}{T_\infty} - 1\right)\alpha\beta^2 \mathrm{Re}\quad(1-Pr)\right)} \\ B_{3\pm} &= \frac{-\beta^2 \mathrm{Re}^2 Pr(1-Pr)}{\lambda_{3\pm}^2 - i\left(\frac{T_f}{T_\infty} - 1\right)\alpha\beta^2 \mathrm{Re}\quad(1-Pr)} \end{aligned}\right\} \tag{3.42c}$$

The general solution of equations (3.38)-(3.40) which must match the numerical solution of equations (3.21)-(3.23) at the edge of the boundary layer, $y = y_e$, is

$$\left.\begin{aligned} f &= c_{1+}e^{\lambda_{1+}y_e} + c_{1-}e^{\lambda_{1-}y_e} + c_{2+}e^{\lambda_{2+}y_e} + c_{2-}e^{\lambda_{2-}y_e} + c_{3+}e^{\lambda_{3+}y_e} + c_{3-}e^{\lambda_{3-}y_e} \\ f' &= \lambda_{1+}c_{1+}e^{\lambda_{1+}y_e} + \lambda_{1-}c_{1-}e^{\lambda_{1-}y_e} + \lambda_{2+}c_{2+}e^{\lambda_{2+}y_e} + \lambda_{2-}c_{2-}e^{\lambda_{2-}y_e} + \\ &\quad \lambda_{3+}c_{3+}e^{\lambda_{3+}y_e} + \lambda_{3-}c_{3-}e^{\lambda_{3-}y_e} \end{aligned}\right\}$$

$$
\left.
\begin{aligned}
f'' &= \lambda_{1+}^2 c_{1+} e^{\lambda_{1+} y_e} + \lambda_{1-}^2 c_{1-} e^{\lambda_{1-} y_e} + \lambda_{2+}^2 c_{2+} e^{\lambda_{2+} y_e} + \lambda_{2-}^2 c_{2-} e^{\lambda_{2-} y_e} + \\
&\quad \lambda_{3+}^2 c_{3+} e^{\lambda_{3+} y_e} + \lambda_{3-}^2 c_{3-} e^{\lambda_{3-} y_e} \\
\varphi &= A_{1+} c_{1+} e^{\lambda_{1+} y_e} + A_{1-} c_{1-} e^{\lambda_{1-} y_e} + A_{2+} c_{2+} e^{\lambda_{2+} y_e} + A_{2-} c_{2-} e^{\lambda_{2-} y_e} + \\
&\quad A_{3+} c_{3+} e^{\lambda_{3+} y_e} + A_{3-} c_{3-} e^{\lambda_{3-} y_e} \\
s &= B_{3+} c_{3+} e^{\lambda_{3+} y_e} + B_{3-} c_{3-} e^{\lambda_{3-} y_e} \\
s' &= \lambda_{3+} B_{3+} c_{3+} e^{\lambda_{3+} y_e} + \lambda_{3-} B_{3-} c_{3-} e^{\lambda_{3-} y_e}
\end{aligned}
\right\} \quad (3.43)
$$

In order to satisfy the condition that all disturbances vanish as $y \to \infty$, it is necessary that $c_{1+} = c_{2+} = c_{3+} = 0$.

Solving equations (3.43) for c_{1+}, c_{2+} and c_{3+} using Cramer's rule gives three 6x6 determinants which when equated to zero provide three boundary condition equations to be applied at $y = y_e$. These are

$$s' + \lambda_{3+} s = 0 \qquad (3.44)$$

$$
f'' + \lambda_{1+} f' - \lambda_{2+}^2 (f + i\lambda_{1+}\varphi) - \frac{\left[\lambda_{3+}^2 - i\alpha\beta^2 \mathrm{Re}\left[\frac{T_f}{T_\infty} - 1\right] \quad (1 - Pr)\right]}{\lambda_{3+}^2 (\lambda_{1+} + \lambda_{3+})} s'
$$

$$
+ \left[\frac{T_f}{T_\infty} - 1\right] c \frac{\lambda_{2+}^2 \lambda_{1+}}{\lambda_{3+}^2} s' = 0 \qquad (3.45)
$$

$$f'' + \lambda_{2+}f' - \lambda_{1+}^2(f + i\lambda_{2+}\varphi) - \frac{\left[\lambda_{3+}^2 - i\alpha\beta^2 \mathrm{Re}\left[\frac{T_f}{T_\infty} - 1\right] \quad (1 - Pr)\right]}{\lambda_{3+}^2(\lambda_{2+} + \lambda_{3+})} s'$$

$$+ \left[\frac{T_f}{T_\infty} - 1\right] c \frac{\lambda_{1+}^2 \lambda_{2+}}{\lambda_{3+}^2} s' = 0 \qquad (3.46)$$

To avoid numerical difficulties when β is small, equation (3.45) is subtracted from equation (3.46) to give

$$f' + (\lambda_{1+} + \lambda_{2+})f + i\lambda_{1+}\lambda_{2+}\varphi + \frac{\left[\lambda_{3+}^2 - i\alpha\beta^2 \mathrm{Re}\left[\frac{T_f}{T_\infty} - 1\right] \quad (1 - Pr)\right]}{(\lambda_{1+} + \lambda_{3+})(\lambda_{2+} + \lambda_{3+})\lambda_{3+}^2} s'$$

$$+ \left[\frac{T_f}{T_\infty} - 1\right] c \frac{\lambda_{1+}\lambda_{2+}}{\lambda_{3+}^2} s' = 0 \qquad (3.47)$$

3.3. Numerical Solution

The eigenvalue problem posed by equations (3.21)-(3.23) with matching conditions, equations (3.35) at $y = 0$ and boundary conditions, equations (3.44),(3.45) and (3.47) at $y = y_e$ is solved using two different numerical algorithms. The first is the shooting method of Hieber and Gebhart, reference (3.12), 1971. In this method, the asymptotic expressions for f ,φ and s given by equations (3.41) and (3.42) are used directly as the starting point for the integration. Since the governing equations are linear, three bounded, linearly independent solutions can be obtained by separately using each of the exponentially decaying

asymptotic forms in turn. If the undisturbed flow is asymmetric, three more solutions are obtained by integrating from $y = -y_e$. That is f_i, φ_i and s_i must be found such that

$$f_i = e^{\lambda_i - y_e}\ ,\ \varphi_i = A_i - f_i\ ,\ s_i = B_i - f_i \qquad i = 1, 3 \quad at\ y = y_e$$

$$f_i = e^{\lambda_i + y_e}\ ,\ \varphi_i = A_i + f_i\ ,\ s_i = B_i + f_i \qquad i = 4, 6 \quad at\ y = -y_e$$

The solution can then be expressed as

$$f = f_1 + C_2 f_2 + C_3 f_3 + C_4 f_4 + C_5 f_5 + C_6 f_6$$

$$\varphi = \varphi_1 + C_2\varphi_2 + C_3\varphi_3 + C_4\varphi_4 + C_5\varphi_5 + C_6\varphi_6$$

$$s = s_1 + C_2 s_2 + C_3 s_3 + C_4 s_4 + C_5 s_5 + C_6 s_6$$

where the coefficient of f_1 has been chosen as unity, thereby fixing the arbitrary scale of the disturbance level. The six complex constants C_2–C_6 and ζ (the flame position) are determined by satisfying six of the seven matching conditions at $y = 0$. The seventh matching condition at $y = 0$ will be satisfied only if the four parameters, real and imaginary parts of α, β and Re , are appropriate. Note that since there is only one remaining complex boundary condition to be satisfied, two of these four parameters may be specified, the other two constituting the eigenvalues of the problem. Since the governing equations are nonlinear in α, β and Re , the eigenvalue must be determined using an iteration procedure. If, for example, the remaining boundary condition to be satisfied is φ continuous at $y = 0$, the real and imaginary parts of $z = \varphi(0^+) - \varphi(0^-)$ can be used as nonlinear functions of α, β and Re. By taking small increments in two of

the parameters, approximate derivatives of the real and imaginary parts of z with respect to those parameters can be obtained. Newton's method, or any other non-linear equation solver can then be used to find the values of the two parameters which satisfy $z = 0$.

The routine employed to integrate the governing equations was a CIT library routine using a Runge-Kutta-Gill starting procedure and an Adams-Moulton predictor-corrector formula for each subsequent step. Hieber and Gebhart, reference (3.12) obtained 1% accuracy in determining the real and imaginary parts of α when using this method to calclate the stability of a natural convection boundary layer generated by a vertical plate dissipating a uniform heat flux.

The second numerical method is a finite difference technique due to Keller and Cebeci described in Bradshaw and Cebeci, reference (3.13), 1977. It involves writing the governing equations as a system of twelve real first order equations of the form

$$\mathbf{f}_i' = fn\left\{\mathbf{f}_i, y, \alpha, \beta, Re; Pr, \left[\frac{T_f}{T_\infty} - 1\right]\right\} \qquad i = 1,2,\ldots 12, \quad y > 0$$

where

$$\mathbf{f}_1 = \mathrm{Re}(\varphi_+),\ \mathbf{f}_2 = \mathrm{Im}(\varphi_+),\ \mathbf{f}_3 = \mathrm{Re}(f_+),\ \mathbf{f}_4 = \mathrm{Im}(f_+)$$

$$\mathbf{f}_5 = \mathrm{Re}(f_+'),\ \mathbf{f}_6 = \mathrm{Im}(f_+'),\ \mathbf{f}_7 = \mathrm{Re}(f_+''),\ \mathbf{f}_8 = \mathrm{Im}(f_+'')$$

$$\mathbf{f}_9 = \mathrm{Re}(s_+),\ \mathbf{f}_{10} = \mathrm{Im}(s_+),\ \mathbf{f}_{11} = \mathrm{Re}(s_+'),\ \mathbf{f}_{12} = \mathrm{Im}(s_+')$$

If the undisturbed flow is asymmetric twelve more equations are obtained for

variables in the negative half plane, $y < 0$, by substituting $y' = -y$ in the governing equations (3.21)-(3.23). Both sets of equations are thenvalid in the range $0 < y < y_e$, which is divided into J segments. The derivatives are then replaced by a finite difference approximation evaluated at the mid-point of each segment.

$$\mathbf{f}_i^j - \mathbf{f}_i^{j-1} = \Delta y_j \, fn\left\{\left[\frac{\mathbf{f}_i^j + \mathbf{f}_i^{j-1}}{2}\right], \left[\frac{y_j + y_{j-1}}{2}\right], \alpha, \beta, Re; Pr, \left[\frac{T_f}{T_\infty} - 1\right]\right\}$$

$$i = 1, 24 \qquad j = 0, J \tag{3.48}$$

where $\mathbf{f}_i^j$ is the value of $\mathbf{f}_i$ evaluated at $y = y_j$, the end point of the jth segment. An additional twelve conditions, six at each of $y = y_e$ and $y = -y_e$, $(j = J)$, are obtained from the boundary conditions, equations (3.44), (3.45) and (3.47). ζ can be eliminated from the matching conditions, equations (3.35) to leave twelve more equations for the variables at $y = 0$, $(j = 0)$. These equations are of the form

$$\left.\begin{aligned} fn\left\{\mathbf{f}_i^0, 0, \alpha, \beta, Re; Pr, \left[\frac{T_f}{T_\infty} - 1\right]\right\} = 0 \\ fn\left\{\mathbf{f}_i^J, y_J, \alpha, \beta, Re; Pr, \left[\frac{T_f}{T_\infty} - 1\right]\right\} = 0 \end{aligned}\right\} \tag{3.49}$$

Equations (3.48) and (3.49) constitute a 24(J+1) set of homogeneous equations in the 24(J+1) unknowns $\mathbf{f}_i^j$, $j = 0,..J$, $i = 1,..24$. To obtain a non-trivial solution for the $\mathbf{f}_i^j$'s, the determinant of the 24(J+1) x 24(J+1) coefficient matrix, which is non-linear in α,β and Re , must be zero. To find the eigenvalues which

accomplish this, a special iteration procedure is employed. Instead of using the homogeneous boundary conditions, equations (3.49), at $y = 0$, the condition $(s_+' + \zeta\vartheta_+'') + f^*(s_-' + \zeta\vartheta_-'')$ is replaced by

$$s_+ - s_- = 1 \tag{3.50}$$

thus fixing the arbitrary amplitude of the disturbance. The value of the two unspecified parameters, say α_R and α_I, where the subscripts refer to the real and imaginary parts of α, must be determined so that the dropped boundary condition is satisfied.

The complete system of difference equations and altered boundary conditions can be written as

$$\mathbf{R}_{kl}\Delta_l = R_k \tag{3.51}$$

where $\Delta_l = \mathbf{f}_i^j$ such that $l = i + 24j$, $i = 1,..24$, $j = 0,..J$ i.e the Δ_l's are the unknown quantities $\mathbf{f}_i$ evaluated at each of the (J+1) mesh points in turn. The solution of equation (3.51) can be obtained by the block elimination method described in Bradshaw and Cebeci, reference (3.13), Appendix 7A. Now with β and Re fixed

$$\Delta_l = \Delta_l(\alpha_R,\alpha_I)$$

The boundary condition which must still be satisfied is

$$z_1(\alpha_R,\alpha_I) = \left[\Delta_{11} - \frac{\vartheta_+''}{\vartheta_+'}\Delta_9\right] - f^*\left[\Delta_{23} + \frac{\vartheta_-''}{\vartheta_-'}\Delta_{21}\right] = 0 \tag{3.52a}$$

$$z_2(\alpha_R,\alpha_I) = \left[\Delta_{12} - \frac{\vartheta_+''}{\vartheta_+'}\Delta_{10}\right] - f^*\left[\Delta_{24} + \frac{\vartheta_-''}{\vartheta_-'}\Delta_{22}\right] = 0 \qquad (3.52b)$$

Here ζ has been eliminated using equations (3.49) and the substitution $y' = -y$ has been made for $y < 0$ as it was in the governing equations. The two equations (3.52) are solved using Newton's method. Specifically if α_R^ν and α_I^ν are the νth iterates, then the $(\nu+1)th$ iterates are determined by using $\alpha_R^{(\nu+1)} = \alpha_R^\nu + \delta\alpha_R^\nu$ and $\alpha_I^{(\nu+1)} = \alpha_I^\nu + \delta\alpha_I^\nu$ in equation (3.52), expanding about $\delta\alpha_R^\nu = \delta\alpha_I^\nu = 0$ and retaining only linear terms in the expansion. This gives the linear system

$$z_1^\nu + \left(\frac{\partial z_1}{\partial \alpha_R}\right)^\nu \delta\alpha_R^\nu + \left(\frac{\partial z_1}{\partial \alpha_I}\right)^\nu \delta\alpha_I^\nu = 0 \qquad (3.53a)$$

$$z_2^\nu + \left(\frac{\partial z_2}{\partial \alpha_R}\right)^\nu \delta\alpha_R^\nu + \left(\frac{\partial z_2}{\partial \alpha_I}\right)^\nu \delta\alpha_I^\nu = 0 \qquad (3.53b)$$

where $z_i^\nu = z_i(\alpha_R^\nu,\alpha_I^\nu)$. Equations (3.53) can be solved to give

$$\delta\alpha_R^\nu = \frac{z_1^\nu\left(\frac{\partial z_2}{\partial \alpha_R}\right)^\nu - z_2^\nu\left(\frac{\partial z_1}{\partial \alpha_R}\right)^\nu}{D}$$

$$D = \left(\frac{\partial z_1}{\partial \alpha_R}\right)^\nu\left(\frac{\partial z_2}{\partial \alpha_I}\right)^\nu - \left(\frac{\partial z_2}{\partial \alpha_R}\right)^\nu\left(\frac{\partial z_1}{\partial \alpha_I}\right)^\nu$$

$$\delta\alpha_I^\nu = -\frac{z_1^\nu + \delta\alpha_I^\nu\left(\frac{\partial z_1}{\partial \alpha_I}\right)^\nu}{\left(\frac{\partial z_1}{\partial \alpha_R}\right)^\nu}$$

The derivatives of z_1 and z_2 are easily obtained by differentiating equation (3.51)

$$\mathrm{R}\left(\frac{\partial \Delta}{\partial \alpha_R}\right)^{\nu} = -\left(\frac{\partial \mathrm{R}}{\partial \alpha_R}\right)^{\nu} \Delta^{\nu}$$

$$\mathrm{R}\left(\frac{\partial \Delta}{\partial \alpha_I}\right)^{\nu} = -\left(\frac{\partial \mathrm{R}}{\partial \alpha_I}\right)^{\nu} \Delta^{\nu}$$

and substituting in equations (3.52). Solving for all of the required derivatives is therefore accomplished by solving two linear systems with the *same coefficient matrix* R , already computed and factored, that was used to solve equation (3.51). This provides an efficient way to improve the guessed values of α_R and α_I. The disadvantage of this method is the large amount of storage required by the coefficient matrix.

3.4. Inviscid Stability Equations

By setting $Re = \infty$ in equations (3.21)-(3.23), the inviscid Orr-Sommerfeld equation for variable density flow is found to be

$$(u - c)\left(\varphi'' - \alpha^2 \varphi\right) - u'' \varphi = \left(\frac{T_f}{T_\infty} - 1\right) \frac{\vartheta'}{T} \left(\varphi'(u - c) - u' \varphi\right) \qquad (3.54)$$

with boundary conditions

$$\varphi(0) = 0\,, \quad \varphi \to 0 \quad as\ y \to \infty \qquad (Symmetric\ Disturbance) \qquad (3.55a)$$

$$\varphi'(0) = 0\,, \quad \varphi \to 0 \quad as\ y \to \infty \qquad (Antisymmetric\ Disturbance) \qquad (3.55b)$$

The solution for the eigenvalue is easily obtained by employing a shooting method starting from the asymptotic behaviour $\varphi \to e^{-\alpha y}$ *as* $y \to \infty$, integrating

to $y = 0$, and iterating to satisfy the appropriate boundary condition. If the undisturbed flow is asymmetric the integration is also performed from negative infinity using $\varphi \to e^{\alpha y}$ as $y \to -\infty$ and the matching conditions φ, φ' continuous are imposed at $y = 0$. A discussion of the difficulties associated with calculating neutral and stable eigenvalues (i.e $\alpha_I \geq 0$) is contained in Lin, reference (3.14), 1955, chapter 8.

References.

(3.1) R. BETCHOV and W. O CRIMINALE, Jr. ,Stability of Parallel Flows, *Academic Press* (1967)

(3.2) S. I PAI, On the Stability of Two-Dimensional Laminar Jet Flow of Gas, *J. Aero. Sci.* **18**, 731, (1951)

(3.3) N. CURLE, On Hydrodynamic Stability in Unlimited Fields of Viscous Flow, *Proc. Roy. Soc. Series A*, **238**, 489, (1956)

(3.4) T. TATSUMI and T. KAKUTANI, The Stability of a Two-Dimensional Laminar Jet, *JFM* **4** 261, (1958)

(3.5) R. E. KAPLAN, The Stability of Laminar Incompressible Boundary Layers in the Presense of Compliant Boundaries, *MIT Report ASRL TR116-1* Chapter 8, (1964)

(3.6) J. E. PLAPP, I. Laminar Boundary Layer Stability in Free Convection. II. Laminar Free Convection with Variable Fluid Properties, *Ph.D Thesis, California Institute of Technology*, (1957)

(3.7) J. E. PLAPP, The Analytic Study of Laminar Boundary-Layer Stability in Free Convection, *J. Aero. Sci.* **24**, 318, (1957)

(3.8) P. R. NACHTSHEIM, Stability of Free-Convection Boundary-Layer Flows, *NASA TN D-2089*, (1963)

(3.9) L. PERA and B. GEBHART, On the Stability of Laminar Plumes: Some Numerical Solutions and Experiments, *Int. J. Heat Mass Trans.* **14**, 975, (1971)

(3.10) L. LEES and C. C. LIN, Investigation of the Stability of the Laminar Boundary Layer in a Compressible Fluid, *NACA TN 1115*, (1946)

(3.11) L. LEES and E. RESHOTKO, Stability of the Compressible Laminar Boundary Layer, *JFM* **12**, 555, (1962)

(3.12) C. A. HIEBER and B. GEBHART, Stability of Vertical Natural Convection Boundary Layers: Some Numerical Solutions, *JFM* **48**, 625, (1971)

(3.13) T. CEBECI and P. BRADSHAW, Momentum Transfer in Boundary Layers, *McGraw-Hill* , Chapter 9, (1977)

(3.14) C. C. LIN, The Theory of Hydrodynamic Stability, *Camb. Univ. Press*, Chapter 8, (1955)

Chapter 4.

THE INSTABILITY OF BUOYANT DIFFUSION FLAMES

Although the stability of the convecting flow generated by a diffusion flame bears a superficial similarity to the corresponding problem for the laminar buoyant plume, Pera and Gebhart, reference (4.1), 1971, the differences are very significant.

First, the steady velocity and temperature profiles are quite different from those of the buoyant plume, particularly the temperature profile, which has both a constant value and a discontinuity in its slope at the flame. The differences are even more pronounced by non-unit stoichiometry, when the flame becomes very asymmetric. Second, the presence of the flame sheet introduces a set of matching conditions on the velocity and temperature disturbances at $y=0$, quite different from the simple continuity requirements for the plume. Finally, all analyses of the buoyant plume have assumed that density variations are important only in the body force term of the equations of motion. This approximation, attributed to Boussinesq, is not applicable for the flame, where density differences in the steady flow are large compared to unity.

Four different base flows have been considered in this chapter, these being the symmetric flame, i.e unit stoichiometric ratio, employing the Boussinesq approximation, which is obtained by artificially setting $\left[\frac{T_f}{T_\infty}-1\right]=0$ in all terms of the stability equations except the Reynolds number, and with $\left[\frac{T_f}{T_\infty}-1\right]=6$, and the asymmetric flame with a stoichiometric ratio the same as methane burning in air, also with both the Boussinesq approximation and $\left[\frac{T_f}{T_\infty}-1\right]=6$. In all cases, the fuel and oxidizer are assumed to have the same density at infinity and are therefore quiescent outside the boundary layer. These base

profiles are shown in figures (2.2)-(2.5), and have unit Lewis number and $Pr = 0.72$. Symmetric disturbances were found to be much more stable than antisymmetric disturbances, so the results presented in this chapter are for the antisymmetric mode.

The results for a symmetric flame using the Boussinesq approximation are given in figures (4.1)-(4.7). Figures (4.1) and (4.2) show the dimensionless frequency, β, and real part of the wave number α_R plotted against Reynolds number for several choices of the dimensionless spatial amplification rate α_I. At a Reynolds number of 200, the neutral stability curve ($\alpha_I = 0$) has closely approached its asymptote of $\beta = 0.444$, $\alpha_R = 1.42$ obtained by solving the inviscid Orr-Sommerfeld equation. Lowering the Reynolds number decreases the frequency and wave number of the neutral curve but increases the amplification rates, especially for low frequency disturbances. Since it is the growth in the amplitude of the disturbance as it is convected downstream which leads to transition and turbulence, Smith, reference (4.2), 1956, the increased amplification rates at low Reynolds number indicate that viscosity has a destabilising influence on the flow.

An important feature of the stability diagram, figure (4.1), is that the neutral stability curve has no minimum. This is somewhat surprising, since laminar jet flow does exhibit a critical Reynolds number, below which all disturbances are stable. This was first demonstrated analytically by Curle, reference (4.3), 1956, and calculated numerically by Kaplan, reference (4.4), 1964. In the case of the buoyant plume, Pera and Gebhart, reference (4.1), 1971, no critical Reynolds number was found, indicating that this might be a feature of boundary-free, natural convection flows, in which, unlike the laminar jet, total momentum is not constant due to the effects of buoyancy. In the present case, the neutral stability curve is found to cross the zero frequency axis and continue to indefinitely large negative frequencies as the Reynolds number is reduced. It can also be seen in figure (4.1) that some of the constant amplification rate

contours also cross the $\beta = 0$ axis.

At first it might seem that these disturbances, which have a phase velocity vertically downwards, must be stable since amplification occurs as disturbances propagate in the upwards direction, however the group velocity, given by $c_G = \frac{\partial \beta_R}{\partial \alpha_R}$ is positive, and since the group velocity is associated with the energy propagation of the disturbance, these disturbances are amplified. In a series of papers, references (4.5)-(4.8), (1963, 1965a,b, 1968), Gaster proposed that spatial and temporal amplification rates can be related by the linearized formula

$$\alpha_I = \frac{-\alpha_R}{c_G} c_{I\,temp} + O(c_I^2) \qquad (4.1)$$

Thus for the disturbances to grow with time, the product $\alpha_I c_G$ must be negative. By considering a laminar boundary layer disturbed by a point source of the form

$$q(x,t) = \delta(x)\cos\omega t \qquad t > 0$$

$$= 0 \qquad t < 0$$

which simulates a vibrating ribbon, Gaster, 1965b, showed that spatially growing disturbances result and that the disturbance propagates downstream if $\frac{\partial \alpha_R}{\partial \beta_R} > 0$.

Consider figure (4.3) which gives α_R and α_I as functions of β at a Reynolds number of 10. The eigenvalue solution at this Reynolds number is quite complicated due to the presence of discontinuities which will be discussed presently. First, consider the branch of the solution which exists for $\beta > 0$. At a frequency

$\beta = 0.149$, $\alpha_I = 0$, thus the disturbance is neutrally stable. As β is reduced, the wave number α_R decreases to a minimum near $\beta = -0.018$, after which it increases until this branch ceases to be valid at $\beta \approx -0.045$. The minimum at $\beta \approx -0.018$ represents a change in the sign of c_G, and is therefore a limiting stability curve for this solution branch. Consider β to be a complex function of α. Then

$$\frac{d\beta}{d\alpha} = \frac{\partial \beta_R}{\partial \alpha_R} + i \frac{\partial \beta_I}{\partial \alpha_R} = \frac{1}{\frac{d\alpha}{d\beta}}$$

$$= \frac{\frac{\partial \alpha_R}{\partial \beta_R} - i \frac{\partial \alpha_I}{\partial \beta_R}}{\left(\frac{\partial \alpha_R}{\partial \beta_R}\right)^2 + \left(\frac{\partial \alpha_I}{\partial \beta_R}\right)^2}$$

thus

$$c_G = \frac{\partial \beta_R}{\partial \alpha_R} = \frac{\frac{\partial \alpha_R}{\partial \beta_R}}{\left(\frac{\partial \alpha_R}{\partial \beta_R}\right)^2 + \left(\frac{\partial \alpha_I}{\partial \beta_R}\right)^2} \tag{4.2}$$

The group velocity is therefore positive for $-0.18 < \beta < -0.149$, so these disturbances propagate vertically upwards. Thus, since $\alpha_I < 0$, these disturbances are unstable. For $-0.45 < \beta < -0.018$, c_G is negative and the disturbances are stable.

Now consider the behaviour near $\beta = -0.045$. The asymptotic behaviour as $y \to \infty$ of the solution is given by equations (3.41) and (3.42). One of the three independent solutions as $y \to \infty$ is given by

$$f \rightarrow e^{-(\alpha^2 - i\beta Re)^{\frac{1}{2}} y} \qquad as\ y \rightarrow \infty$$

Consider $\lambda^2 = \alpha^2 - i\beta \mathrm{Re} = (\alpha_R^2 - \alpha_I^2) + i(2\alpha_R\alpha_I - \beta Re)$. When $\beta > 0$, $\alpha_I < \alpha_R$ and λ^2 is in the fourth quadrant of the complex plane, figure (4.4). As β is reduced, α_I increases and α_R decreases until at $\beta \approx -0.011$, α_I and α_R are equal. λ^2 now enters the third quadrant of the complex plane. At $\beta \approx -0.045$, the imaginary part of λ^2 becomes zero. If the same branch of the square root is used as the imaginary part of λ^2 crosses zero to become positive, the real part of λ^2 will change sign from positive to negative, thus violating the boundary condition that disturbances must vanish as $y \rightarrow \infty$. This solution branch therefore is no longer valid for $\beta < -0.045$.

Now consider the branch which exists for large negative β in figure (4.3). The group velocity is positive for $-0.159 \leq \beta \leq -0.03$ then changes sign for $-0.03 \leq \beta \leq -0.019$. At $\beta \approx -0.019$, by an argument exactly analogous to the preceding one, it can be seen that the boundary condition at infinity is violated due to a change of sign in the asymptotic form $f \rightarrow e^{-(\alpha^2 - i\beta Pr Re)^{\frac{1}{2}} y}$. Similarly at $\beta \approx -0.159$, α_R changes sign, causing this branch to become invalid. A third branch also exists which does not lose validity in this manner, however over its entire calculated range, its group velocity remains negative, therefore this branch is not investigated further. Below $\beta = -0.159$, no unstable solutions appeared.

Returning to figure (4.1), this behaviour has been summarised. The dashed line which marks the limiting stability curve for negative β corresponds to the loss of validity of the solution when α_R changes sign. The dashed lines which are shown near the $\beta = 0$ axis for small Reynolds numbers indicate either the loss of validity of a solution branch, or the change in sign of c_G if this occurs first, as it did in figure (4.3). The position of these lines is very approximate due to the

excessive number of calculations necessary to obtain accuracy. Note that at very low Reynolds numbers, where the amplification rates start to decline, these discontinuities in the solution no longer occur. It is therefore possible to take a path between any two points in the $\beta - \mathrm{Re}$ plane, along which α_R and α_I vary continuously.

The solution of the inviscid Orr-Sommerfeld equations for this flow is presented in figure (4.5). Note that the maximum amplification rate is slightly less than $\alpha_I = -0.18$, so the $\alpha_I = -0.18$ contours shown in figures (4.1) and (4.2) close at some finite Reynolds number. The negative phase velocity branch of the solution is also present in the inviscid limit, but could not be determined in the range $-0.0058 < \beta < 0$. This difficulty can be examined by considering the inviscid equation for the function $f(y) = \frac{\varphi(y)}{(u-c)}$, Lin, reference (4.9), 1955, chapter 8.

$$\frac{d}{dy}\left[(u-c)^2 f'\right] - \alpha^2 (u-c)^2 f = 0 \tag{4.3}$$

Multiplying this equation by the complex conjugate of f and integrating over the range $-\infty < y < \infty$ gives

$$I = \int_{-\infty}^{\infty} (u-c)^2 \left[|f'|^2 + \alpha^2 |f|^2\right] dy = 0 \tag{4.4}$$

where the first term has been integrated by parts once. Consider the real part of this integral

$$\mathrm{Re}(I) = \int_{-\infty}^{\infty} \left[(u-c_R)^2 - c_I^2\right]\left[|f'|^2 + (\alpha_R^2 - \alpha_I^2)|f|^2\right] dy$$

$$+ 2c_I \int_{-\infty}^{\infty} (u - c_R) 2\alpha_I \alpha_R |f|^2 dy = 0 \qquad \Bigg\} \quad (4.5)$$

where

$$c = c_R + ic_I = \frac{\beta}{(\alpha_R^2 + \alpha_I^2)} (\alpha_R - i\alpha_I)$$

If $\alpha_R^2 < \alpha_I^2$, this relation can clearly be satisfied, however if $\alpha_I^2 < \alpha_R^2$ and α_I^2 is sufficiently small, the second term in this expression can become small compared to the first and the solution will not exist. In figure (4.5), α_I^2 becomes less than α_R^2 at $\beta \approx -0.0058$. The solution either ceases to exist shortly after this point, or it changes very rapidly. There is some numerical evidence to suggest that the latter is the case, however convergence became very slow, making the results inconclusive. Note that the inviscid solution for the symmetric flame with $\left[\frac{T_f}{T_\infty} - 1\right] = 6$, figure (4.13), and also for the buoyant plume, presented in the next chapter, do not display this behaviour; the negative phase velocity solution is continuous up to $\beta = 0$.

It should be noted that at low Reynolds number, both the parallel flow assumption used in the stability theory, and the boundary layer simplification used to find the steady base flow become poor approximations. Non-parallel effects have been studied for the laminar jet by Haaland, reference (4.10), 1972, and Bajaj and Garg, reference (4.11), 1977, who accounted for only some of the non-parallel terms, and more recently by Garg, reference (4.12), 1981, who included the effects of the transverse velocity component, the streamwise variation of the base flow and of the disturbance amplitude, wave number and growth rate. Garg found that including these effects increased the critical Reynolds number from $Re_c \approx 4$ to $Re_c \approx 21.6$ and moved the lower branch of the neutral stability curve to higher frequencies. For the buoyant plume, non-parallel

effects have been studied by Haaland and Sparrow, reference (4.13), 1973, and more comprehensively by Hieber and Nash, reference (4.14), 1975. Hieber and Nash used a higher order boundary-layer theory for the steady base flow, but did not consider streamwise variation of the disturbance amplitude. They found that a critical Reynolds number, $Re_c \approx 15$, does exist, below which all disturbances are stable, and that the neutral stability curve does have a lower branch. It is therefore expected that the low Reynolds number region in the present analysis would also be considerably modified by removing the parallel flow assumption. In particular, the negative phase velocity region of the stability region of the diagram is likely to be significantly different, since these disturbances have very long wavelengths.

Figures (4.6) and (4.7) give a more physical representation of the solution. Here the frequency and wave number have been non-dimensionalised using fixed time and length scales, rather than using the boundary layer thickness and velocity to supply scales which vary with Reynolds number. The new variables, denoted by a superscript +, are related to the dimensional variables, denoted by a superscript * and the previous dimensionless variables by

$$\left.\begin{aligned} \beta^+ &= \beta^* \left(\frac{\nu^*}{\left(\frac{T_f}{T_\infty} - 1 \right) g^{*2}} \right)^{\frac{1}{3}} = \beta \, \mathrm{Re}^{\frac{1}{3}} \\ \alpha^+ &= \alpha^* \left(\frac{\nu^{*2}}{\left(\frac{T_f}{T_\infty} - 1 \right) g^*} \right)^{\frac{1}{3}} = \alpha \, \mathrm{Re}^{\frac{-1}{3}} \end{aligned}\right\} \qquad (4.6)$$

It is now clear that all frequencies eventually become unstable as the Reynolds number is increased, since the neutral curve has an asymptote $\beta^+ \rightarrow 0.444 \mathrm{Re}^{\frac{1}{3}}$. The most amplified disturbances will, however, be at the lower frequencies which

become unstable at small Reynolds numbers.

The effect of non-unit stoichiometry is examined in figures (4.8) and (4.9). This calculation is for a stoichiometric ratio the same as methane burning in air, and also uses the Boussinesq approximation. The stability diagrams are very similar in form to those for the symmetric flame, figures (4.1) and (4.2). The neutral stability curve has moved to lower frequencies, however the amplification rates are somewhat increased. The asymmetry of the flame therefore slightly destabilises the flame.

The coupling between the temperature and momentum disturbance equations is inversely proportional to Reynolds number, and furthermore, when the Boussinesq approximation is employed, the steady temperature profile appears only in the temperature disturbance equation. Any differences between the stability of the symmetric and asymmetric flames at large Reynolds numbers must therefore arise from differences in the velocity profiles alone. Consider figures (2.2) and (2.4). Most of the asymmetry of the flow in figure (2.4) is contained in the temperature and mass fraction profiles. If these are ignored, the velocity profile is seen to be quite similar to that for the symmetric flame. It is therefore not unreasonable that non-unit stoichiometry has a relatively small effect on the stability of the flame, especially at large Reynolds numbers.

A much greater effect on the stability curve is obtained when the Boussinesq approximation is removed. Consider the stability of the symmetric flame with $\left[\frac{T_f}{T_\infty} - 1\right] = 6$, shown in figures (4.10) to (4.15). In this calculation, the relation between viscosity and temperature is taken to be $\frac{\mu^*}{\mu_\infty^*} = \left[\frac{T^*}{T_\infty^*}\right]^{0.66}$, from White, reference (4.15), 1974. This formula is accurate to within $\pm 4\%$ in the temperature range $210° - 1900° K$. The neutral stability curve has shifted to frequencies a factor of ten lower than when the Boussinesq approximation was employed and the amplification rates are also considerably reduced. Furthermore, the

neutral stability curve for positive phase velocity waves is no longer the limiting curve for instability. Instead it has been replaced by the line of discontinuity corresponding to the loss of validity of the solution as α_R changes sign. This is shown in figure (4.10) by a dashed line which starts at Re = 20, $\beta = -0.045$, and continues to larger Reynolds numbers. These disturbances have positive group velocities, despite a negative phase velocity, and clearly play an important role in the instability of the flame when large density variations are considered.

The dashed line which extends to smaller Reynolds numbers, starting at Re = 20, $\beta = -0.045$, also indicates a limiting stability curve, but now it corresponds to a change in the sign of the group velocity rather than in the sign of α_R. This is shown more clearly in figure (4.12) which shows the variation of α_R and α_I with β at Re = 10. The change in the sign of $\frac{\partial \alpha_R}{\partial \beta}$ near $\beta = -0.04$ indicates a change in the sign of the group velocity. For $\beta < -0.04$, disturbances are propagated in the vertically downward direction and decay in amplitude. Once again the dashed lines near the $\beta = 0$ axis in figure (4.10) indicate a loss of validity of a branch of the solution as discussed previously.

The inviscid solution is presented in figure (4.13). In comparison with figure (4.5) where the Boussinesq approximation was employed, there are several points of interest. The maximum amplification rates are approximately the same in the two cases, which is somewhat surprising since for Reynolds numbers less than 200, the amplification rates were significantly smaller when the Boussinesq approximation was removed. The relative importance of the positive and negative frequency regions has changed considerably, the negative frequency branch now extending to higher frequencies than the positive branch. The negative branch also exhibits a change in the sign of the group velocity at $\beta \approx -0.018$. For disturbances with frequencies in the range $0 < \beta < -0.018$, amplification does not occur, but for $-0.112 < \beta < -0.018$, the disturbances are unstable.

In figures (4.14) and (4.15), the dimensionless form of equation (4.6) is used. Once again, it is clear that all frequencies eventually become unstable, however frequencies less than 10 Hz will undergo greater amplification than higher frequencies. These highly amplified disturbances have wavelengths of a few centimeters.

In figures (4.16) and (4.17) the asymmetry of the base flow is again seen to modify the stability diagram by a relatively small amount. The flame is somewhat destabilised however, since both the limiting stability curves and the amplification rates are moved to higher values.

The effect of removing the Boussinesq approximation is demonstrated in figures (4.18) and (4.19). Here the inviscid Orr-Sommerfeld equation for variable density flows had been solved for the range of flame temperatures $0 < \left[\frac{T_f}{T_\infty} - 1\right] < 10$. Figure (4.18) shows the inviscid asymptote α_R^N and β^N for the neutral stability curve, $\alpha_I^N = 0$, the phase velocity of the neutral disturbance c^N and the asymptote α_I^L, β^L, of the limiting stability curve $\alpha_R^L = 0$, as a function of $\left[\frac{T_f}{T_\infty} - 1\right]$. All show a large change as $\left[\frac{T_f}{T_\infty} - 1\right]$ increases from zero to ten, especially β^N which decreases by a factor of ten and α_R^N which decreases by a factor of three.

In figure (4.19) the temperature dependence of the length and time scales used for non-dimensionalisation has been removed. The new variables are

$$\bar{\beta} = \frac{\beta^*}{\left[\frac{g^* x^{*3}}{\nu^{*2}}\right]^{\frac{1}{4}} \left[\frac{2g^*}{x^*}\right]^{\frac{1}{2}}} = \beta \left[\frac{T_f}{T_\infty} - 1\right]^{\frac{3}{4}}$$

$$\left.\begin{aligned} \bar{\alpha} &= \frac{\alpha^* \sqrt{2} x^*}{\left[\frac{g^* x^{*3}}{\nu^{*2}}\right]^{\frac{1}{4}}} = \alpha \left[\frac{T_f}{T_\infty} - 1\right]^{\frac{1}{4}} \\ \bar{c} &= \frac{c^*}{2\sqrt{g^* x^*}} = c \left[\frac{T_f}{T_\infty} - 1\right]^{\frac{1}{2}} \end{aligned}\right\} \qquad (4.7)$$

For $\left[\frac{T_f}{T_\infty} - 1\right] > 2$, these show little variation with flame temperature except for $\bar{\beta}^L$, the negative frequency at which $\alpha_R = 0$, and c^r, which is the ratio between the phase velocity of the neutral disturbance c^N, and the maximum velocity in the flow.

In summary, it has been found that the convective flow generated by a vertical diffusion flame is very unstable, all disturbance frequencies eventually becoming unstable at sufficiently large Reynolds numbers. A new unstable regime has been discovered, consisting of waves with negative phase velocity but positive group velocity. These disturbances have very long wavelengths making the parallel flow assumption questionable, however their existence is confirmed by solving the inviscid disturbance equations. Since the wavelength of these disturbances is long compared to the plume thickness, the stability of the plume might profitably be investigated by an analysis considering the plume thickness to be negligibly small compared to the wavelength. Variation of flow parameters, such as momentum flux and buoyancy, with Reynolds number could then be included and their effects on the stability of the flow examined. This has been undertaken in Chapter 6.

Comparison of the flame stability diagrams using the Boussinesq approximation with those for the buoyant plume, determined by Pera and Gebhart, reference (4.1), 1971, shows some similarity in the neutral stability curve, however

more extensive calculations are required for the buoyant plume before other features of the stability diagrams can be compared. This will be pursued in Chapter 5.

Finally, it is found that the variable density effects due to high temperature differences in the flame can not be adequately handled using the Boussinesq approximation. Instead the full variable density stability equations, developed in Chapter 3 must be employed.

References.

(4.1) L. PERA and B. GEBHART, On the Stability of Laminar Plumes: Some Numerical Solutions and Experiments, *Int. J. Heat Mass Trans.* **14**, 975, (1971)

(4.2) A. M. O. SMITH, Transition, Pressure Gradient, and Stability Theory, *9th Int. Congress of App. Mech.* **4**, 234, (1956)

(4.3) N. CURLE, On Hydrodynamic Stability in Unlimited Fields of Viscous Flow, *Proc. Roy. Soc. Series A*, **238**, 489, (1956)

(4.4) R. E. KAPLAN, The Stability of Laminar Incompressible Boundary Layers in the Presense of Compliant Boundaries, *MIT Report ASRL TR116-1* Chapter 8, (1964)

(4.5) M. GASTER, A Note on the Relation between Temporally-Increasing and Spatially-Increasing Disturbances in Hydrodynamic Stability, *JFM* **14** 222, (1963)

(4.6) M. GASTER, The Role of Spatially Growing Waves in the Theory of Hydrodynamic Stability, *Prog. in Aero. Sci.* **6** 251, (1965a)

(4.7) M. GASTER, On the Generation of Spatially Growing Waves in a Boundary Layer, *JFM* **22** 433, (1965b)

(4.8) M. GASTER, Growth of Disturbances in Both Space and Time, *The Physics of Fluids* **11** 723, (1968)

(4.9) C. C. LIN, The Theory of Hydrodynamic Stability, *Camb. Univ. Press*, Chapter 8, (1955)

(4.10) S. E. HAALAND, Contributions to Linear Stability Theory of Nearly Parallel Flows, *PhD Thesis, Fluid Mechanics Program, University of Minnesota, Minneapolis Minnesota* , (1972)

(4.11) A. K. BAJAJ and V. K. GARG, Linear Stability of Jet Flows, *J. App. Mech.* **44** 378, (1977)

(4.12) V. K. GARG, Spatial Stability of the Non-Parallel Bickley Jet, *JFM* **102** 127, (1981)

(4.13) S. E. HAALAND and E. M. SPARROW, Stability of Buoyant Boundary Layers and Plumes, Taking Account of Nonparallelism of the Basic Flows, *J. Heat Trans.* **95c** 295, (1973)

(4.14) C. A. HIEBER and E. J. NASH, Natural Convection above a Line Heat Source: Higher-Order Effects and Stability, *Int. J. Heat Mass Trans.* **18** 1473, (1975)

(4.15) F. M. WHITE , Viscous Fluid Flow, *McGraw-Hill, (1974)*

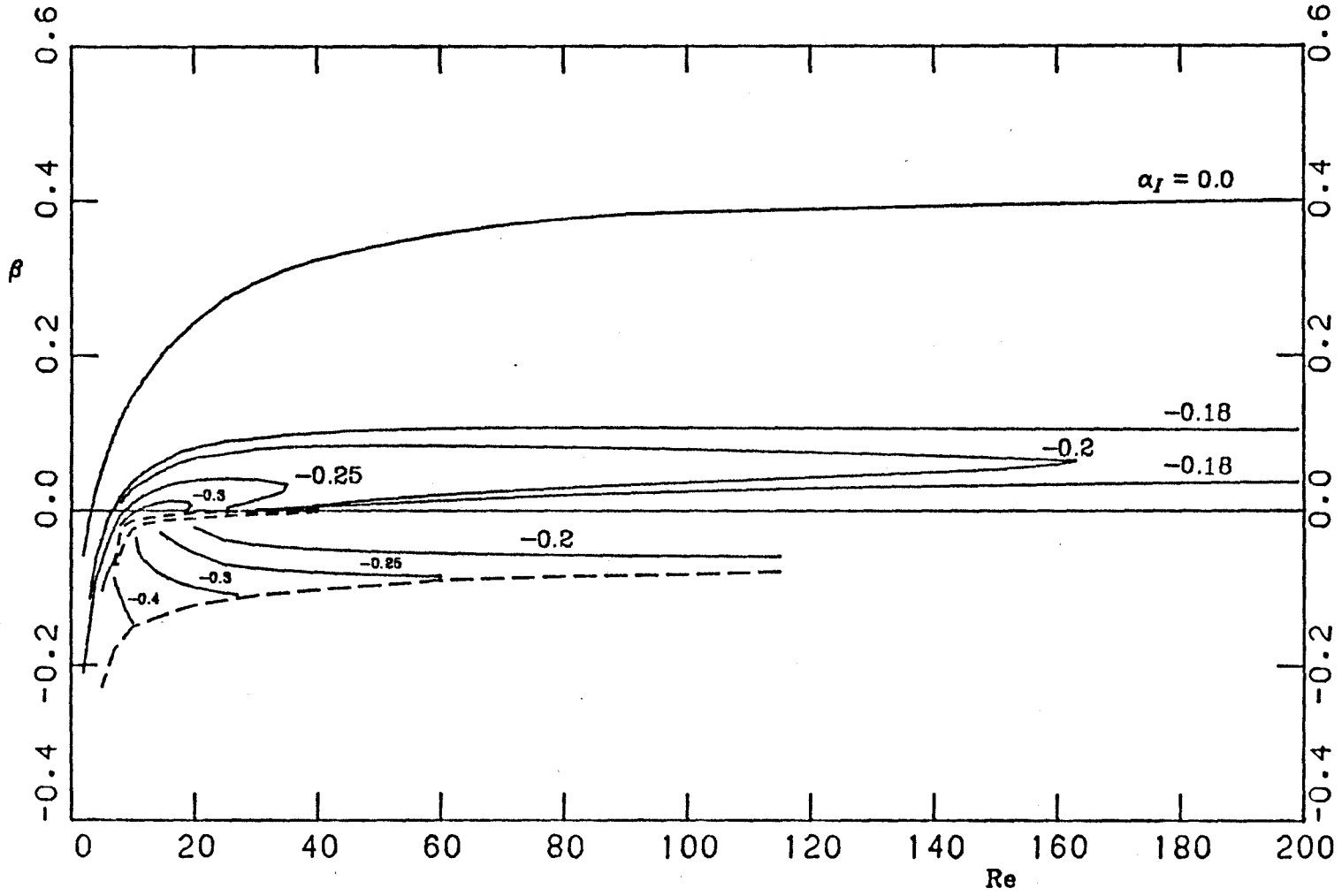

Figure (4.1) Neutral stability and amplification contours for symmetric buoyant diffusion flame using Boussinesq approximation. Frequency-Reynolds number diagram with local non-dimensionalisation.

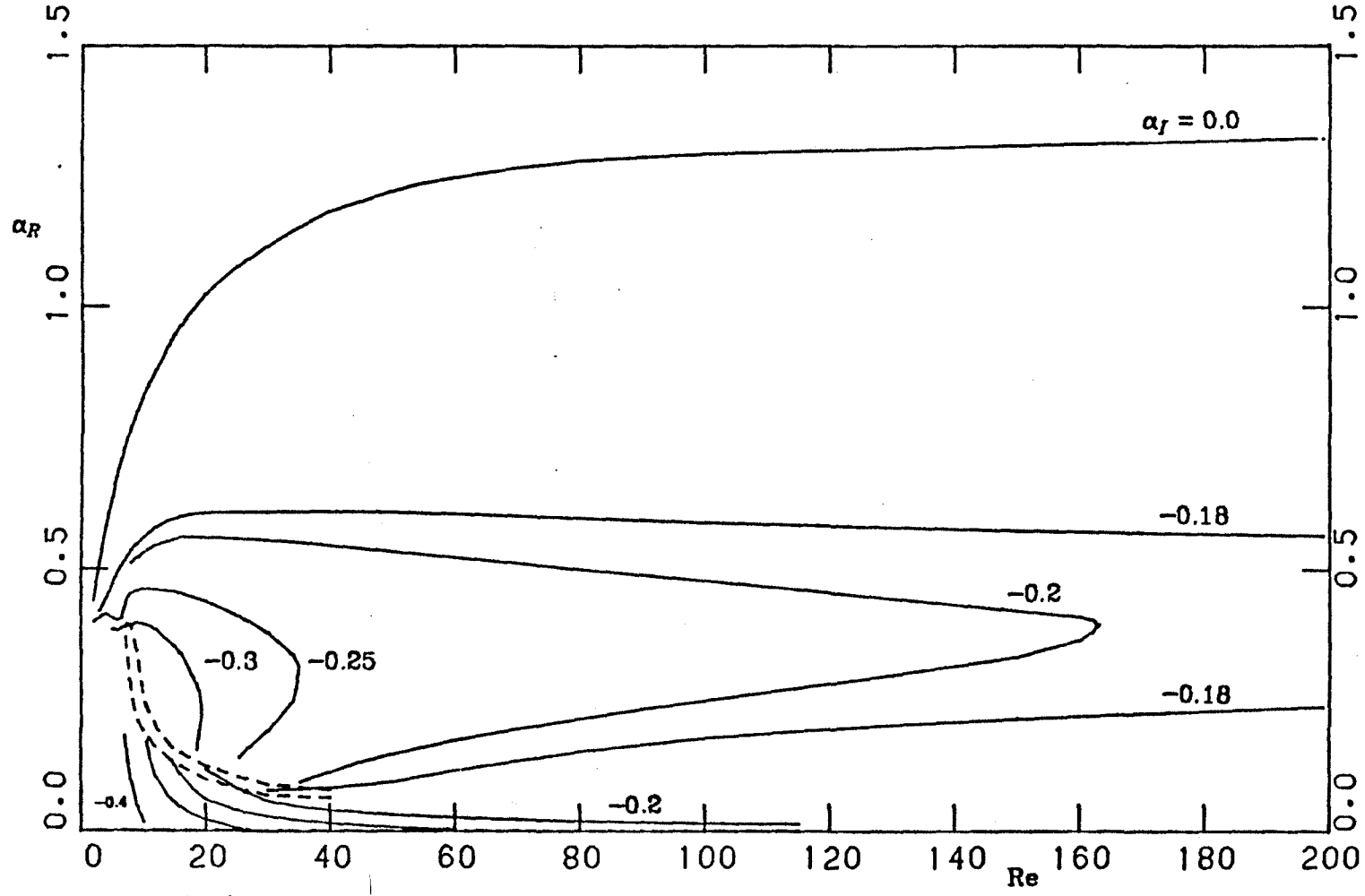

Figure (4.2) **Neutral stability and amplification contours for symmetric buoyant diffusion flame using Boussinesq approximation. Wave number-Reynolds number diagram with local non-dimensionalisation.**

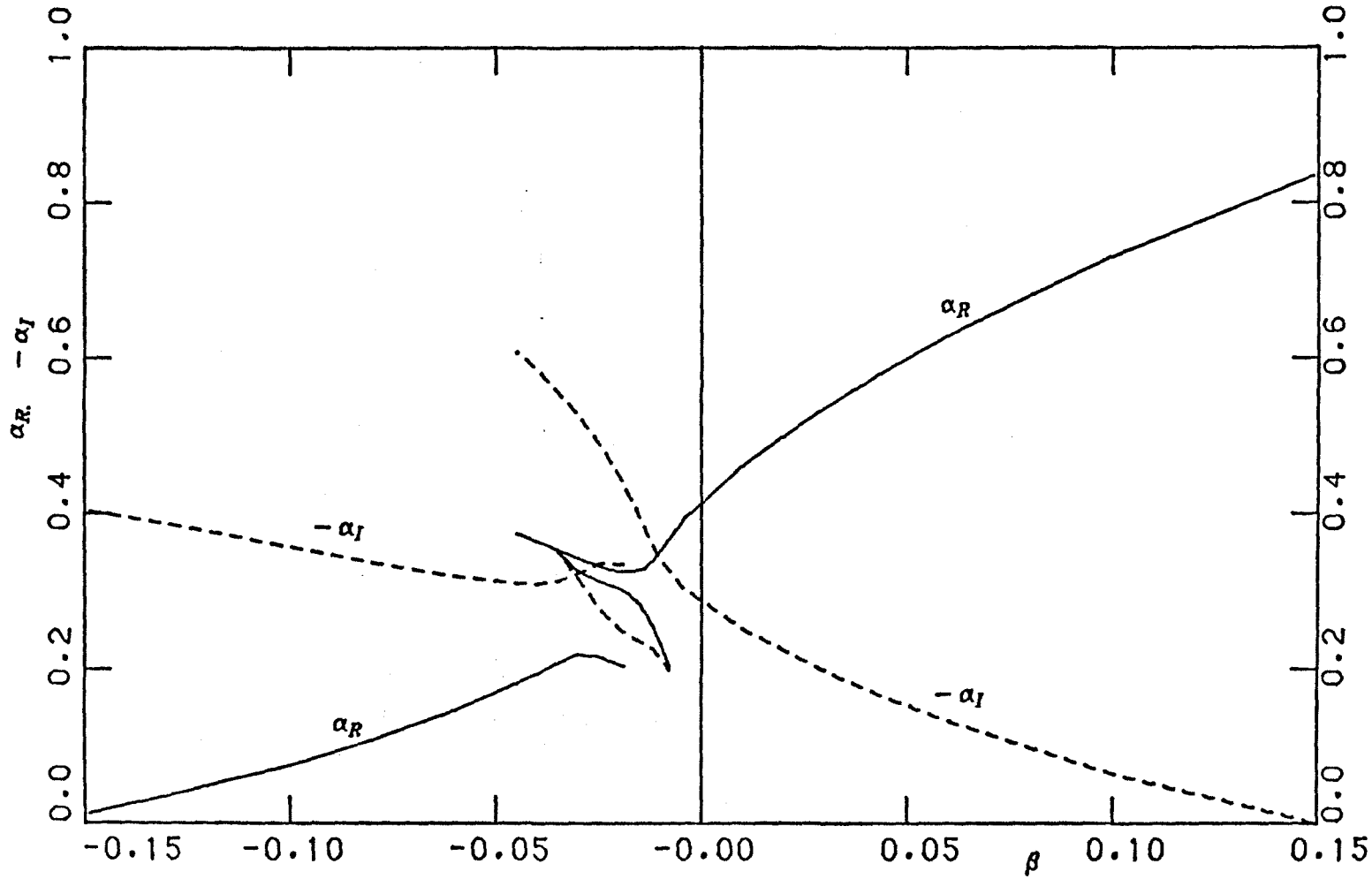

Figure (4.3) Stability of symmetric buoyant diffusion flame using Boussinesq approximation. Variation of wave number and amplification rates with frequency at Re = 10.

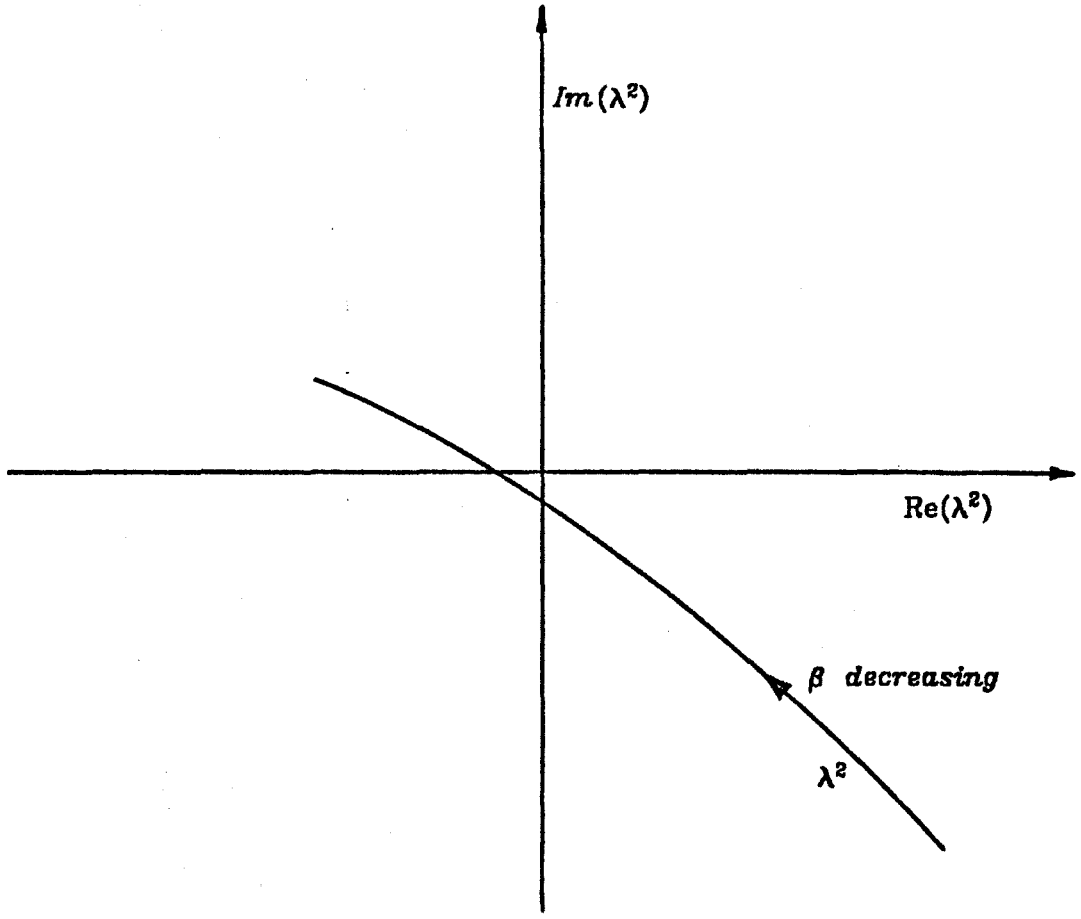

Figure (4.4) Variation of the exponent in the asymptotic expression for the disturbance quantities with frequency.

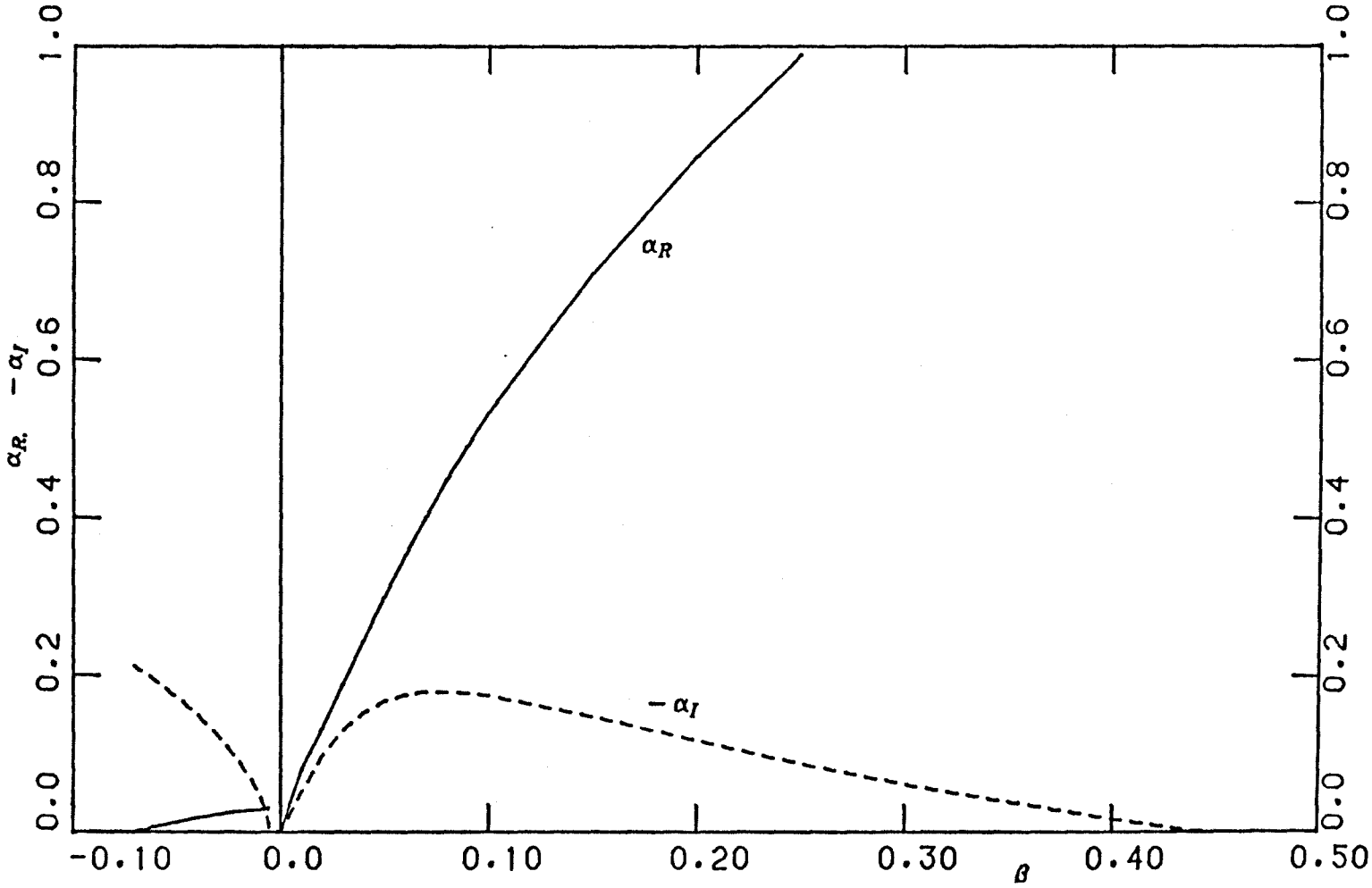

Figure (4.5) Inviscid asymptote for the stability of symmetric buoyant diffusion flame using Boussinesq approximation. Variation of wave number and amplification rates with frequency.

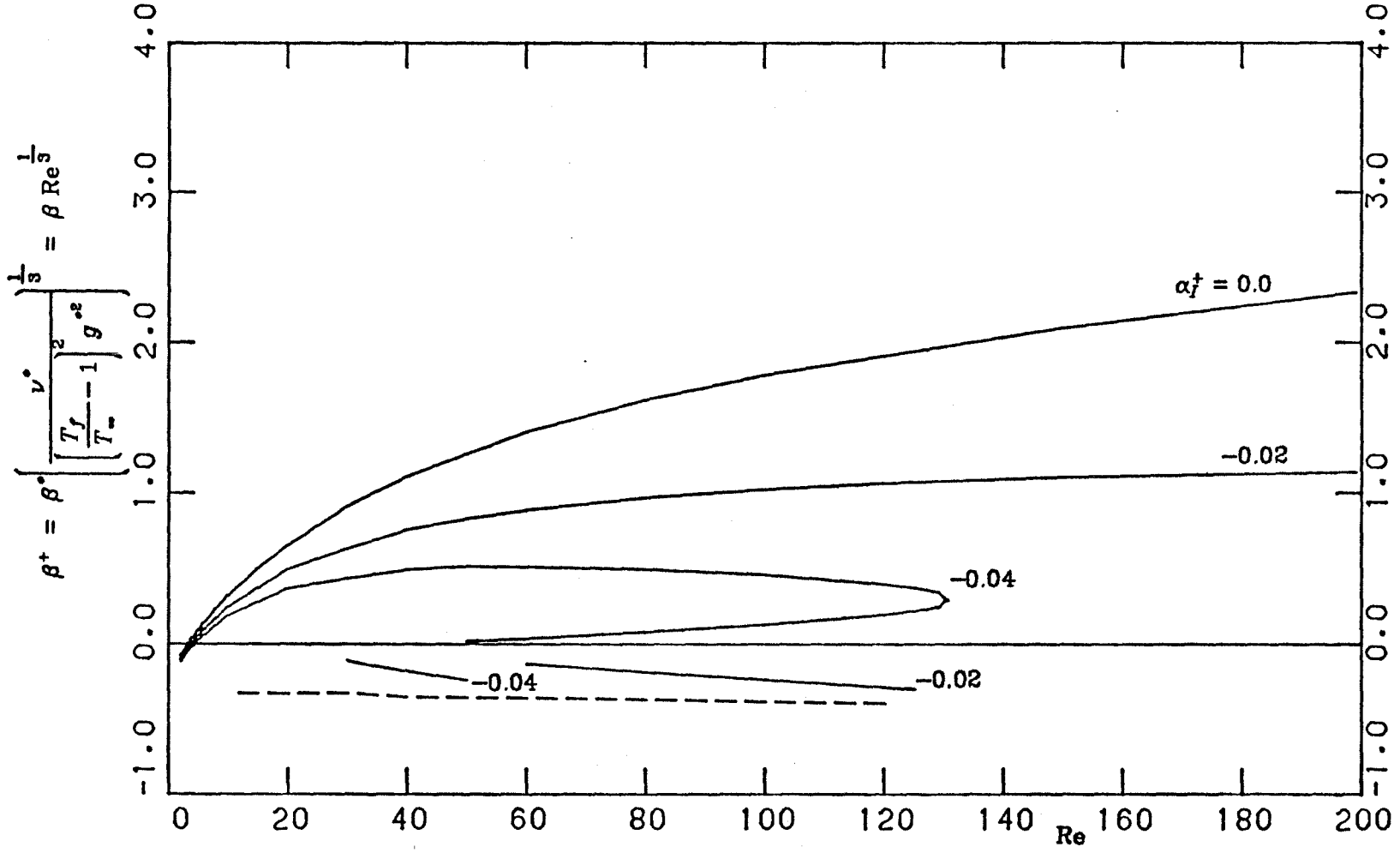

Figure (4.6) **Neutral stability and amplification contours for symmetric buoyant diffusion flame using Boussinesq approximation. Frequency-Reynolds number diagram with global non-dimensionalisation.**

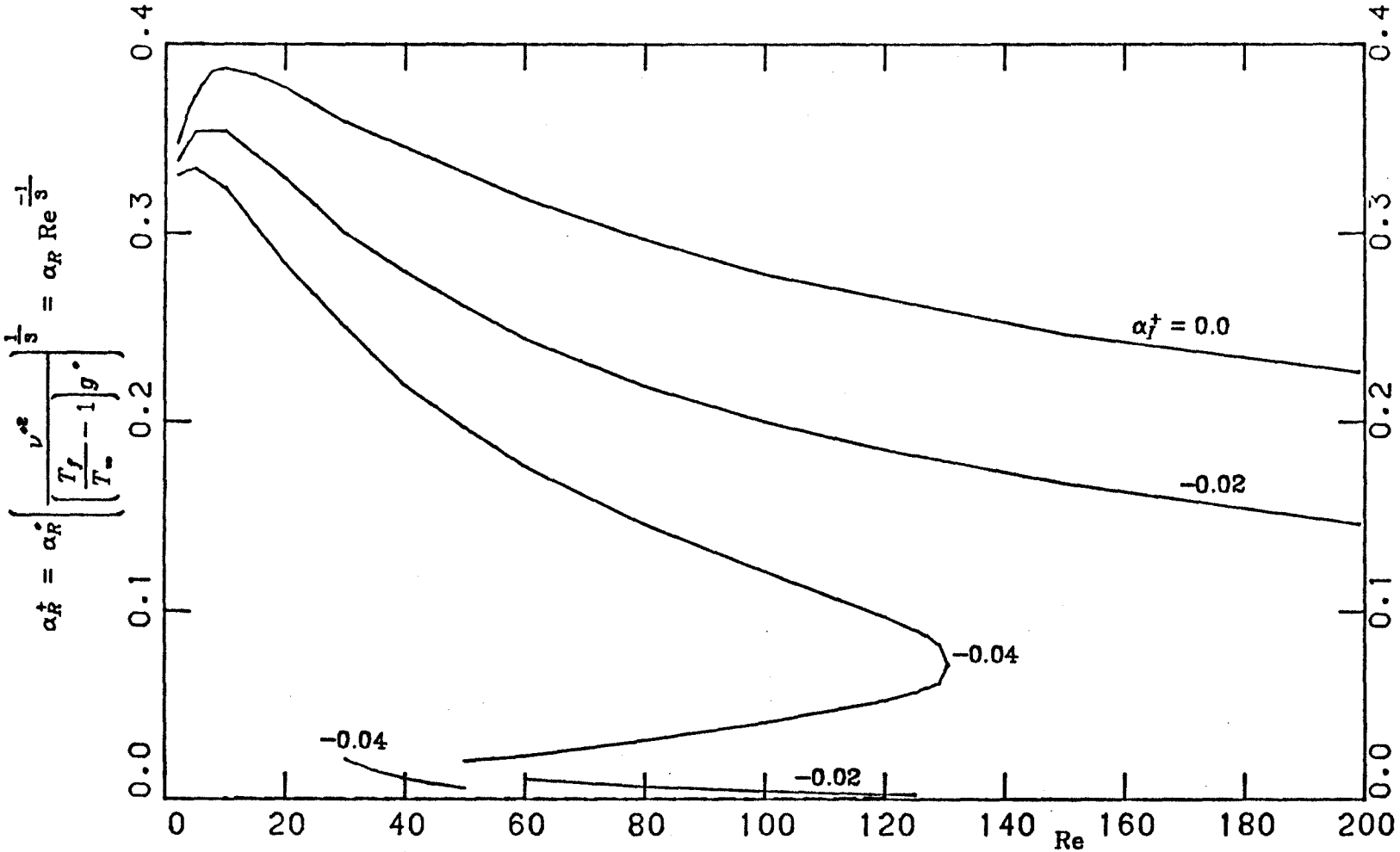

Figure (4.7) Neutral stability and amplification contours for symmetric buoyant diffusion flame using Boussinesq approximation. Wave number-Reynolds number diagram with global non-dimensionalisation.

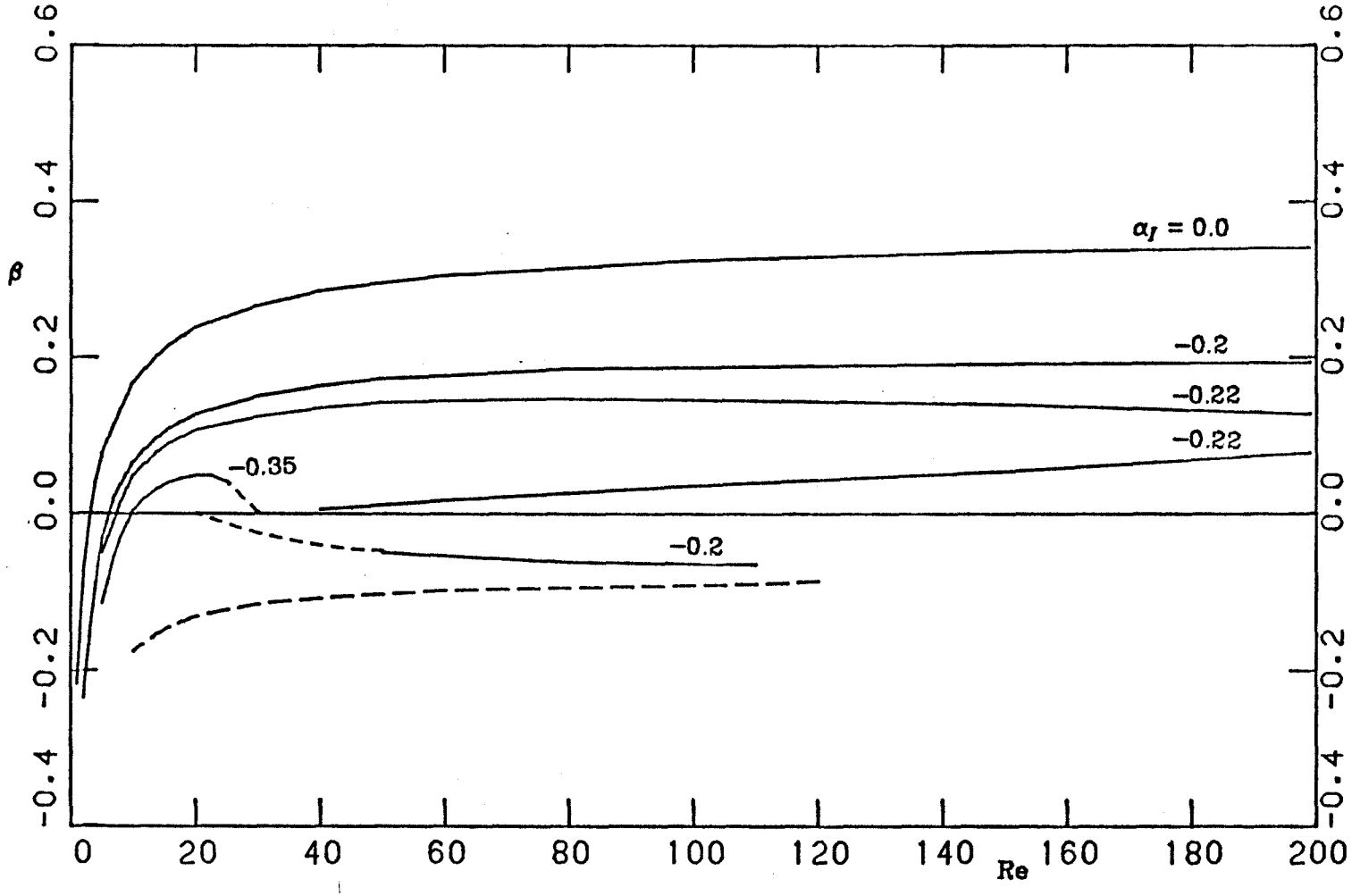

Figure (4.8) Neutral stability and amplification contours for asymmetric buoyant diffusion flame ($\tilde{\varphi}$ = 0.058) using Boussinesq approximation. Frequency-Reynolds number diagram with local non-dimensionalisation.

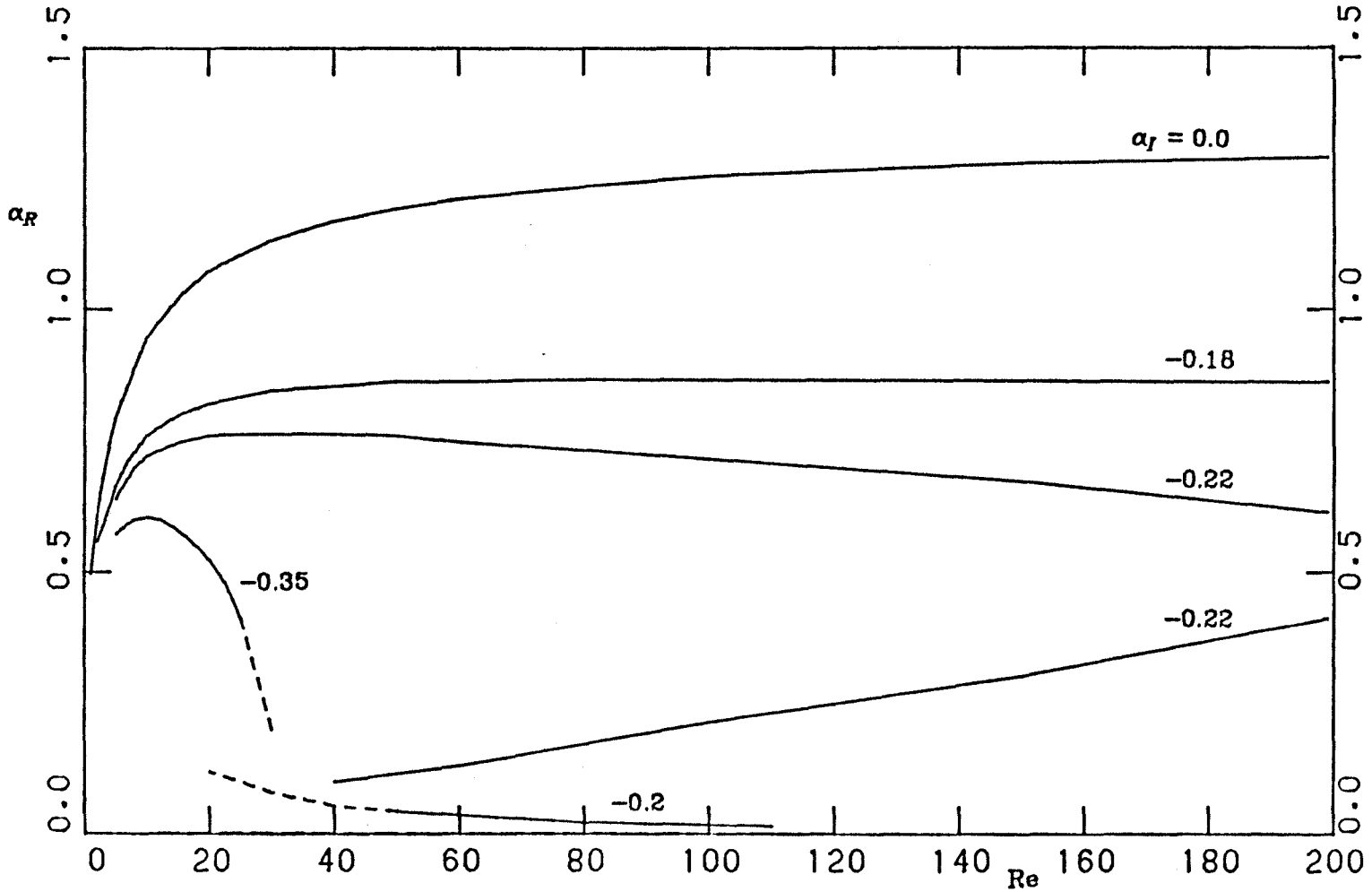

Figure (4.9) Neutral stability and amplification contours for asymmetric buoyant diffusion flame ($\tilde{\varphi}$ = 0.058) using Boussinesq approximation. Wave number-Reynolds number with local non-dimensionalisation.

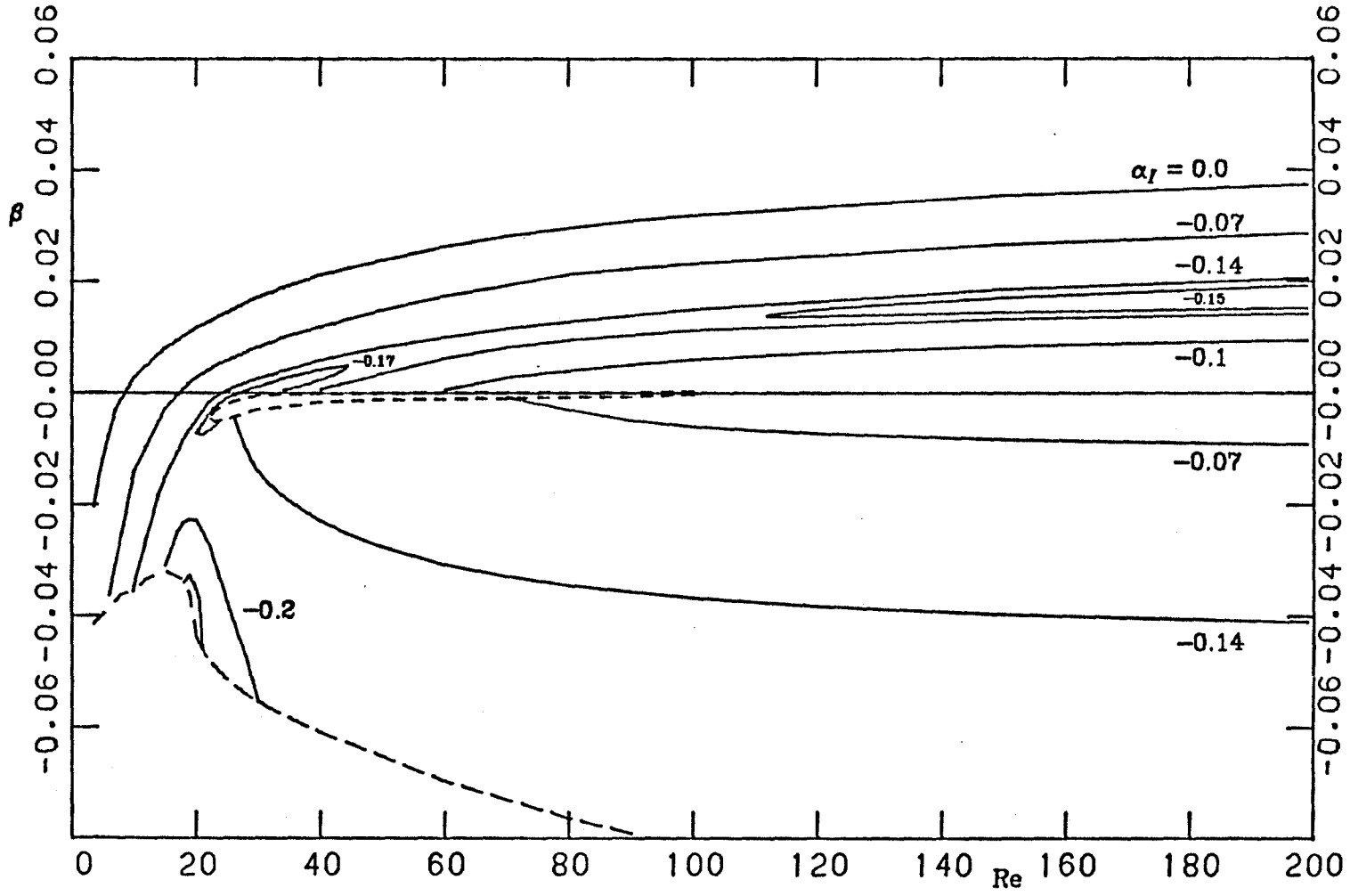

Figure (4.10) Neutral stability and amplification contours for symmetric buoyant diffusion flame with $\left[\frac{T_f}{T_\infty} - 1\right] = 6$. Frequency-Reynolds number diagram with local non-dimensionalisation.

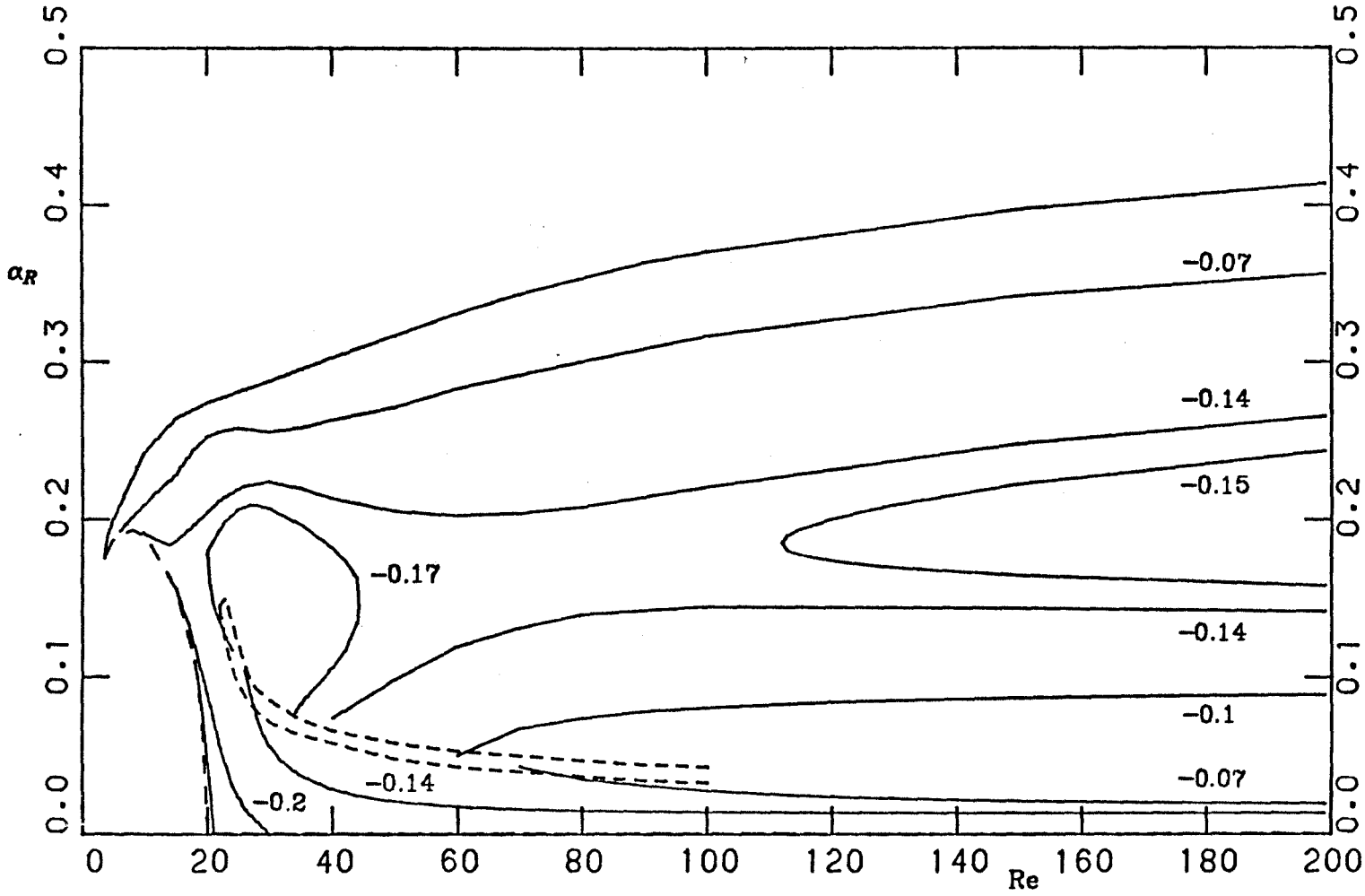

Figure (4.11) Neutral stability and amplification contours for symmetric buoyant diffusion flame with $\left[\frac{T_f}{T_\infty} - 1\right] = 6$. Wave number-Reynolds number diagram with local non-dimensionalisation.

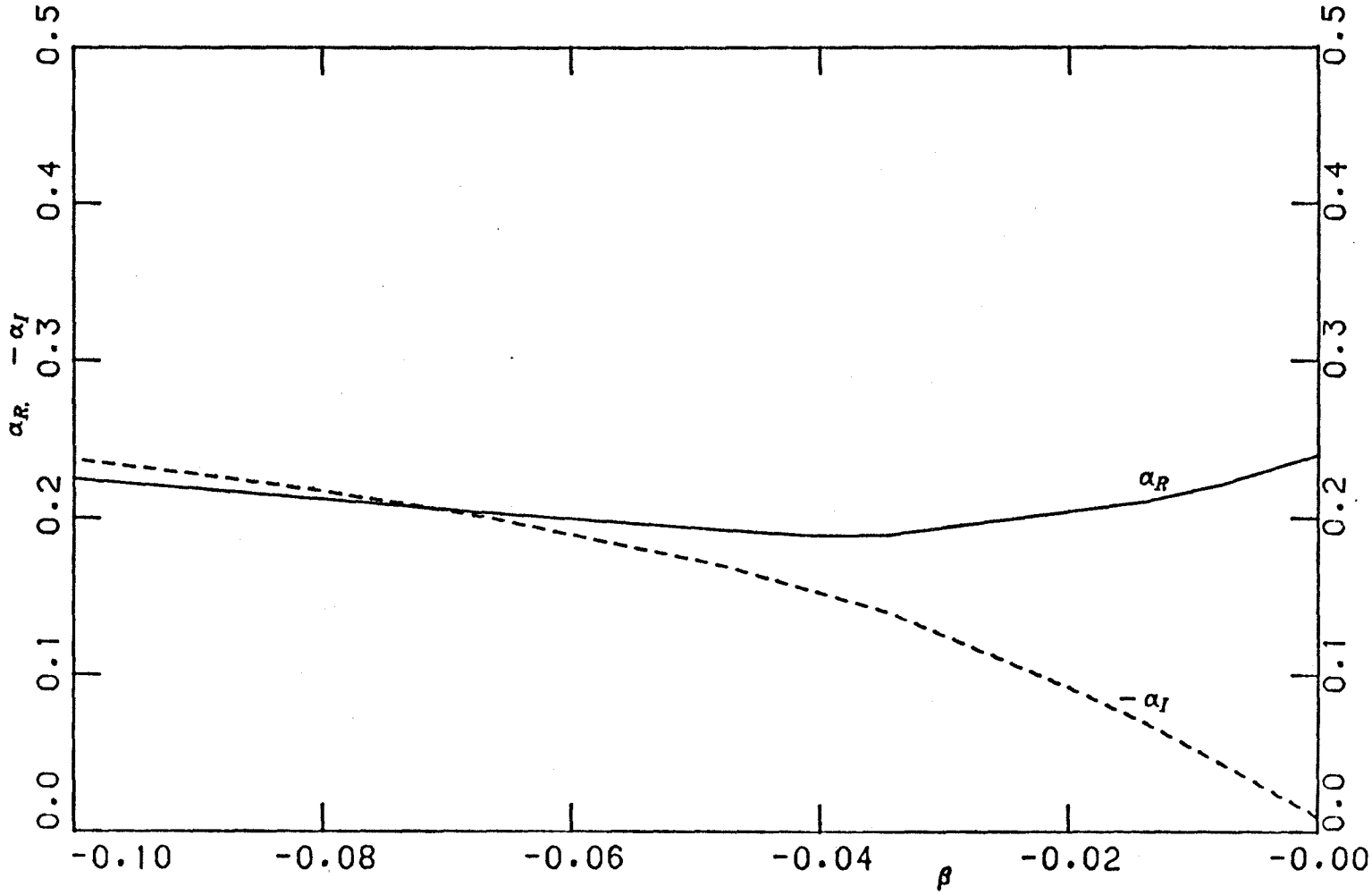

Figure (4.12) Stability of symmetric buoyant diffusion flame with $\left[\frac{T_f}{T_\infty} - 1\right] = 6$. Variation of wave number and amplification rates with frequency at Re = 10.

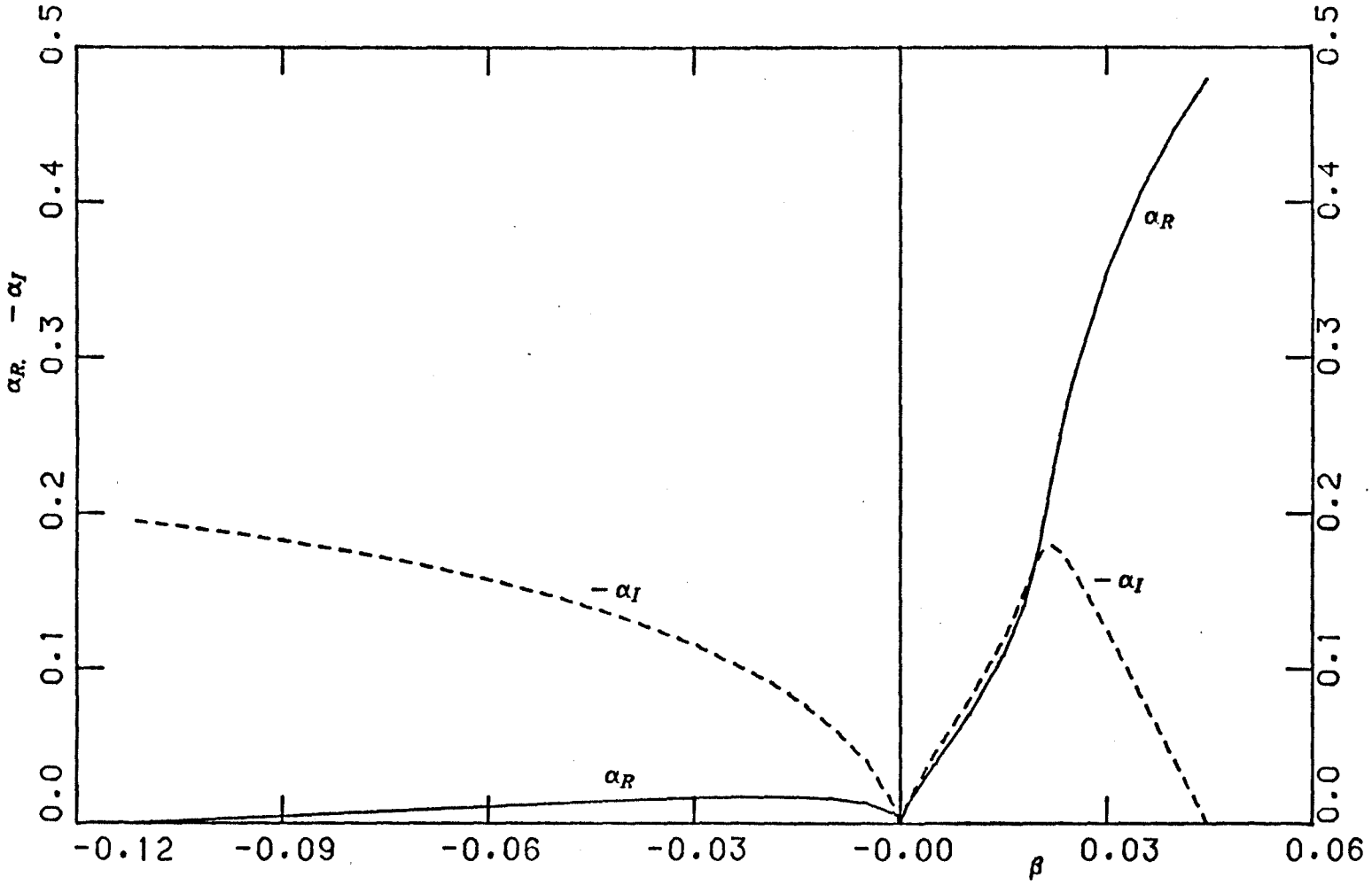

Figure (4.13) Inviscid asymptote for symmetric buoyant diffusion flame with $\left(\frac{T_f}{T_\infty} - 1\right) = 6$. Variation of wave number and amplification rates with frequency.

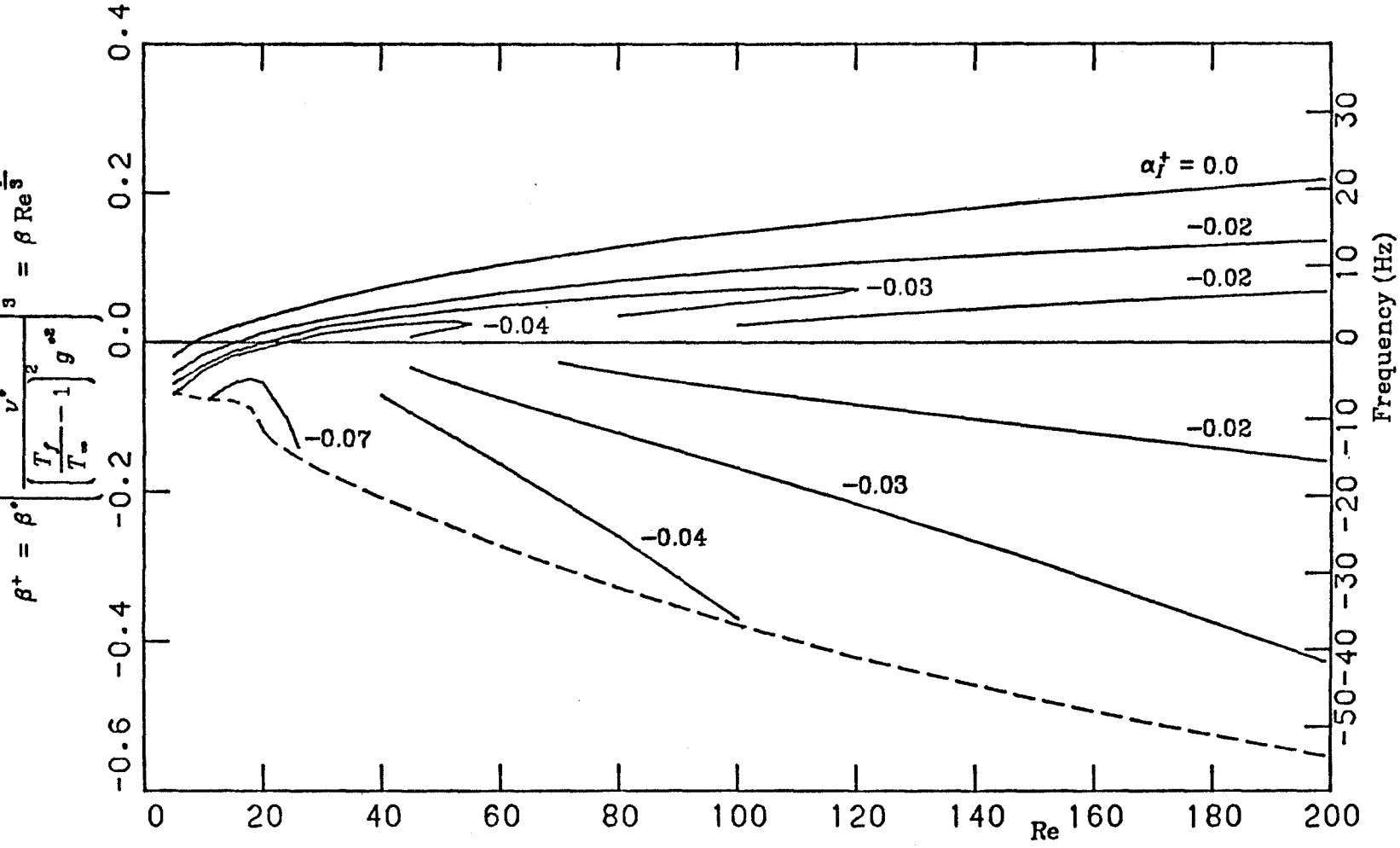

Figure (4.14) Neutral stability and amplification contours for symmetric buoyant diffusion flame with $\left[\frac{T_f}{T_\infty} - 1\right] = 6$. Frequency-Reynolds number diagram with global non-dimensionalisation.

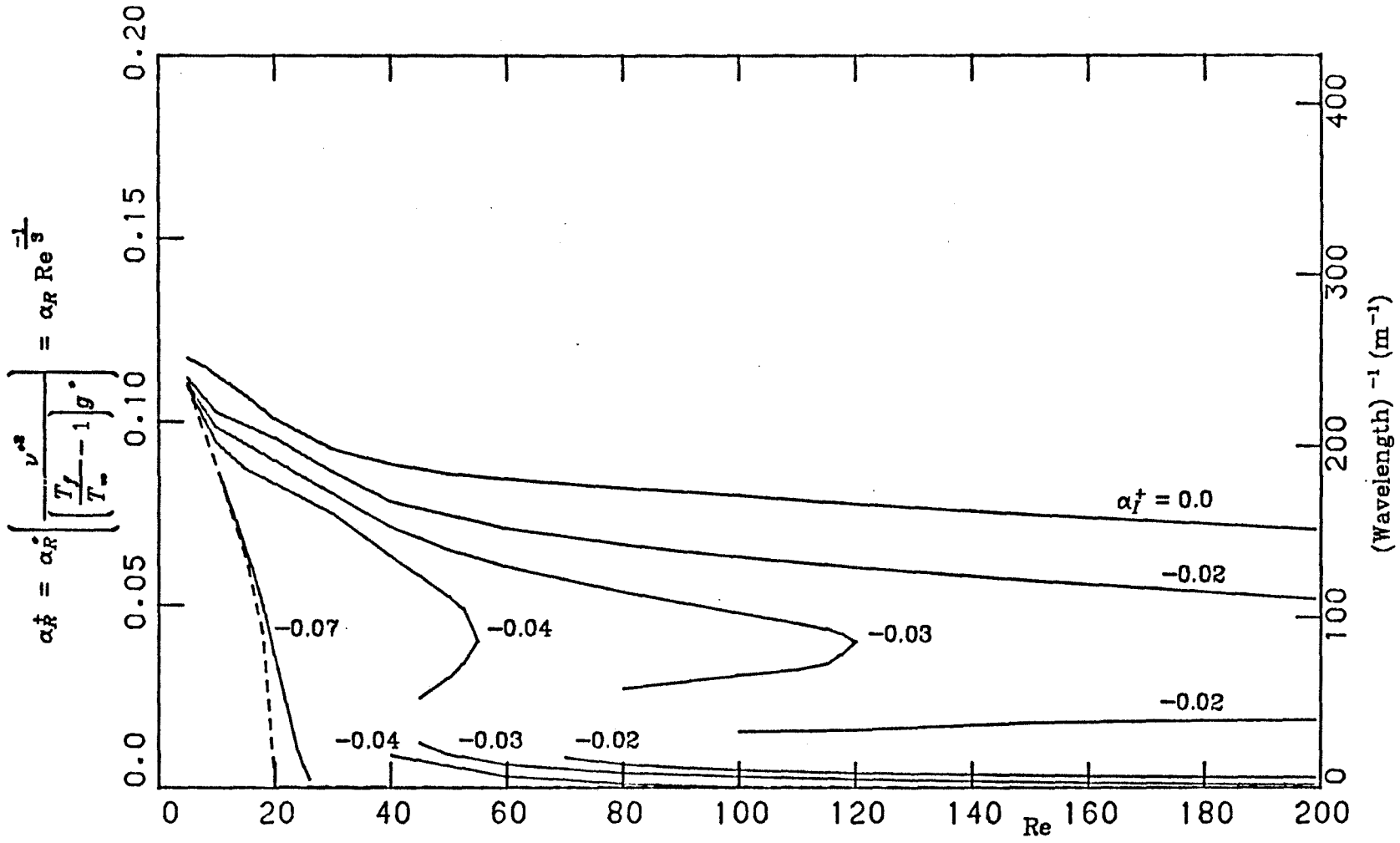

Figure (4.15) Neutral stability and amplification contours for symmetric buoyant diffusion flame with $\left(\frac{T_f}{T_\infty} - 1\right) = 6$. Wave number-Reynolds number diagram with global non-dimensionalisation.

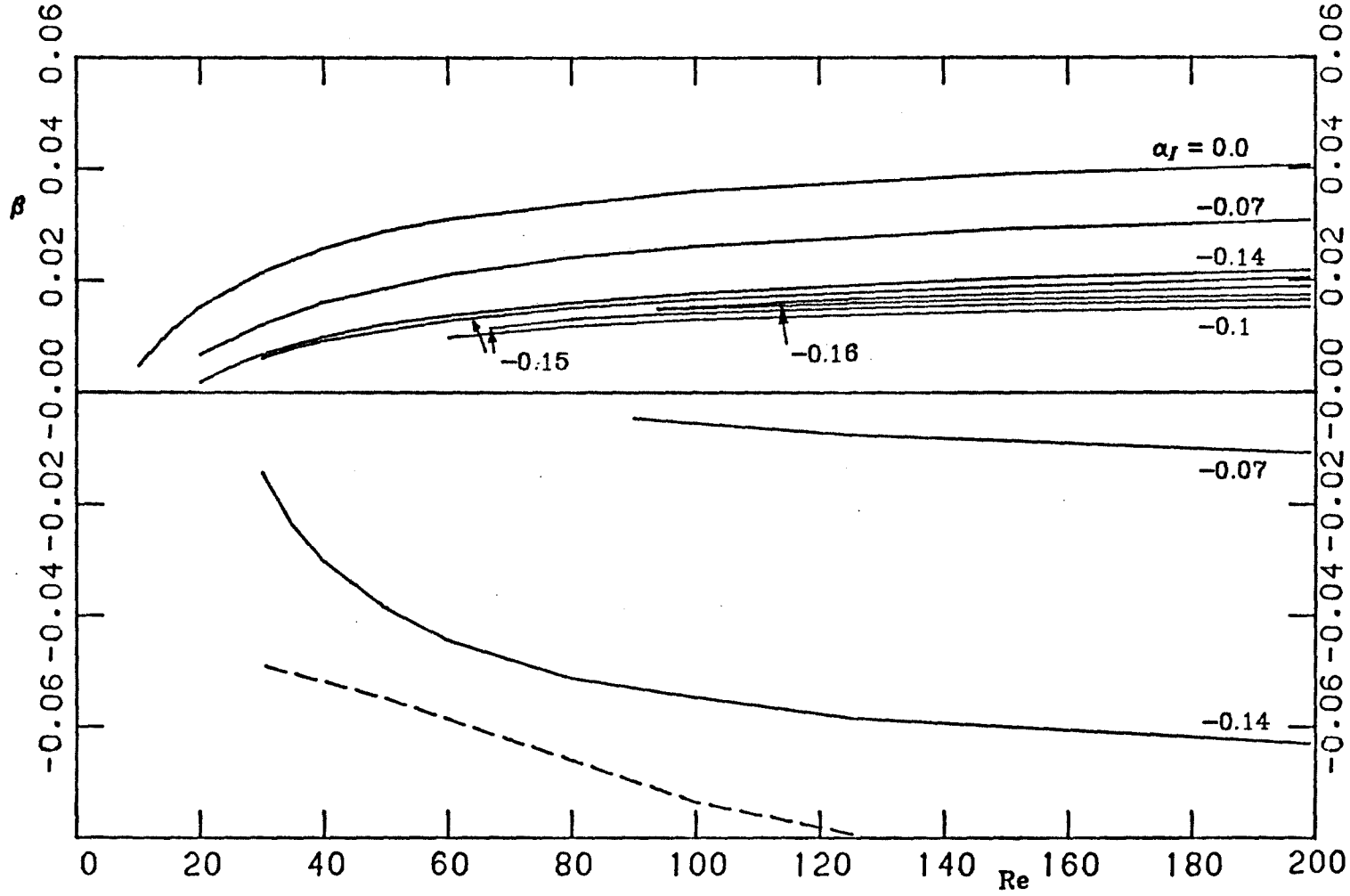

Figure (4.16) Neutral stability and amplification contours for asymmetric buoyant diffusion flame ($\tilde{\varphi}$ = 0.058) with $\left(\frac{T_f}{T_\infty} - 1\right) = 6$. Frequency-Reynolds number diagram with local non-dimensionalisation.

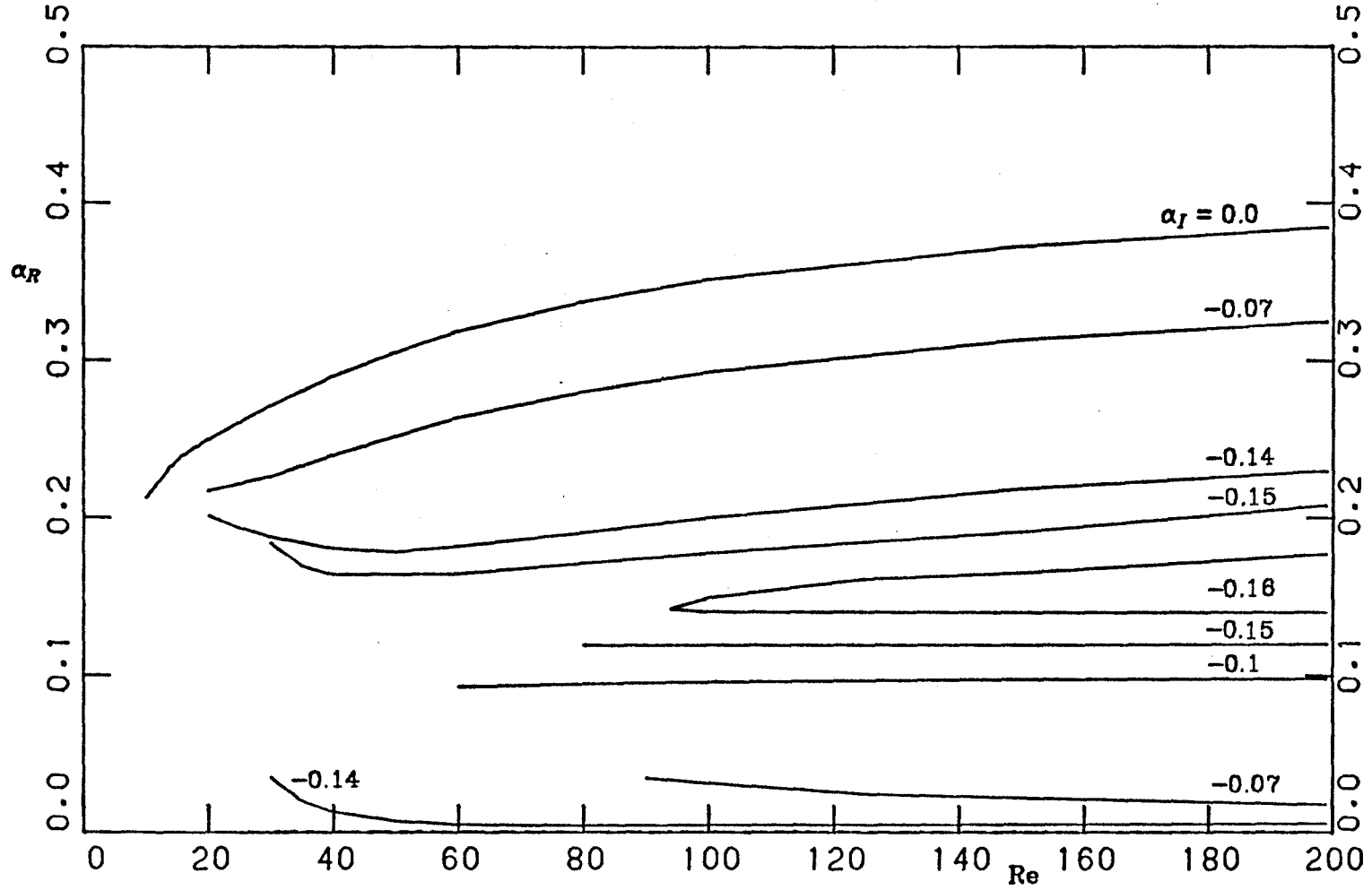

Figure (4.17) Neutral stability and amplification contours for asymmetric buoyant diffusion flame ($\tilde{\varphi}$ = 0.058) with $\left(\frac{T_f}{T_\infty} - 1\right)$ = 6. Wave number-Reynolds number diagram with local non-dimensionalisation.

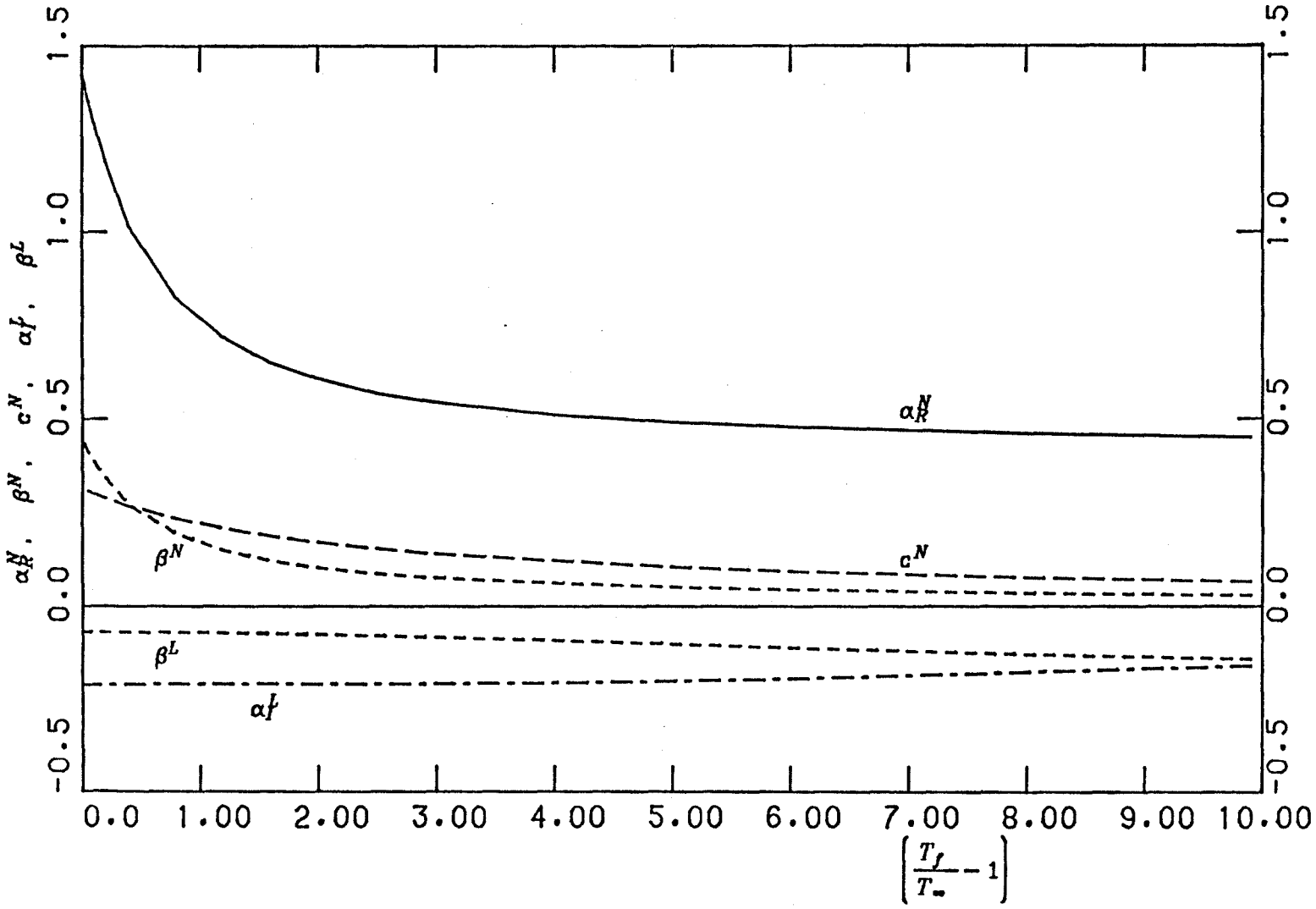

Figure (4.18) Variation of inviscid asymptotes with flame temperature.

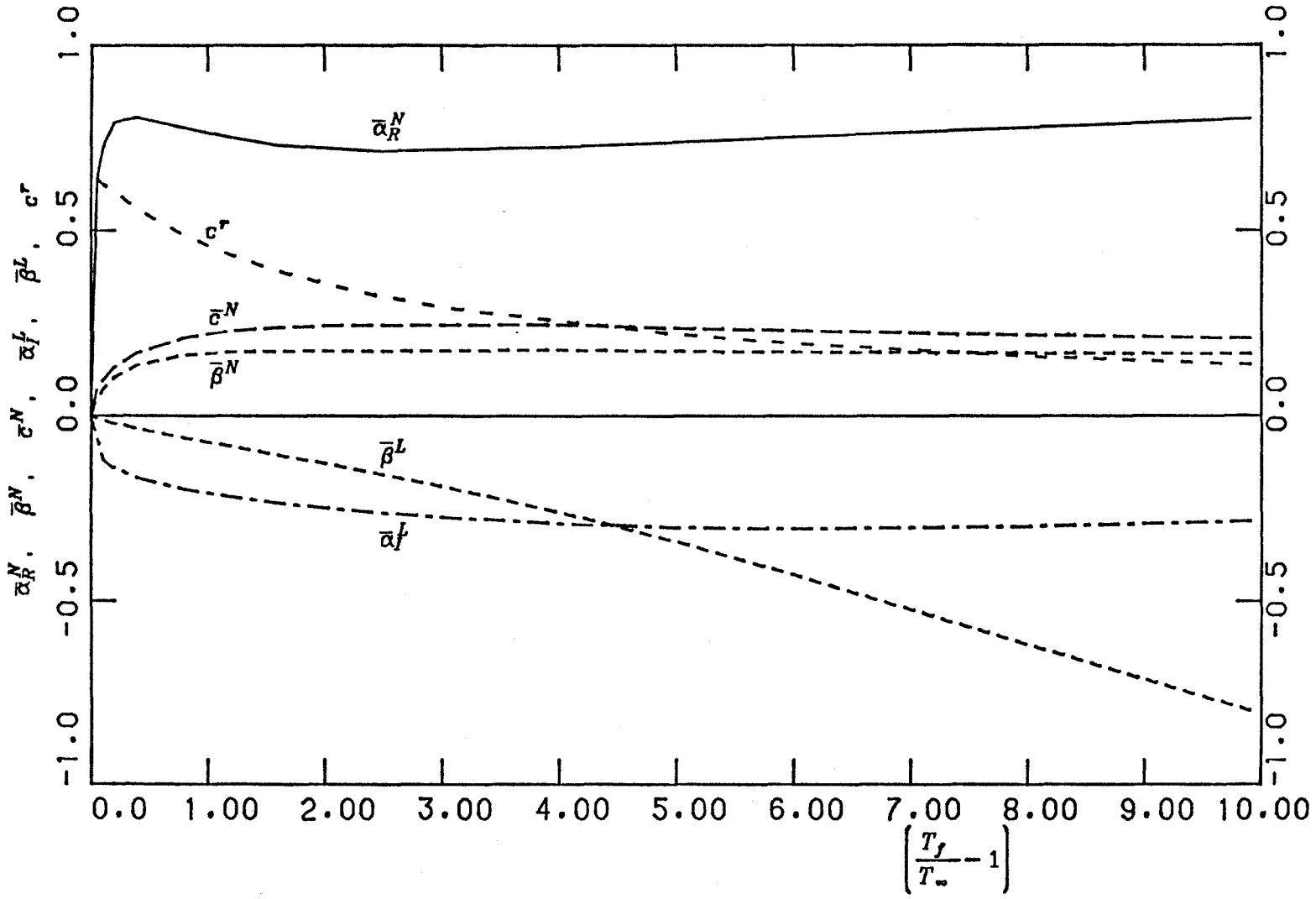

Figure (4.19) Variation of inviscid asymptotes with flame temperature with the non-dimensionalisation independent of temperature.

Chapter 5.

STABILITY OF PLANE BUOYANT PLUMES.

The plane buoyant plume arising from a horizontal line heat source has been the subject of extensive research originating with Zeldovich, reference (5.1), 1937, who described the natural convection plumes arising from a point and from a horizontal line source. More recently, a steady laminar self-similar solution has been obtained by employing the boundary layer and Boussinesq approximations. The solutions have been calculated numerically by Fujii, reference (5.2), 1963, Gebhart, Pera and Schorr, reference (5.3), 1970, who have performed an extensive literature survey, and more accurately by Fujii, Morioka and Uehara, reference (5.4), 1973. Experimental studies of the steady buoyant plume in air have been performed by Brodowicz and Kierkus, reference (5.5), 1966, and Forstrom and Sparrow, reference (5.6), 1967. These experiments exhibited a centerline temperature difference some 15% less than the theoretical prediction, but did obey the similarity scaling laws of the analysis.

The stability of the steady flow was first investigated by Pera and Gebhart, reference (5.7), 1971, who used the Tollmien-Schlichting small disturbance theory to obtain a neutral stability curve for the flow. Their analysis did not reveal a critical Reynolds number or a lower branch to the neutral curve. They also performed some experiments confirming the results of the stability analysis. By taking account of the non-parallel nature of the base flow, Haaland and Sparrow, reference (5.8), 1973, and more recently Hieber and Nash, reference (5.9), 1975, who included a higher-order boundary layer solution for the steady flow, found a critical Reynolds number and established the position of the lower branch of the neutral curve.

For the purpose of comparison with the flame stability results, more extensive calculations employing the parallel flow assumption were performed and

are discussed in this chapter, and the effect of removing the Boussinesq approximation is examined.

5.1. Steady Solution

By employing the boundary layer approximation and the Howarth Transformation in a manner analogous to chapter two, the following similarity equations are obtained

$$\xi''' + \frac{12}{5}\xi\xi'' - \frac{4}{5}(\xi')^2 + \vartheta = 0 \tag{5.1}$$

$$\vartheta'' + \frac{12}{5}Pr(\xi\vartheta)' = 0 \tag{5.2}$$

subject to the boundary conditions

$$\left.\begin{aligned} \xi'' = \xi = \vartheta' = 0 \qquad & at\ \eta = 0 \\ \xi' \to 0, \quad \vartheta \to 0 \qquad & as\ \eta \to \infty \end{aligned}\right\} \tag{5.3}$$

where the prime denotes differentiation with respect to the similarity variable η

$$\eta = \frac{\mathrm{Re}}{4x^*}\int_0^{y^*}\frac{\rho^*}{\rho_\infty^*}dy^* \tag{5.4}$$

and the streamfunction ψ^* is given by

$$\psi^* = \nu_\infty^*\,\mathrm{Re}\,\xi(\eta) \tag{5.5}$$

where

$$\left.\begin{aligned} \mathrm{Re} = 2\sqrt{2}\left[\frac{x^{*3} g^* \left(\frac{T_f}{T_\infty} - 1\right)}{\nu_\infty^{*2}}\right]^{\frac{1}{4}} &= x^{*\frac{3}{5}} \bar{Q}^{\frac{1}{5}} \left[\frac{4^3 g^*}{\nu_\infty^{*2}}\right]^{\frac{1}{5}} \\ \bar{Q} = \left[\frac{Q_p^*}{\mu_\infty^* c_p^* T_\infty^* I}\right], \quad I &= \int_{-\infty}^{\infty} \xi' \vartheta \, d\eta \end{aligned}\right\} \tag{5.6}$$

and Q_p^* is the heat generated by the line source per unit length. The difference between the centerline temperature T_0^* and the ambient temperature T_∞^* is given by

$$\left(\frac{T_0^*}{T_\infty^*} - 1\right) = \frac{\bar{Q}}{\mathrm{Re}} \tag{5.7}$$

the velocity components by

$$\left.\begin{aligned} \tilde{u}^* = \frac{\partial \psi^*}{\partial y^*} &= 4\left[\frac{\left(\frac{T_0}{T_\infty} - 1\right) g^* x^*}{4}\right]^{\frac{1}{2}} \xi' \\ \tilde{v}^* = \left[\frac{\rho^*}{\rho_\infty^*}\right] v^* + u^* \int_0^{y^*} \frac{\partial}{\partial x^*}\left[\frac{\rho^*}{\rho_\infty^*}\right] dy^* &= -\frac{\partial \psi^*}{\partial x^*} \\ = -4\nu_\infty^* \left[\frac{\left(\frac{T_0}{T_\infty} - 1\right) g^*}{4\nu_\infty^{*2} x^*}\right]^{\frac{1}{4}} &\left[\frac{3}{4}\xi - \frac{1}{4}\eta\xi'\right] \end{aligned}\right\} \tag{5.8}$$

and the temperature by

$$T^* = T_\infty^* + (T_o^* - T_\infty^*)\vartheta \tag{5.9}$$

This formulation has assumed that c_p^* is constant, $\rho^*\mu^* = \rho_\infty^*\mu_\infty^*$ and $\rho^*\lambda^* = \rho_\infty^*\lambda_\infty^*$ where λ is the thermal conductivity. The energy equation, (5.2), may be integrated once to give

$$\vartheta' + \frac{12}{5} Pr\, \xi \vartheta = C_1$$

C_1 is determined to be zero from the boundary conditions at $\eta = 0$. Integrating again gives

$$\vartheta = \vartheta(0) e^{-\frac{12}{5} Pr \int_0^\eta \xi d\eta}$$

Since ξ is positive and becomes constant for large η, the condition $\vartheta \to 0$ as $\eta \to \infty$ is not independent, but is implied by the other boundary conditions. Note that for the flame, this was not the case since the energy equation is

$$\vartheta'' + 3Pr\, \xi \vartheta' = 0$$

Integrating once then gives

$$\vartheta' = Ce^{-3Pr \int_0^\eta \xi d\eta}$$

and C is not determined from the boundary conditions at $\eta = 0$.

For the plume, the condition that the total energy convected across any horizontal plane is equal to the total heat input

$$Q_p^* = c_p^* \int_{-\infty}^{\infty} \rho^* T^* u^* dy^*$$

is satisfied automatically because of the chosen dimensionless form. The fifth boundary condition is therefore taken to be an arbitrary normalisation. Gebhart et al., reference (5.3), used the condition $\vartheta(0) = 1$ while Fujii preferred the condition $I = \int_{-\infty}^{\infty} \xi' \vartheta \, d\eta = 1$. In the present work, the normalisation of Gebhart et al. is used. They obtain the value $\xi'(0) = 0.6618$ for a Prandtl number $Pr = 0.7$.

5.2. Linear Stability Analysis

In this section, the small disturbance equations developed in chapter two are used to investigate the stability of the buoyant plume. The matching conditions at the centerline of the plume are not the same as the matching conditions at the flame, however. Instead they are replaced by continuity of the temperature disturbance and its derivative, s, s', and of the velocities, the shear stress and its derivative, φ, f, f', f''. Since the steady flow is symmetric, the disturbances can be decomposed into symmetric and antisymmetric components, the antisymmetric component being the more unstable. The matching conditions at the centerline can then be written as boundary conditions

$$\left.\begin{aligned} \varphi(0) = f'(0) = s'(0) = 0 \qquad & (\textit{Symmetric disturbances}) \\ f(0) = f''(0) = s(0) = 0 \qquad & (\textit{Antisymmetric disturbances}) \end{aligned}\right\} \quad (5.10)$$

The results presented are for the buoyant plume with $Pr = 0.7$ both using the Boussinesq approximation, and with $Q_p^* = 58.6 Btu/hr\,ft$ which was studied experimentally by Pera and Gebhart, reference (5.7). It should be noted that since temperatures are not large in the plume, decaying as the inverse of the Reynolds number, equation (5.7), the use of the Boussinesq approximation

should not greatly affect the resulting stability diagram. As for the flame, the results given are for the more unstable antisymmetric disturbances.

Figures (5.1) and (5.2) show the results for $Q_p^* = 0$. The neutral curve is in excellent agreement with that obtained by Pera and Gebhart in the range of Reynolds numbers they considered. In comparison with the symmetric flame, figures (4.1) and (4.2), the buoyant plume exhibits many of the same features. There is no lower branch to the neutral stability curve since it continues to negative frequencies. A negative phase velocity, positive group velocity region, not considered in previous investigations, does exist and extends from very small Reynolds numbers through to infinite Reynolds number.

The neutral curve occurs, however at dimensionless frequencies some 40% higher than for the flame, while the amplification rates are somewhat reduced at low Reynolds numbers and somewhat higher at large Reynolds numbers. The inviscid results, figure (5.3), are in excellent agreement with the calculations of Haaland and Sparrow, reference (5.8), apart from the negative frequency region which they do not consider. Figure (5.4) gives more detail at Re = 10. Note the considerable similarity between this figure and figure (4.3) which shows the stability of the flame at Re = 10. Once again there are discontinuities in the solution corresponding to a change in the asymptotic behaviour of the solution branch from exponential decay to exponential growth, as discussed in chapter four.

Removing the Boussinesq approximation results in a slightly modified stability diagram. Figures (5.5) and (5.6) show the results for $Q_p^* = 58.6\ Btu/hr\ ft$. The neutral curve and constant amplification rate contours have been shifted to lower frequencies, especially at small Reynolds numbers, otherwise the stability diagram is similar to that employing the Boussinesq approximation.

In figures (5.7) and (5.8), the frequency and wave number have been renormalised using physical scales which do not vary with Reynolds number. The new

variables, denoted by a superscript +, are related to the dimensional variables, denoted by a superscript *, and the previous dimensionless variables by

$$\left.\begin{aligned} \beta^+ &= \beta^* \left[\frac{\nu_\infty}{\bar{Q}^2 g^{*2}} \right]^{\frac{1}{3}} = \beta \, \mathrm{Re}^{-\frac{1}{3}} \\ \alpha^+ &= \alpha^* \left[\frac{\nu_\infty^{*2}}{\bar{Q} \, g^*} \right]^{\frac{1}{3}} = \alpha \, \mathrm{Re}^{\frac{-2}{3}} \end{aligned}\right\} \qquad (5.11)$$

where $\bar{Q}$ is defined in equation (5.6). The differences between the buoyant plume and the symmetric flame now become more apparent. The buoyant plume, employing the Boussinesq approximation, has a critical frequency $\beta^+ \approx 0.13$, above which all disturbances are stable, while all frequencies eventually become unstable in the symmetric flame. The dashed line in figures (5.7) and (5.8) is the neutral curve with $Q_p^* = 58.6$ *Btu/hr ft*, ($\bar{Q} = 7.56$). The critical frequency for this curve $\beta^+ = 0.105$ corresponds to a real frequency of 11.5Hz, which agrees well with the experimentally determined value of 12Hz obtained by Pera and Gebhart. They suggested that the discrepancy between this frequency and their calculated critical frequency of 15 Hz might be explained by the difference between the experimentally introduced disturbance and the perfect antisymmetric form assumed for the computations. The present analysis indicates, however, that the primary reason for this discrepancy is instead the neglect of density variation effects in terms other than the buoyancy term in the equation of vertical momentum when using the Boussinesq approximation.

There is a considerable change in the stability diagram when non-parallel effects are accounted for, particularly at low Reynolds numbers. The calculations of Haaland and Sparrow, reference (5.8), and Hieber and Nash, reference (5.9), show the existence of a lower branch of the neutral stability curve with a

critical Reynolds number Re = 15. At a Reynolds number Re = 120, however, the neutral curve and the $\alpha_I = -0.1$ contour obtained by Haaland and Sparrow are quite close to the results presented in this chapter using the parallel flow assumption. The maximum amplification rate obtained from the present analysis is however somewhat higher. Neither Haaland and Sparrow, nor Hieber and Nash considered disturbances with negative phase velocity. The exact shape of the negative phase velocity region when non-parallel effects are included is therefore unknown, however it seems reasonable to hypothesize that this region will also exhibit a critical Reynolds number and will become in effect a second unstable mode of disturbance.

Hieber and Nash comment that the characteristic slow meandering of buoyant plumes is not accounted for by the previous linear stability analyses, since the observed frequencies at low Reynolds number are much less than those predicted by the lower branch of the neutral stability curve. It is possible that a full non-parallel analysis of the negative phase velocity region might account for this instability.

Transition to turbulence may be predicted from figure (5.5) for the plume and figure (4.10) for the flame, using the empirically based correlation between the observed transition to turbulence and the growth in the amplitude of the disturbance. For forced-flow boundary layers, Smith, reference (5.10), 1957, established that transition occurred when the disturbance was amplified by a factor of e^9. For natural convection boundary layers, Hieber and Gebhart, reference (5.11), 1971, obtained better correlation with a value of e^{10}. Assuming this latter value is appropriate for the buoyant plume and flame, figure (5.5) leads to a transition around $Re_T = 140$ for the plume, while the positive phase velocity region of figure (4.10) predicts $Re_T \approx 250$ for the flame. The negative phase velocity region would lead to somewhat earlier transition, around $Re_T = 200$, however this region is likely to be greatly modified by non-parallel effects. The buoyant flame is thus considerably more stable than the plume.

References.

(5.1) Y. B. ZELDOVICH, Limiting Laws of Freely Rising Convection Currents, *Zh. Eksp. Teor. Fiz.* **7(12)**, 1463, (1937)

(5.2) T. FUJII, Theory of Steady Laminar Natural Convection above a Horizontal Line Heat Source and a Point Heat Source, *Int. J. Heat Mass Trans.* **6**, 597, (1963)

(5.3) B. GEBHART, L. PERA and A. W. SCHORR, Steady Laminar Natural Convection Plumes above a Horizontal Line Heat Source, *Int. J. Heat Mass Trans.* **13**, 161, (1970)

(5.4) T. FUJII, I. MORIOKA and H. UEHARA, Buoyant Plume above a Horizontal Line Heat Source, *Int. J. Heat Mass Trans.* **16**, 755, (1973)

(5.5) K. BRODOWICZ and W. T. KIERKUS, Experimental Investigation of Laminar Free-Convection Flow in Air above a Horizontal Heated Wire with Constant Heat Flux, *Int. J. Heat Mass Trans.* **9**, 81, (1966)

(5.6) R. J. FORSTROM, and E. M. SPARROW, Experiments on the Buoyant Plume above a Heated Horizontal Wire, *Int. J. Heat Mass Trans.* **10**, 321, (1967)

(5.7) L. PERA and B. GEBHART, On the Stability of Laminar Plumes: Some Numerical Solutions and Experiments, *Int. J. Heat Mass Trans.* **14**, 975, (1971)

(5.8) S. E. HAALAND and E. M. SPARROW, Stability of Buoyant Boundary Layers and Plumes, Taking account of Nonparallelism of the Basic Flows, *J. Heat Trans.* **95c** 295, (1973)

(5.9) C. A. HIEBER and E. J. NASH, Natural Convection above a Line Heat Source: Higher-Order Effects and Stability, *Int. J. Heat Mass Trans.* **18** 1473, (1975)

(5.10) A. M. O. SMITH, Transition, Pressure Gradient, and Stability Theory, *9th Int. Congress of App. Mech.* **4**, 234, (1956)

(5.11) C. A. HIEBER and B. GEBHART, Stability of Vertical Natural Convection Boundary Layers: Some Numerical Solutions, *JFM* **48**, 625, (1971)

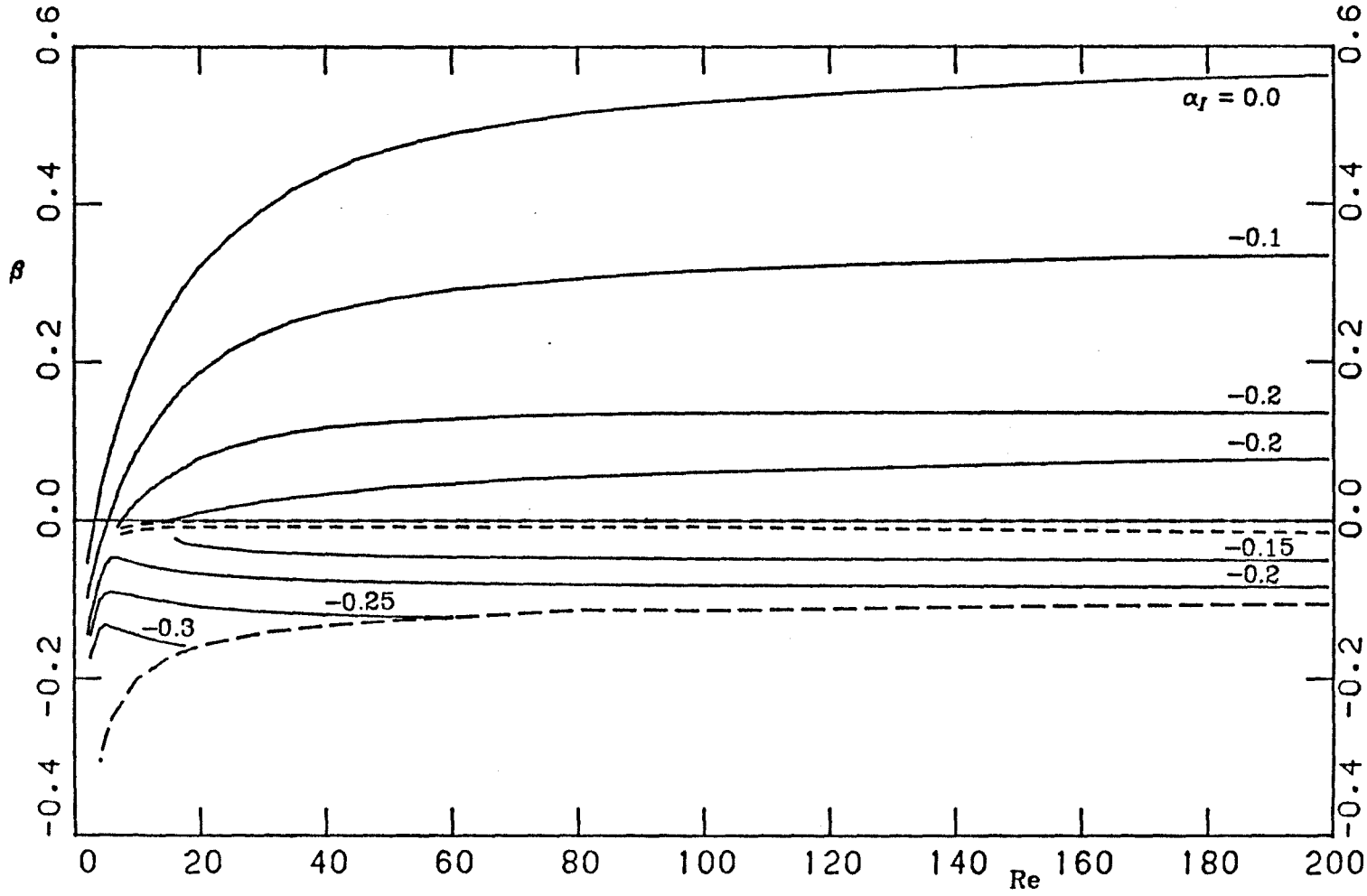

Figure (5.1) Neutral stability and amplification contours for a plane buoyant plume using Boussinesq approximation. Frequency-Reynolds number diagram with local non-dimensionalisation.

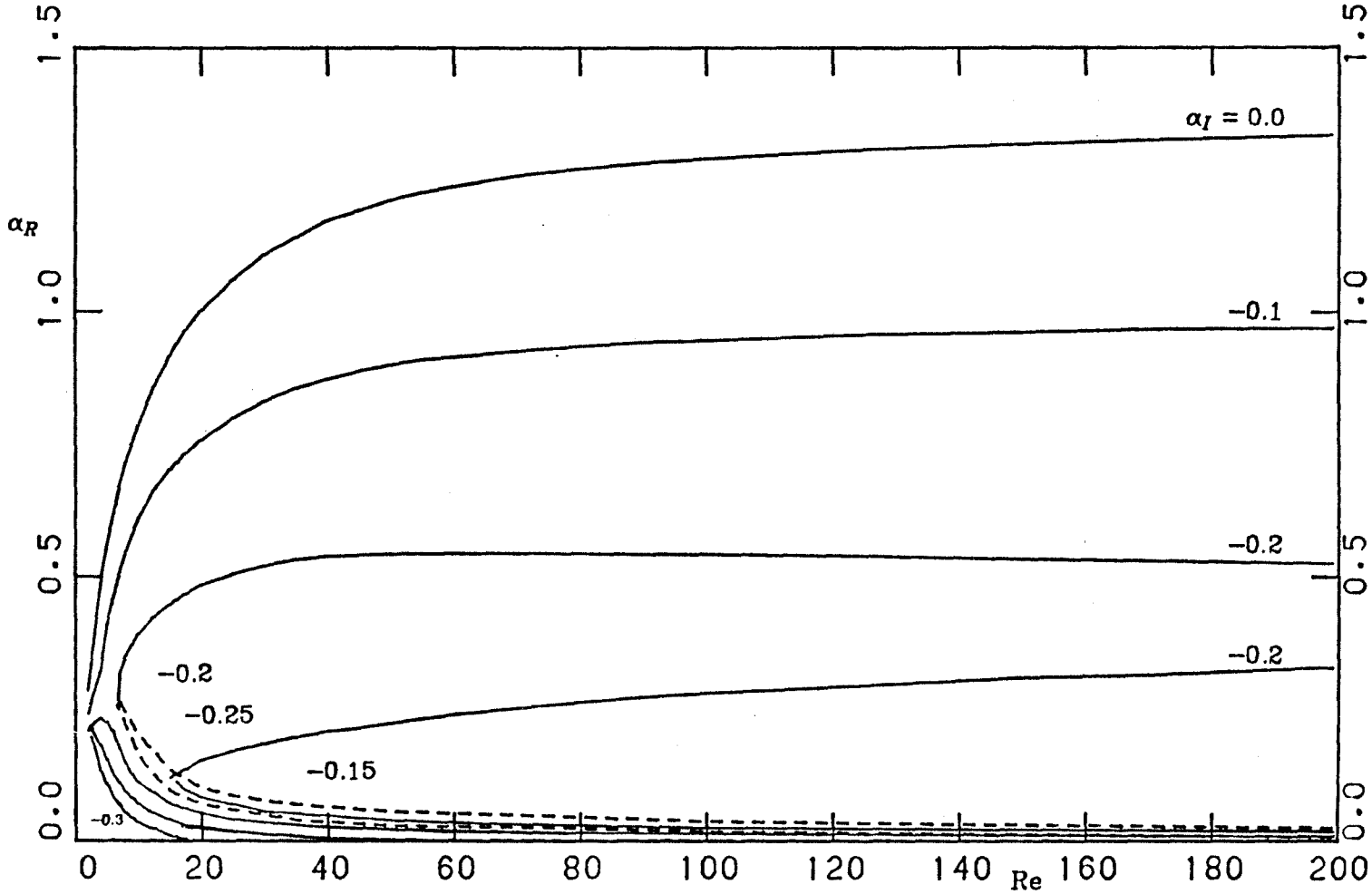

Figure (5.2) Neutral stability and amplification contours for a plane buoyant plume using Boussinesq approximation. Wave number-Reynolds number diagram with local non-dimensionalisation.

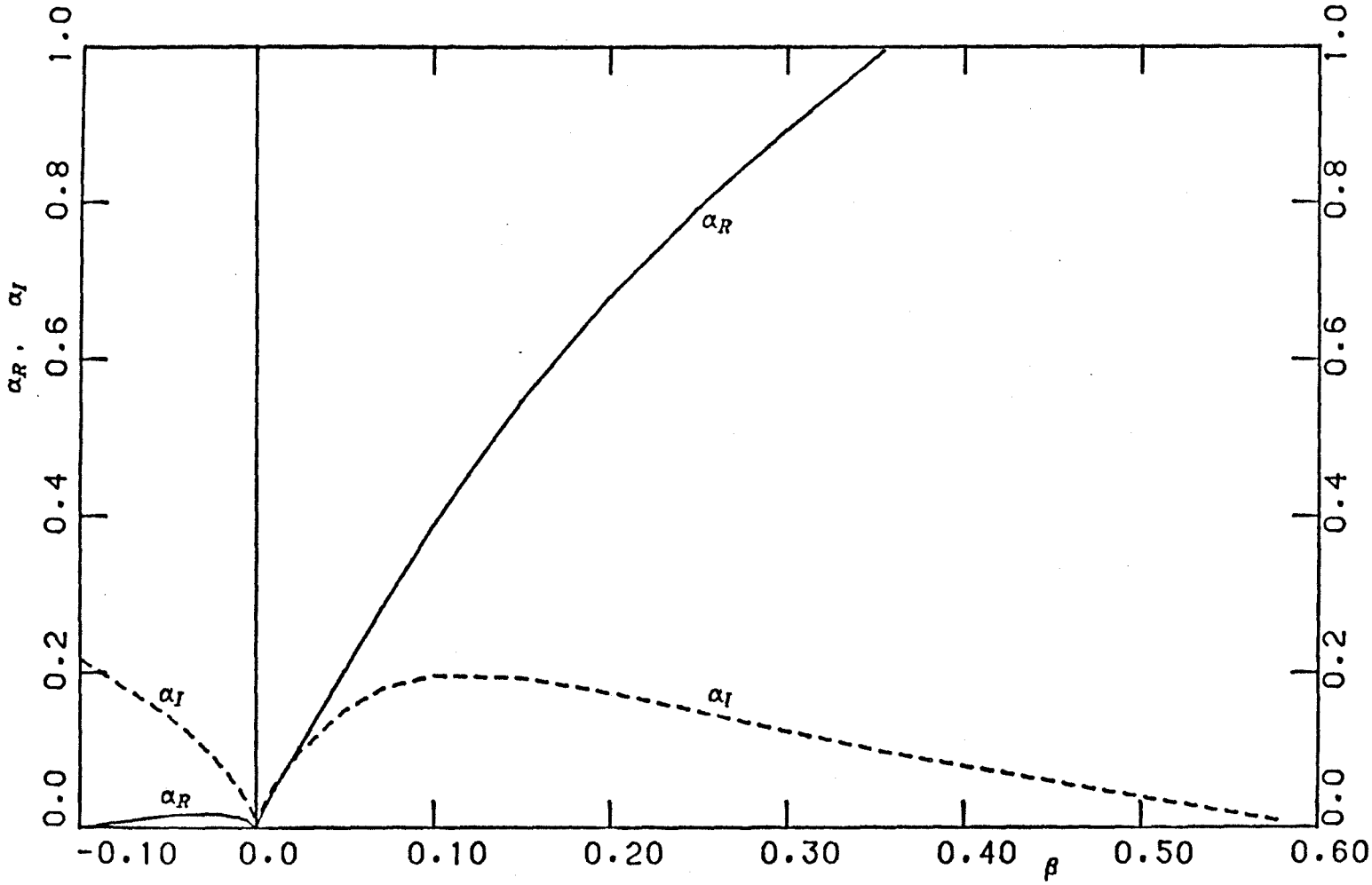

Figure (5.3) Inviscid asymptote for the stability of a plane buoyant plume using Boussinesq approximation. Variation of wave number and amplification rates with frequency.

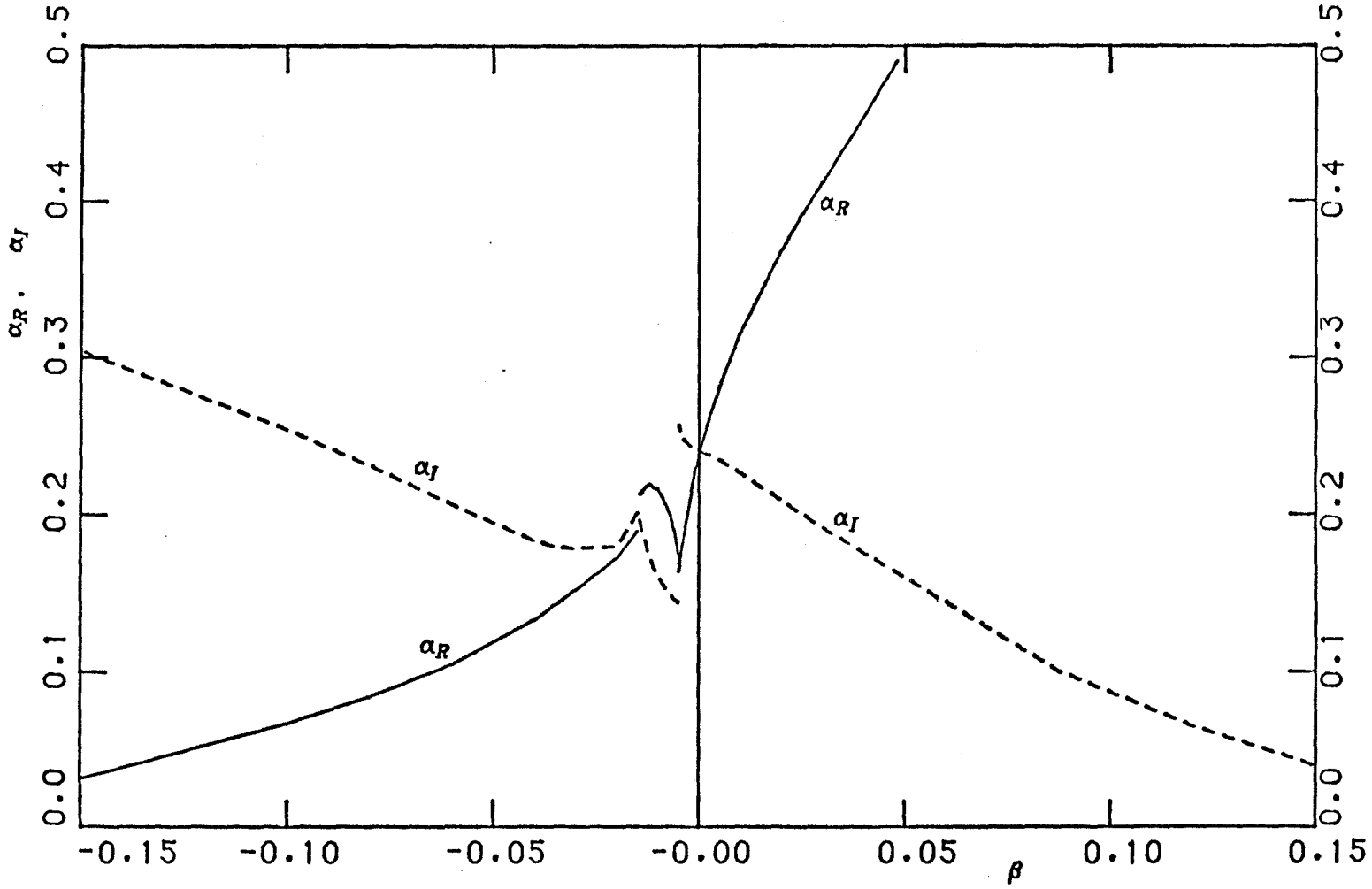

Figure (5.4) Stability a of plane buoyant plume using Boussinesq approximation. Variation of wave number and amplification rates with frequency at Re = 10.

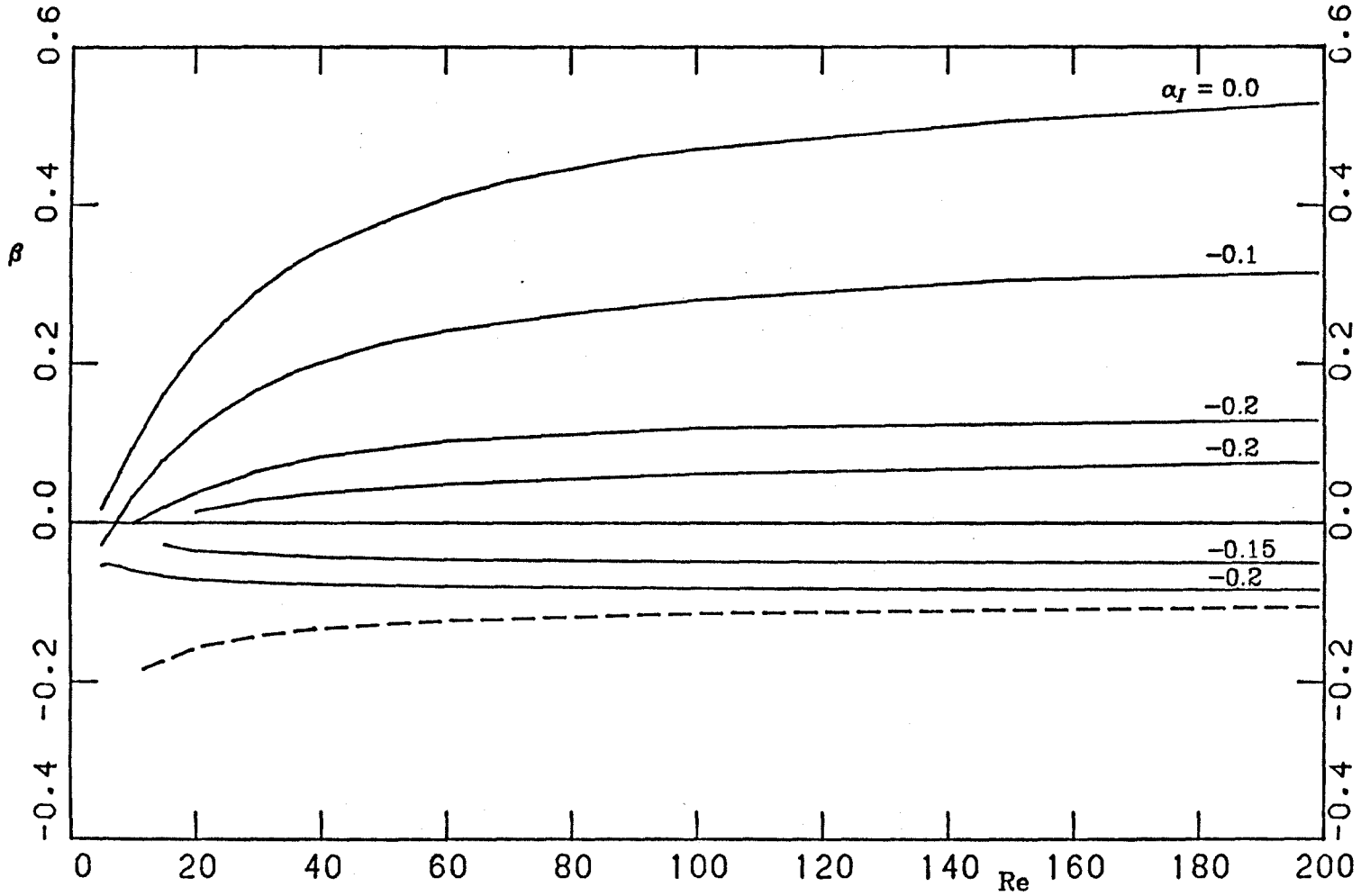

Figure (5.5) Neutral stability and amplification contours for a plane buoyant plume with $Q_p^* = 58.6\ Btu/hr\ ft.$ Frequency-Reynolds number diagram with local non-dimensionalisation.

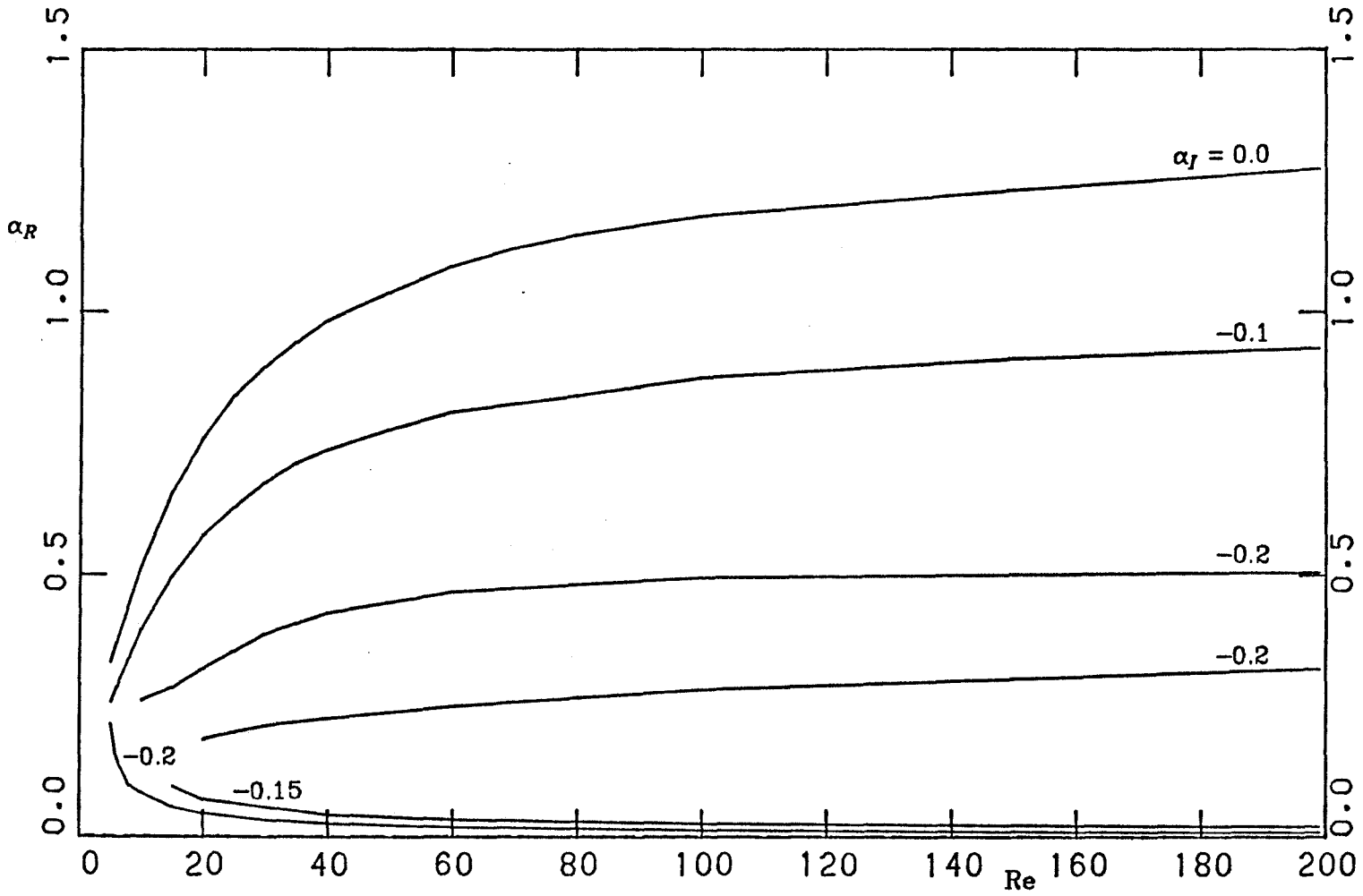

Figure (5.6) Neutral stability and amplification contours for a plane buoyant plume with $Q_p^* = 58.6 Btu/hr\ ft$. Wave number-Reynolds number diagram with local non-dimensionalisation.

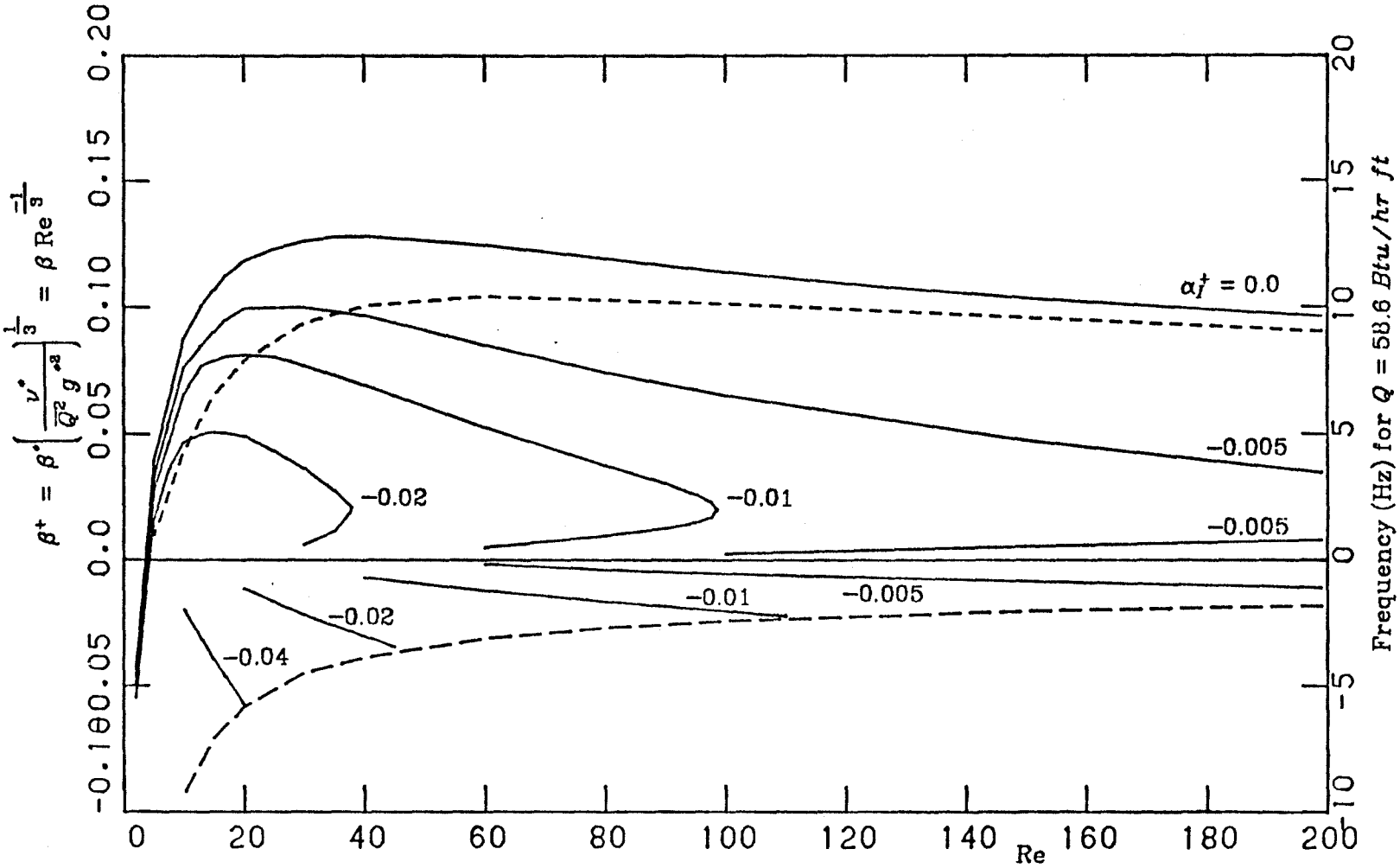

Figure (5.7) Neutral stability and amplification contours for a plane buoyant plume. Frequency-Reynolds number diagram with global non-dimensionalisation.

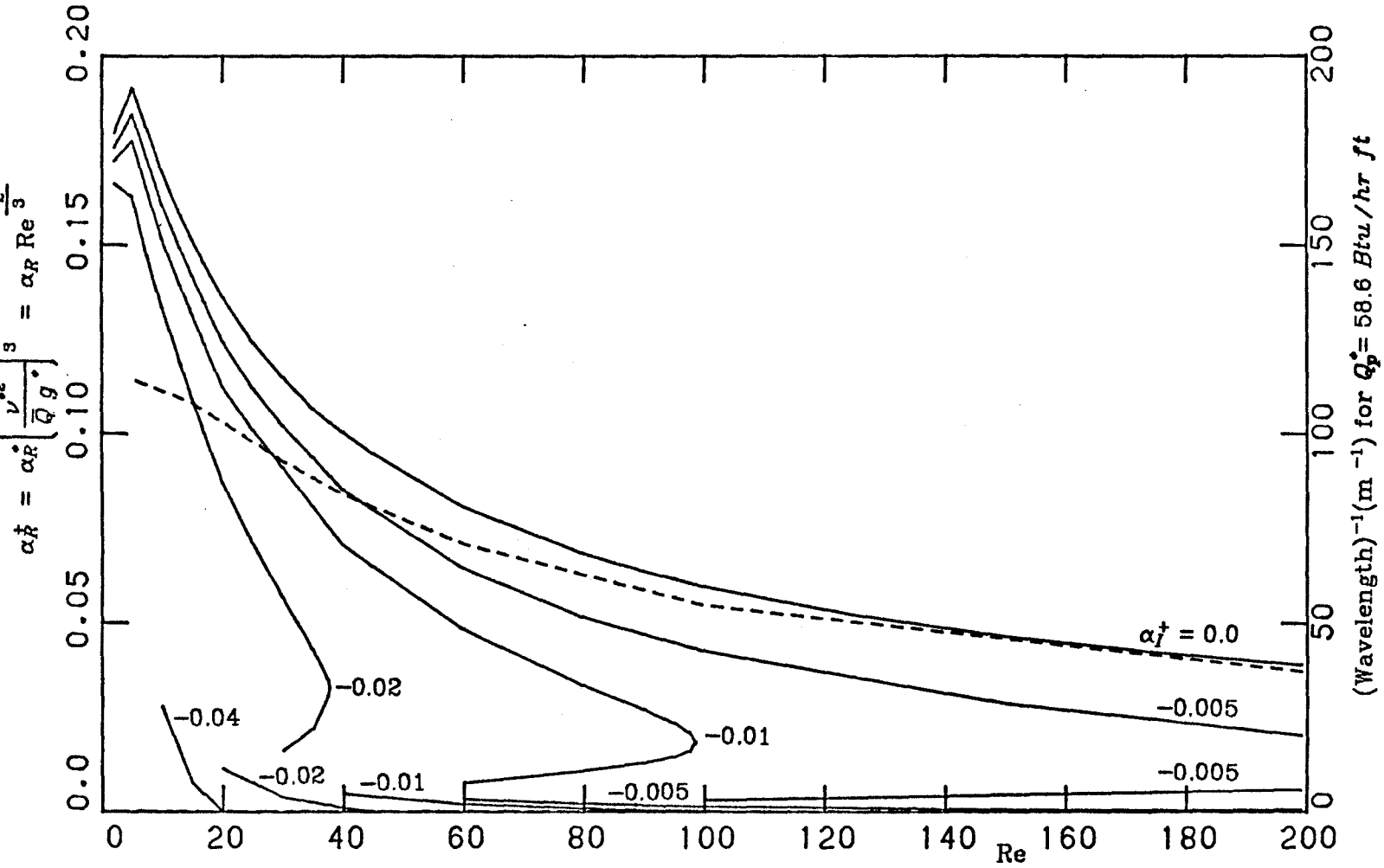

Figure (5.8) Neutral stability and amplification contours for a plane buoyant plume. Wave number-Reynolds number with global non-dimensionalisation.

Chapter 6.

STABILITY OF A BUOYANT FLAME SHEET TO LONG WAVELENGTH DISTURBANCES

6.1. Formulation

In Chapter 4, the importance of long wavelength disturbances was discussed, especially for waves with negative phase velocity. Disturbances of this kind are amenable to an analytic treatment where the thickness of the flame and associated convecting fluid layer is considered to be negligibly small compared to the disturbance wavelength. The resulting simplification of the problem allows the dependence of the integrated flow properties, such as momentum flux and buoyancy, on vertical height to be considered. The flow properties of interest are:
The mass flux M^*, given by

$$\frac{M^*}{\mu_\infty^* L^*} = m^* w^* = C_1 x^{\frac{3}{4}} \tag{6.1}$$

where

$$C_1 = \int_{-\infty}^{\infty} \zeta' d\eta \tag{6.2}$$

and

$$x \equiv \mathrm{Re}^{\frac{4}{3}} = 4\left[\frac{g^*\left(\frac{T_f}{T_\infty} - 1\right)}{\nu_\infty^{*2}}\right]^{\frac{1}{3}} x^* \tag{6.3}$$

The quantities m^* and w^* are the effective density and velocity of the flame averaged over its thickness, and L is the length of flame in the transverse direction. The momentum flux J^*, given by

$$\frac{J^*}{\rho_\infty^* \left[g^* \left(\frac{T_f}{T_\infty} - 1 \right) \nu_\infty^4 \right]^{\frac{1}{3}} L} \equiv m^* w^{*2} = C_2 x^{\frac{5}{4}} \tag{6.4}$$

where

$$C_2 = \int_{-\infty}^{\infty} \zeta'^2 d\eta \tag{6.5}$$

The entrainment velocities in the fuel and oxidizer, $v_{e\pm}^*$, given by

$$\frac{v_{e\pm}^*}{\left[g^* \left(\frac{T_f}{T_\infty} - 1 \right) \nu_\infty^* \right]^{\frac{1}{3}}} = -3\, \xi_{\pm\infty}\, x^{\frac{-1}{4}} \tag{6.6}$$

Using the expressions for the mass and momentum flux in the plume, the average density m^* can be obtained.

$$\frac{m^*}{\rho_\infty^* \left[\frac{\nu_\infty^{*2}}{g^* \left(\frac{T_f}{T_\infty} - 1 \right)} \right]^{\frac{1}{3}} L} = \frac{C_1^2}{C_2} x^{\frac{1}{4}} \tag{6.7}$$

For a symmetric flame, the constants are found to be

$$C_1 = 1.32,\ C_2 = 0.394,\ \xi_{\pm\infty} = \pm 0.6599 \tag{6.8}$$

In order to formulate the stability problem, it is necessary to find the steady velocity field generated by entrainment of fluid into the flame. This depends on the particular geometry being considered, so for the remainder of this chapter, it will be assumed that the flow is bounded by a wall at $x = 0$, as shown in figure

(6.1). To further simplify the problem, the flame will also be assumed to be symmetric. The steady potential flow must then satisfy the following governing equations and boundary conditions

$$\left.\begin{aligned} &\nabla^2 \varphi^*_{0+} = 0 \qquad x^* > 0,\ y^* > 0 \\ &\frac{\partial \varphi^*_{0+}}{\partial x^*} = 0 \qquad on\ x^* = 0 \\ &\frac{\partial \varphi^*_{0+}}{\partial y^*} = -A\, x^{*\frac{-1}{4}} \qquad on\ y^* = 0 \\ &\varphi^*_{0-}(x^*, y^*) = \varphi_{0+}(x^*, -y^*) \qquad x^* > 0,\ y^* < 0 \end{aligned}\right\} \tag{6.9}$$

where the + and - subscripts refer to the fuel and oxidizer side of the flame respectively and A is a known positive constant from equation (6.6). These equations are satisfied by the corner flow whose complex potential W^*_{0+} is given by

$$\left.\begin{aligned} W^*_{0+}(z) &= \varphi^*_{0+}(x^*, y^*) + i\psi^*_{0+}(x^*, y^*) \\ &= \frac{-4A}{3\cos\frac{\pi}{8}} (-iz)^{*\frac{3}{4}} \end{aligned}\right\} \tag{6.10}$$

where $z^* = x^* + iy^*$. Then the vertical velocity at the flame, v^*_{0+}, is given by

$$u_{0+}^{*} = \mathrm{Re}\left(\frac{dW^{*}}{dz^{*}}\right)\Bigg|_{x^{*}=x^{*}} = -A\tan\frac{\pi}{8}\,x^{*\frac{-1}{4}} \tag{6.11}$$

Other quantities which will be required are

$$\left.\begin{aligned}\frac{\partial^2\varphi_{0+}^{*}}{\partial y^{*2}} &= \frac{-A}{4}\tan\frac{\pi}{8}\,x^{*\frac{-5}{4}}\\[2ex] \frac{\partial^2\varphi_{0+}^{*}}{\partial x^{*}\partial y^{*}} &= \frac{A}{4}x^{*\frac{-5}{4}}\end{aligned}\right\} \tag{6.12}$$

For small disturbances, the complete potential describing non-steady motion of the flame can be found by considering a small perturbation about the steady solution

$$\varphi_{\pm}^{*}(x^{*},y^{*}) = \varphi_{0\pm}^{*}(x^{*},y^{*}) + \varphi_{1\pm}^{*}(x^{*},y^{*},t^{*}) \tag{6.13}$$

Two matching conditions are obtained across the flame from the kinematic and dynamic requirements which must be satisfied. The kinematic condition is obtained by expanding equation (6.13) in a Taylor series about $y^{*} = 0$ to obtain the horizontal velocity at the flame

$$\left.\begin{aligned}v_{+}^{*} &= \frac{\partial\varphi_{0+}^{*}}{\partial y^{*}} + \zeta^{*}\frac{\partial^2\varphi_{0+}^{*}}{\partial y^{*2}} + \ldots. + \frac{\partial\varphi_{1+}^{*}}{\partial y^{*}} + \ldots.\\[2ex] &= v_{s+}^{*} + \frac{\partial\zeta^{*}}{\partial t^{*}} + u_{+}^{*}\frac{\partial\zeta^{*}}{\partial x^{*}}\end{aligned}\right\} \tag{6.14}$$

thus

$$\frac{\partial \varphi_{1+}^{*}}{\partial y^{*}} = \frac{\partial \zeta^{*}}{\partial t^{*}} + u_{0+}^{*} \frac{\partial \zeta^{*}}{\partial x^{*}} - \zeta \frac{\partial^2 \varphi_{0+}^{*}}{\partial y^{*2}} \Bigg|_{y^{*}=0} \tag{6.15}$$

Similarly

$$\frac{\partial \varphi_{1-}^{*}}{\partial y^{*}} = \frac{\partial \zeta^{*}}{\partial t^{*}} + u_{0-}^{*} \frac{\partial \zeta^{*}}{\partial x^{*}} - \zeta \frac{\partial^2 \varphi_{0-}^{*}}{\partial y^{*2}} \Bigg|_{y^{*}=0} \tag{6.16}$$

The dynamic matching condition is obtained by considering conservation of horizontal momentum for the control volume shown in figure (6.2).

$$p_{-}^{*} - p_{+}^{*} + (\rho_{\infty}^{*} v_{-}^{*2} - \rho_{\infty}^{*} v_{+}^{*2}) - \frac{\partial}{\partial x^{*}} \left[m^{*} w^{*} \left(\frac{\partial \zeta^{*}}{\partial t^{*}} + w^{*} \frac{\partial \zeta^{*}}{\partial x^{*}} \right) \right]$$

$$- m^{*} \frac{\partial}{\partial t^{*}} \left(\frac{\partial \zeta^{*}}{\partial t^{*}} + w^{*} \frac{\partial \zeta^{*}}{\partial x^{*}} \right) = 0 \tag{6.17}$$

Using the Bernoulli equation, the pressure difference across the flame is found to be

$$p_{-}^{*} - p_{+}^{*} = \rho_{\infty}^{*} \left(\frac{\partial \varphi_{+}^{*}}{\partial t^{*}} - \frac{\partial \varphi_{-}^{*}}{\partial t^{*}} \right) + \frac{\rho_{\infty}^{*}}{2} \left[(u_{+}^{*2} + v_{+}^{*2}) - (u_{-}^{*2} + v_{-}^{*2}) \right] \tag{6.18}$$

Subtracting equation (6.17) from equation (6.18) gives

$$\rho_{\infty}^{*} \left(\frac{\partial \varphi_{+}^{*}}{\partial t^{*}} - \frac{\partial \varphi_{-}^{*}}{\partial t^{*}} \right) + \frac{\rho_{\infty}^{*}}{2} \left[(v_{-}^{*2} - u_{-}^{*2}) - (v_{+}^{*2} - u_{+}^{*2}) \right]$$

$$\left.- \frac{\partial}{\partial x^*}\left[m^* w^* \left[\frac{\partial \zeta^*}{\partial t^*} + w^* \frac{\partial \zeta^*}{\partial x^*}\right]\right] - m^* \frac{\partial}{\partial t^*}\left[\frac{\partial \zeta^*}{\partial t^*} + w^* \frac{\partial \zeta^*}{\partial x^*}\right] = 0 \right\} (6.19)$$

Substituting from equation (6.14) for v_+^*, using

$$u_+^* = u_{0+}^* + \zeta^* \frac{\partial^2 \varphi_{0+}^*}{\partial x^* \partial y^*}\bigg|_{y^*=0} + \ldots + \frac{\partial \varphi_{1+}^*}{\partial x^*} + \ldots$$

and linearising, noting that the zeroeth order is satisfied identically, i.e. the steady potentials, φ_{0+}^* and φ_{0-}^*, satisfy the dynamic matching condition, gives

$$\left.\begin{aligned} &\rho_\infty^*\left[\frac{\partial \varphi_{1+}^*}{\partial t^*} - \frac{\partial \varphi_{1-}^*}{\partial t^*}\right] + \rho_\infty^*(v_{s-}^* - v_{s+}^*)\left[\frac{\partial \zeta^*}{\partial t^*} + u_{0+}^* \frac{\partial \zeta^*}{\partial x^*}\right] + \\ &\rho_\infty^*\left[u_{0+}^*\left[\frac{\partial \varphi_{1+}^*}{\partial x^*} + \zeta^* \frac{\partial^2 \varphi_{0+}^*}{\partial x^* \partial y^*}\bigg|_{y^*=0}\right] - u_{0-}^*\left[\frac{\partial \varphi_{1-}^*}{\partial x^*} + \zeta^* \frac{\partial^2 \varphi_{0-}^*}{\partial x^* \partial y^*}\bigg|_{y^*=0}\right]\right] \\ &- \frac{\partial}{\partial x^*}\left[m^* w^* \left[\frac{\partial \zeta^*}{\partial t^*} + w^* \frac{\partial \zeta^*}{\partial x^*}\right]\right] - m^* \frac{\partial}{\partial t^*}\left[\frac{\partial \zeta^*}{\partial t^*} + w^* \frac{\partial \zeta^*}{\partial x^*}\right] = 0 \end{aligned}\right\} (6.20)$$

This can be somewhat simplified by use of the steady mass conservation equation

$$\rho_\infty^*(v_{s-}^* - v_{s+}^*) = \frac{d}{dx^*}(m^* w^*)$$

and by noting that, from conservation of vertical momentum, the buoyancy, $\tilde{\beta}^*$, of the plume can be related to the momentum flux by

$$\tilde{\beta}^* = \int_{-\infty}^{\infty}(\rho_\infty^* - \rho^*)g^* dy^* = \frac{d}{dx^*}\int_{-\infty}^{\infty}\rho^* u^{*2} dy^* = \frac{dJ^*}{dx^*}$$

The dynamic matching condition at $y^* = 0$ is thus given by

$$\rho_\infty^*\left[\frac{\partial\varphi_{1+}^*}{\partial t^*} - \frac{\partial\varphi_{1-}^*}{\partial t^*}\right] + \rho_\infty^*(v_{e-}^* - v_{e+}^*)u_{0+}^* \frac{\partial\zeta^*}{\partial x^*} +$$

$$\underbrace{\rho_\infty^* u_{0+}^*\left[\frac{\partial\varphi_{1+}^*}{\partial x^*} + \zeta^* \frac{\partial^2\varphi_{0+}^*}{\partial x^* \partial y}\bigg|_{y^*=0} - \left[\frac{\partial\varphi_{1-}^*}{\partial x^*} + \zeta^* \frac{\partial^2\varphi_{0-}^*}{\partial x^{*2}}\bigg|_{y^*=0}\right]\right]}_{\text{Pressure difference across the flame due to non-steady perturbation}} =$$

$$\underbrace{m^*\left[\frac{\partial}{\partial t^*} + w^*\frac{\partial}{\partial x^*}\right]\frac{\partial\zeta^*}{\partial t^*}}_{\text{Inertial reaction due to acceleration mass}} + \underbrace{m^* w^*\left[\frac{\partial}{\partial t^*} + w^*\frac{\partial}{\partial x^*}\right]\frac{\partial\zeta^*}{\partial x^*}}_{\text{Inertial reaction due to momentum flux}} + \underbrace{\frac{\partial}{\partial x^*}(m^* w^{*2})\frac{\partial\zeta^*}{\partial x^*}}_{\text{Component of buoyancy force perpendicular to flame sheet}}$$

The symmetry of the problem allows the simplification of determining only one potential, $\varphi^*(x^*,y^*,t^*) = \varphi_{1+}^*(x^*,y^*,t^*) = -\varphi_{1-}^*(x^*,-y^*,t^*)$. Using this and the following length and time scales for non-dimensionalisation

$$l = \frac{1}{4}\left[\frac{\nu_\infty^{*2}}{g^*\left(\frac{T_f}{T_\infty} - 1\right)}\right]^{\frac{1}{3}}$$

$$\left.\begin{aligned} \tau = \frac{1}{4}\left[\frac{\nu_\infty^*}{g^{*2}\left(\frac{T_f}{T_\infty}-1\right)^2}\right]^{\frac{1}{3}} \end{aligned}\right\} \qquad (6.21)$$

the dynamic matching condition reduces to

$$\frac{\partial\varphi}{\partial t} - C_3 x^{\frac{-1}{2}}\frac{\partial\tilde{\xi}}{\partial x} - C_4 x^{\frac{-1}{4}}\frac{\partial\varphi}{\partial x} - \frac{C_3}{4}x^{\frac{-3}{2}}\tilde{\xi} =$$

$$\frac{2C_1^2}{C_2}x^{\frac{1}{4}}\frac{\partial^2\tilde{\xi}}{\partial t^2} + 4C_1 x^{\frac{3}{4}}\frac{\partial^2\tilde{\xi}}{\partial x\,\partial t} + 2C_2\frac{\partial}{\partial x}\left[x^{\frac{5}{4}}\frac{\partial\tilde{\xi}}{\partial x}\right] \qquad at\ y = 0 \qquad (6.22)$$

where all variables are non-dimensional. The kinematic conditon, equation (6.15), becomes

$$\frac{\partial\varphi}{\partial y} = \frac{\partial\tilde{\xi}}{\partial t} - C_4\frac{\partial}{\partial x}(x^{\frac{-1}{4}}\tilde{\xi}) \qquad at\ y = 0 \qquad (6.23)$$

The constants in these equations are given in equation (6.8) and (6.24).

$$C_3 = 9\xi_{+\infty}^2\tan\frac{\pi}{8},\quad C_4 = 3\,\xi_{+\infty}\tan\frac{\pi}{8}, \qquad (6.24)$$

The problem has thus been reduced to determining a potential $\varphi(x,y,t)$ and flame position $\tilde{\xi}(x,t)$ such that

$$\nabla^2\varphi = 0 \qquad x > 0,\ y > 0$$

$$\left.\begin{aligned} &\frac{\partial \varphi}{\partial x} = 0 && \text{on } x = 0 \\ &\frac{\partial \tilde{\xi}}{\partial x} = 0 && \text{on } x = 0 \\ &|\nabla \varphi| \to 0 && \text{as } \sqrt{x^2 + y^2} \to \infty \end{aligned}\right\} \qquad (6.25)$$

and satisfying matching conditions at $y = 0$ given by equations (6.22) and (6.23) and initial conditions $\tilde{\xi}$ and $\frac{\partial \tilde{\xi}}{\partial t}$ specified at $t = 0$.

6.2. Asymptotic Solution

Consider the non-dimensional variable

$$x = \frac{x^*}{l} = 4x^* \left[\frac{g^* \left[\frac{T_f}{T_\infty} - 1 \right]}{\nu_\infty^{*2}} \right]^{\frac{1}{3}} = \mathrm{Re}^{\frac{4}{3}}$$

If $\nu_\infty^* = 2\text{x}10^{-6} m^2/s$, the kinematic viscosity of air at $350^\circ K$, and $\left[\frac{T_f}{T_\infty} - 1 \right] = 5$, then $x > 1$ if $x^* > 0.05mm$. It would therefore seem reasonable to examine the asymptotic behaviour of the solution for large x.

Consider a harmonic function φ with $\frac{\partial \varphi}{\partial y}$ specified on $y = 0$. Then

$$\frac{\partial \varphi}{\partial y}(x,y) = \frac{1}{\pi} \int_{-\infty}^{\infty} \frac{y}{(x - \xi)^2 + y^2} \frac{\partial \varphi}{\partial y}(\xi,0) d\xi$$

thus

$$\frac{\partial \varphi}{\partial x}(x,y) = \frac{1}{\pi}\int_{-\infty}^{\infty} \frac{(x-\xi)}{(x-\xi)^2 + y^2} \frac{\partial \varphi}{\partial y}(\xi,0)d\xi$$

If φ is symmetric about $x = 0$ then

$$\frac{\partial \varphi}{\partial x} = \frac{2}{\pi}\, p.v \int_0^{\infty} \frac{x}{x^2 - \xi^2} \frac{\partial \varphi}{\partial y}(\xi,0)d\xi \qquad on\ y = 0$$

where the integral is to be evaluated as a principal value. Thus from equation (6.23), an expression can be obtained for $\frac{\partial \varphi}{\partial x}$ in terms of $\tilde{\zeta}$ and $\frac{\partial \tilde{\zeta}}{\partial t}$. Substituting in equation (6.22) and differentiating with respect to x yields the following integro-differential equation for $\tilde{\zeta}$.

$$\left.\begin{aligned} &\frac{2}{\pi}\left(\frac{\partial}{\partial t} - C_4 \frac{\partial}{\partial x} x^{-\frac{1}{4}}\right) p.v \int_0^{\infty} \frac{x}{x^2 - \xi^2}\left(\frac{\partial \tilde{\zeta}}{\partial t}(\xi,t) - C_4 \frac{\partial}{\partial \xi}(\xi^{\frac{-1}{4}} \tilde{\zeta}(\xi,t))\right) d\xi = \\ &C_3 \frac{\partial}{\partial x}\left(x^{\frac{-1}{2}} \frac{\partial \tilde{\zeta}}{\partial x}\right) + \frac{C_3}{4}\frac{\partial}{\partial x}(x^{\frac{-3}{2}} \tilde{\zeta}) + \\ &\frac{\partial}{\partial x}\left(\frac{2C_1^2}{C_2} x^{\frac{1}{4}} \frac{\partial^2 \tilde{\zeta}}{\partial t^2} + 4C_1 x^{\frac{3}{4}} \frac{\partial^2 \tilde{\zeta}}{\partial x \partial t} + 2C_2 \frac{\partial}{\partial x}\left(x^{\frac{5}{4}} \frac{\partial \tilde{\zeta}}{\partial x}\right)\right) \end{aligned}\right\} \quad (6.26)$$

Because all coefficients are independent of time, solutions may be restricted to the form

$$\tilde{\zeta}(x,t) = \zeta(x) e^{\lambda t} \qquad (6.27)$$

Now consider the integral on the left-hand side of equation (6.26)

$$I = p.v \int_0^\infty \frac{x}{x^2 - \xi^2} \left[\lambda \frac{\partial \zeta}{\partial t} - C_4 \frac{\partial}{\partial \xi} (\xi^{\frac{-1}{4}} \zeta) \right] d\xi$$

Since equation (6.26) is linear, ζ can be taken to be a complex valued function of x, which can be extended analytically into the $z = x + iy$ plane by substituting $z = x$. The integral I can then be determined by integration around a contour in the first quadrant of the $\tilde{z} = \xi + i\chi$ plane, as shown in figure (6.3). Then

$$\oint_C \frac{x}{x^2 - \tilde{z}^2} fn(\tilde{z}) d\tilde{z} = p.v \int_0^\infty \frac{x}{x^2 - \xi^2} fn(\xi) d\xi -$$

$$\int_0^\infty \frac{x}{x^2 + \chi^2} fn(i\chi) i d\chi + \int_0^\pi \frac{x}{x^2 - R^2 e^{2i\vartheta}} R\, e^{i\vartheta} fn(Re^{i\vartheta}) d\vartheta$$

$$- \pi i \ (Residue \ at \ \tilde{z} = x) = 0$$

assuming that the only pole occurs at $\tilde{z} = x$. The first integral on the right-hand side is the desired integral I, the second term is of order $\frac{1}{x}$ assuming $\int_0^\infty fn(i\chi) d\chi$ exists, and the third integral vanishes as $R \to \infty$ provided $\frac{1}{R} |fn(z)| \to 0$ as $|z| \to \infty$. Thus the integral equation (6.26) can be approximated by

$$-i \left[\lambda - C_4 \frac{\partial}{\partial x} x^{\frac{-1}{4}} \right] \left[\lambda \zeta - C_4 \frac{\partial}{\partial x} (x^{\frac{-1}{4}} \zeta) \right] = C_3 \frac{\partial}{\partial x} \left[x^{\frac{-1}{2}} \frac{\partial \zeta}{\partial x} \right]$$

$$+ \frac{C_3}{4} \frac{\partial}{\partial x} (x^{\frac{-3}{2}} \zeta) + \frac{\partial}{\partial x} \left[\frac{2C_1^2}{C_2} \lambda^2 x^{\frac{1}{4}} \zeta + 4C_1 x^{\frac{3}{4}} \lambda \frac{\partial \zeta}{\partial x} + 2C_2 \frac{\partial}{\partial x} \left[x^{\frac{5}{4}} \frac{\partial \zeta}{\partial x} \right] \right] \quad (6.28)$$

$$+ O\left[\frac{1}{x}\right] \quad as\ x \to \infty$$

This equation has an irregular singular point at $x = \infty$, therefore a solution of the form, see Bender and Orszag, reference (6.1), 1978, chapter 3,

$$\zeta = e^{S(x)} \tag{6.29}$$

is assumed. Substituting in equation (6.28) gives

$$-i\left[\lambda^2 - 2\lambda C_4 x^{\frac{-1}{4}} S' + \frac{1}{2}\lambda C_4 x^{\frac{-5}{4}} + C_4^2\left[x^{\frac{-1}{2}}(S'' + S'^2)\right.\right.$$

$$\left.\left. - \frac{3}{4}x^{\frac{-3}{2}} S' + \frac{3}{8}x^{\frac{-5}{2}}\right]\right] = \frac{-1}{2} C_3 x^{\frac{-3}{2}} S' + C_3 x^{\frac{-1}{2}}(S'' + S'^2)$$

$$- \frac{3}{2}\frac{C_3}{4}x^{\frac{-5}{2}} + \frac{C_3}{4}x^{\frac{-3}{2}} S' - \frac{C_1^2}{2C_2}\lambda^2 x^{\frac{-3}{4}} + \frac{2C_1^2}{C_2}\lambda^2 x^{\frac{1}{4}} S'$$

$$- 3C_1 x^{\frac{-1}{4}}\lambda S' + 4C_1 x^{\frac{3}{4}}\lambda(S'' + S'^2) + \frac{5}{8} C_2 x^{\frac{-3}{4}} S'$$

$$+ 5x^{\frac{1}{4}} C_2(S'' + S'^2) + 2x^{\frac{5}{4}} C_2\left[(S')^3 + 3S'S'' + S'''\right]$$

Assuming $(S')^3 >> S'''$, $(S')^3 >> S''S'$, $(S')^2 >> S''$ and keeping only the highest powers in x gives

$$\left.\begin{aligned}
&\left[-i\lambda^2 + \frac{C_1^2}{2C_2}\lambda^2 x^{\frac{-3}{4}} + O\left[x^{\frac{-5}{4}}\right]\right] = \\
&\left[\frac{2C_1^2}{C_2}\lambda^2 x^{\frac{1}{4}} - (3C_1\lambda - 2\lambda i C_4)x^{-\frac{1}{4}} + O\left[x^{\frac{-3}{4}}\right]\right]S' \\
&\left[4C_1 x^{\frac{3}{4}}\lambda + 5C_2 x^{\frac{1}{4}} + O\left[x^{\frac{-1}{2}}\right]\right]S'^2 + 2C_2 x^{\frac{5}{4}}(S')^3 \\
&+ O\left[x^{\frac{5}{4}}S''', x^{\frac{5}{4}}S''\ S', x^{\frac{3}{4}}S'\right]
\end{aligned}\right\} \qquad (6.30)$$

This equation could be solved directly for S' and integrated, however it is easier to try a solution of the form

$$S = k_0 x^{\frac{7}{12}} + k_1 x^{\frac{6}{12}} + k_2 x^{\frac{5}{12}} + \ldots.$$

Substituting in equation (6.30) then gives

$$-i\lambda^2 = 2C_2\left[\frac{7}{12}k_0\right]^3$$

$$0 = 3C_2\left[\frac{7}{12}k_0\right]^2\left[\frac{1}{2}k_1\right] + 2C_1\lambda\left[\frac{7}{12}k_0\right]^2$$

$$0 = 3C_2\left[\left[\frac{7}{12}k_0\right]\left[\frac{1}{2}k_1\right]^2 + \left[\frac{7}{12}k_0\right]^2\left[\frac{5}{12}k_2\right]\right]$$

$$+ 2C_1\lambda\left[\frac{7}{12}k_0k_1\right] + \frac{C_1^2}{C_2}\left[\frac{7}{12}k_0\right]\lambda^2 \Bigg\}$$

etc

Solving these equations gives

$$\left.\begin{aligned} \frac{7}{12}k_0 &= i\left[\frac{\lambda^2}{2C_2}\right]^{\frac{1}{3}},\quad e^{\frac{-i\pi}{6}}\left[\frac{\lambda^2}{2C_2}\right]^{\frac{1}{3}},\quad e^{\frac{7\pi i}{6}}\left[\frac{\lambda^2}{2C_2}\right]^{\frac{1}{3}} \\ \frac{1}{2}k_1 &= \frac{-2C_1}{3C_2}\lambda \\ \frac{5}{12}k_2 &= \frac{1}{\frac{7}{12}k_0}\frac{C_1^2\lambda^2}{9C_2^2} \end{aligned}\right\} \quad (6.31)$$

etc

To find the leading behaviour near the singular point at infinity, let

$$S(x) = k(x) + C(x)$$

where $k(x) = \sum_{n=0}^{k_n} x^{\frac{7-n}{12}} \sim k_0 x^{\frac{7}{12}}$ *as* $x \to \infty$ and $C(x) << k(x)$ *as* $x \to \infty$. Then to leading order

$$3k'^2C' + 3k''k' = 0$$

thus

$$C = \frac{5}{12}\ln Ax + O\left(x^{\frac{-1}{12}}\right)$$

The asymptotic behaviour of the solution is therefore given by

$$\zeta \sim x^{\frac{5}{12}} e^{k(x)} e^{\lambda t} \qquad as\ x \to \infty \tag{6.32}$$

where

$$k(x) \sim \sum_{n=0}^{\infty} k_n x^{\frac{7-n}{12}} \tag{6.33}$$

with the k_n's given in equation (6.31). In order to satisfy the boundary condition $\frac{\partial \zeta}{\partial x} e^{\lambda t} = 0$ at $x = 0$ for all time, either λ must be real or both the real and imaginary parts of $\frac{\partial \zeta}{\partial x}$ at $x = 0$ must vanish. The latter requirement imposes too many conditions on ζ and will not be able to be satisfied in general. The condition that λ is real leaves two solutions that satisfy the conditions for integration around the contour in the first quadrant, these being the solutions with $Re(k(x)) < 0$ as $x \to 0$, and are given by

$$\zeta \sim x^{\frac{5}{12}} e^{\,i\frac{12}{7}\left[\frac{\lambda^2}{2C_2}\right]^{\frac{1}{3}} x^{\frac{7}{12}}\left[1 - i\frac{7}{9}sgn(\lambda)\left[\frac{\lambda^2}{2C_2}\right]^{\frac{1}{6}} x^{\frac{-1}{12}}\right.}$$

$$\left. - \frac{7}{45}\left[\frac{2C_1^2}{C_2}\right]\left[\frac{\lambda^2}{2C_2}\right]^{\frac{1}{3}} x^{\frac{-1}{6}} + \ldots.\right] \qquad \lambda > 0 \tag{6.34}$$

and

$$\zeta \sim x^{\frac{5}{12}} e^{i\frac{12}{7}\left[\frac{\lambda^2}{2C_2}\right]^{\frac{1}{3}} x^{\frac{7}{12}}} \left[e^{\frac{2\pi i}{3}} - i\frac{7}{9}\mathrm{sgn}(\lambda)\left[\frac{\lambda^2}{2C_2}\right]^{\frac{1}{6}} x^{\frac{-1}{12}} \right.$$

$$\left. - \frac{7}{45} e^{\frac{-2\pi i}{3}} \left[\frac{2C_1^2}{C_2}\right]\left[\frac{\lambda^2}{2C_2}\right]^{\frac{1}{3}} x^{\frac{-1}{6}} + \ldots \right] \qquad (6.35)$$

All these solutions decay exponentially with x as $x \to \infty$, and thus become small compared to the neglected portion of the integral, which decreases like $\frac{1}{x}$ as $x \to \infty$. If λ is small however, the exponential decay will be sufficiently slow that a region with x large, but $\lambda\sqrt{x}$ or $\lambda^{\frac{2}{3}} x^{\frac{7}{12}}$ of order one will exist. In this region, the asymptotic forms given in equations (6.34) and (6.35) will be valid.

The preceding analysis indicates that instability results primarily due to the action of centrifugal forces, $F_c = J^* \frac{\partial^2 \zeta^*}{\partial x^{*2}} = \frac{m^* w^{*2}}{r^*}$, where r is the radius of curvature of the flame, balanced by the force required to overcome the inertia of the external fluid, $\rho_\infty^* \frac{\partial \varphi^*}{\partial t^*}$. Shorter wavelengths are therefore amplified at faster rates than long wavelengths, since they have smaller radii of curvature, thus increasing the centrifugal forces. The analysis, however, becomes invalid for small wavelengths so non-linear effects must presumably limit the temporal growth rate.

Direct comparison of these results, which deal with a primarily temporal instability, with the results of the local analysis of Chapter 4, which assumes spatial amplification, is somewhat difficult, however there are some points of similarity. Rewriting the expressions for the asymptotic forms using the local non-dimensionalisation of Chapter 4 shows that the disturbance approaches an inviscid asymptote with the same Reynolds number dependence, apart from the algebraic terms $x^{\frac{5}{12}}$ multiplying the exponential term, as the inviscid asymptote

for the local stability analysis, shown in figure (4.13). Taking just the first term in the exponent of equation (6.34) gives

$$\beta_i \approx 0.4\alpha_R^{\frac{3}{2}} \tag{6.36}$$

To agree well with this, α_R and α_I would have to grow like $\beta^{\frac{2}{3}}$ in figure (4.13), which is not true except for perhaps a small region near $\beta = 0$. However, using Gaster's relation, reference (6.2), 1963, given in equation (4.1), and equation (4.2) for the group velocity, to obtain an estimate of β_i from figure (4.13) gives

$$\beta_i \approx 0.07\alpha_R \qquad 0 \lesssim \alpha_R \lesssim 0.1, \quad \beta_R > 0 \tag{6.36}$$

which when compared to equation (6.36) gives remarkably good agreement in predicting amplification rates.

References.

(6.1) C. M. BENDER, and S. A. ORSZAG, Advanced Mathematical Methods for Scientists and Engineers, *McGraw-Hill*, 1978, chapter 3.

(6.2) M. GASTER, A Note on the Relation between Temporally-Increasing and Spatially-Increasing Disturbances in Hydrodynamic Stability, *JFM* 14 222, (1963)

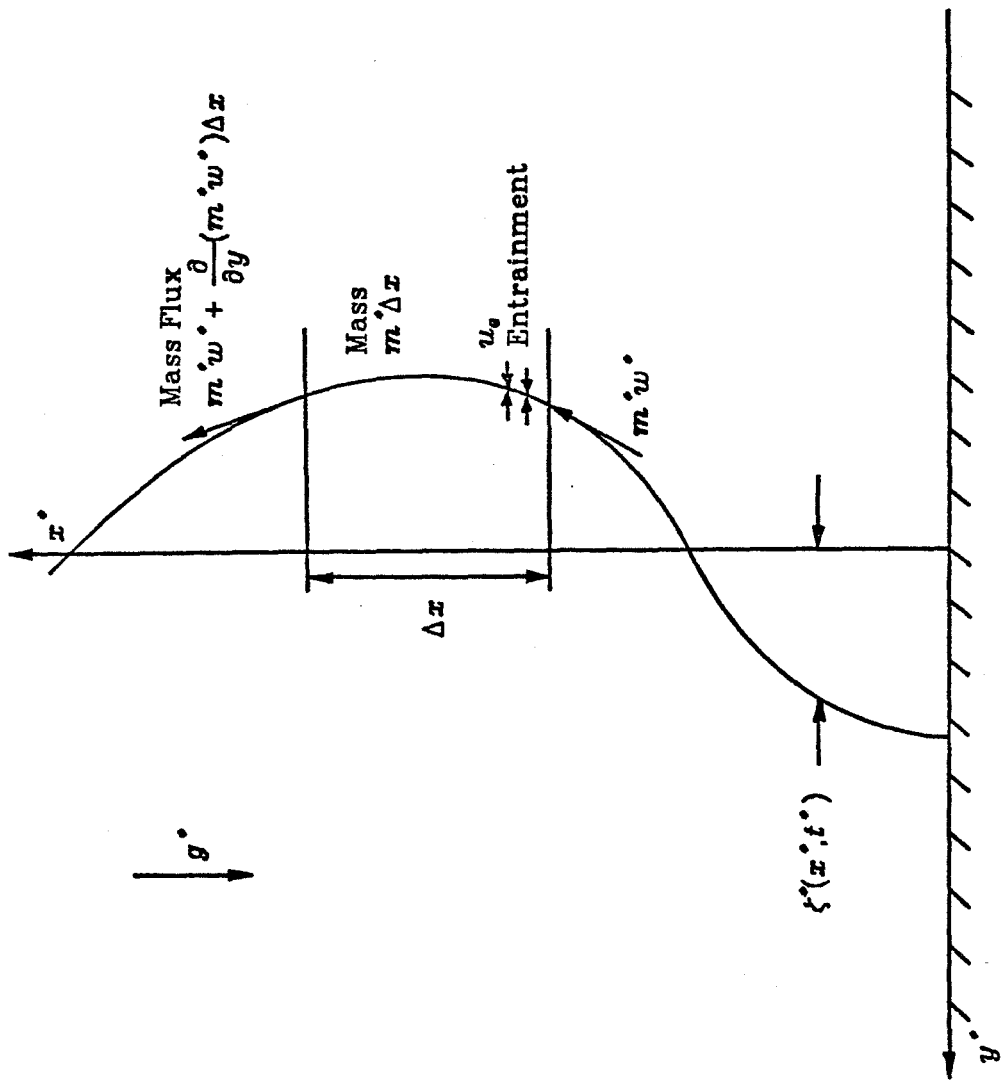

Figure (6.2) Control volume for momentum balance across flame

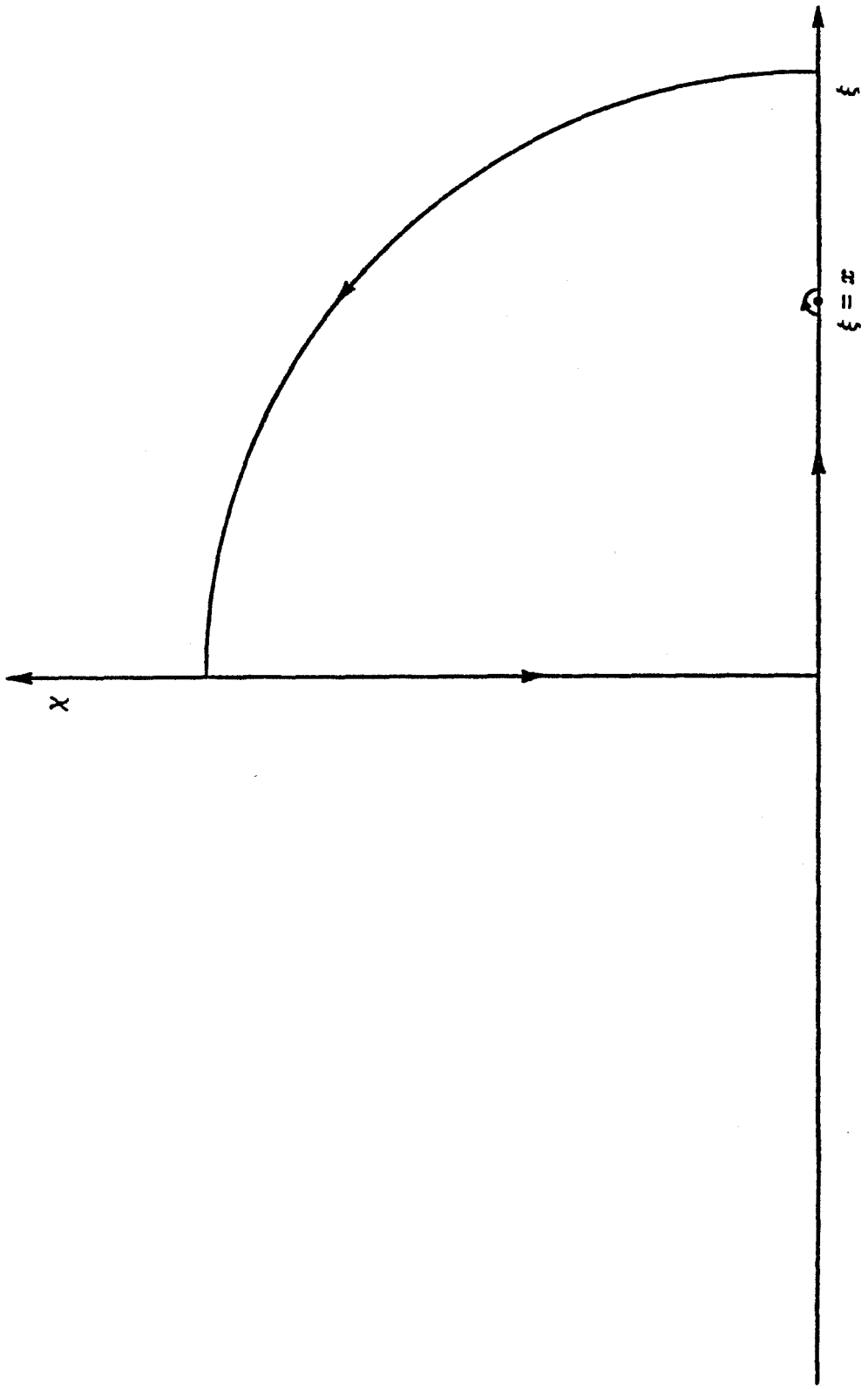

Figure (6.3) Integration contour in $z' = \xi + i\chi$ plane

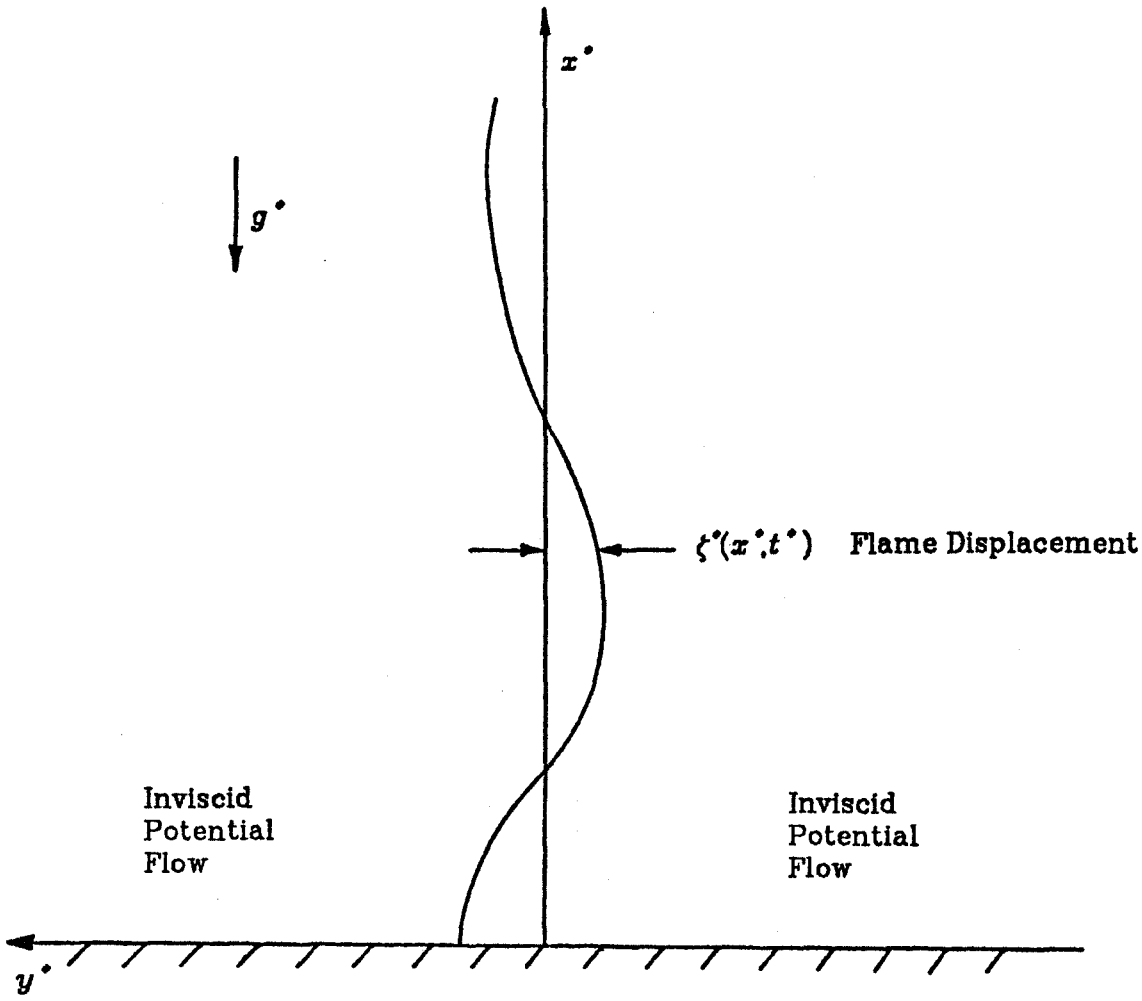

Figure (6.1) Geometry for perturbed flame

Chapter 7.

CONCLUDING REMARKS

It has been the aim of this thesis to present a detailed description of the structure and stability of the convecting fluid flow generated by a diffusion flame. The geometry selected for the steady problem is the most fundamental example of a buoyant diffusion flame available, yet has practical significance for many real situations from candle flames to fires in buildings. Use of the Howarth transformation to allow large density variations to be accommodated is an important part of both this steady analysis and the stability analysis that follows. Modelling of real fuels is accomplished by selecting appropriate stoichiometric ratios and density ratios of fuel to oxidizer, and the results show extreme asymmetries in the flow fields for common reactants, with much of the entrained air being swept through the flame sheet in the form of hot combustion products. This results in a convecting plume on the fuel side of the flame much larger than on the oxidizer side, which retards the diffusion of fuel to the flame and preheats it over a considerable region before reaction with the oxidizer takes place. This might lead to decomposition of the fuel outside of the thin region where the reaction is assumed to occur.

The question of the stability of the laminar solution is of importance in determining when the steady laminar description of the flow is applicable. Local linear stability analysis including all the variable density terms produced some interesting and unusual results. First, it was found that using the Boussinesq approximation to neglect density variations except in the body force term of the vertical momentum equation was not applicable to the flame. Removing this assumption made an order of magnitude difference in the position of the neutral stability curve, dramatically increasing the calculated stability of the flow. Reexamining the stability of the plane buoyant plume without the Boussinesq approximation also produced a marked change in the results, agreement with

experiment being considerably improved. Second, although the flame flow bears a superficial similarity to the buoyant plume above a line source, the several differences cause a large difference in the predicted behaviour of the two flows when perturbed. Third, a new unstable region consisting of waves with negative phase velocity but positive group velocity was found for both the buoyant flame and the buoyant plume. These waves have very long wavelengths, making the parallel flow assumption in the stability analysis questionable near the start of the flame, i.e at low Reynolds number, but persist to infinite Reynolds number where the assumption is valid. Full non-parallel calculations will probably change the shape of this region, however these waves are still expected to play an important role in the instability of buoyant flows. Finally, the asymmetry of the flow for real fuels did not markedly affect the stability. Empirically interpreting the stability diagrams to obtain an expected transition point gives $Re_T \approx 250$ or typically around 7cm above the start of the flame. This is considerably more stable than the buoyant plume with $Re_T \approx 140$.

Since the local analysis can not take account of the changing fluid properties in the flow, such as momentum and mass fluxes, an analytic technique treating the flame and associated plume as having negligible thickness compared to disturbances of long wavelength was undertaken. This showed that the primary cause of instability was centrifugal forces generated by the momentum flux following a curved path. Limited comparison with the local analysis gave reasonable agreement for disturbance amplification rates at large Reynolds numbers.